MIKE 21 & MIKE 3 Flow Model FM

Sand Transport Module

Scientific Documentation

DHI A/S headquarters
Agern Allé 5
DK-2970 Hørsholm
Denmark

+45 4516 9200 Telephone
+45 4516 9333 Support
+45 4516 9292 Telefax

mike@dhigroup.com
www.mikepoweredbydhi.com

PLEASE NOTE

CONTENTS

MIKE 21 & MIKE 3 Flow Model FM
Sand Transport Module
Scientific Documentation

1 Introduction

Traditionally, sediment transport is defined in three modes of transport: Bed load, suspended load and wash load. Among others, a comprehensive description is given by Engelund & Hansen (1967) and Jansen et al. (1979), see Figure 1.1.

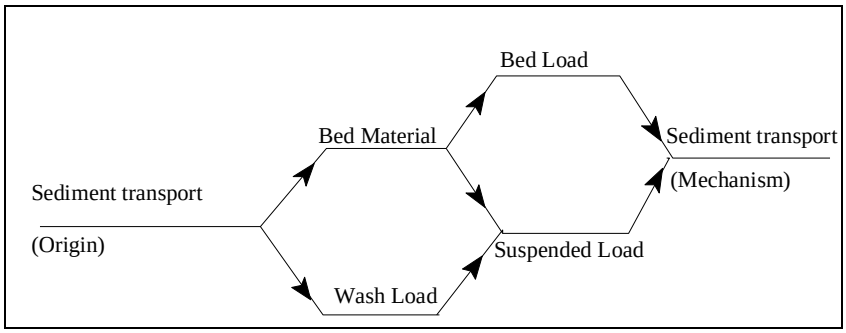

Figure 1.1 Classification of sediment transport. From Jansen et al. (1979)

The latter defines bed load transport as the transport of bed material that is rolling and sliding along the bed. Suspended load transport is defined as the transport of sediment, which is suspended in the fluid for some time. According to the mechanism of suspension, suspended sediment may belong to the bed material load and the wash load. Wash load is defined as the transport of material finer than the bed material. It has no relation to the transport capacity of the stream. Usually, a grain diameter of around 0.06 mm divides the region of wash load and bed material load. The Sand Transport Module only considers the bed material load.

1.1 Model Type

MIKE 21 & MIKE 3 Flow Model FM, Sand Transport Module, calculates the sediment transport rates using two different model types:

- Pure current
- Combined current and waves

The sediment transport calculations are based on the hydrodynamic conditions, sediment properties and, for ‘Combined current and waves’, wave conditions in the individual elements.

The sand transport calculations are carried out using a mean horizontal velocity component. The sand transport calculations in MIKE 3 Flow Model FM are thus not truly three-dimensional, but carried out in two dimensions in the horizontal direction. However, the findings that a more detailed 3D model can give of the hydrodynamic conditions are included.

The sediment transport rates are calculated for sand fractions without taking inertia effects into account. This means that transport rates for shingle sized material often will be overestimated.

For the ‘Pure current’ option the sediment transport rates are calculated directly during the simulation based on the actual conditions. The scientific background behind the calculation of the sediment transport rates for this option is given in Section 2.

For the ‘Combined current and waves’ option the sediment transport rates are found by linear interpolation in a sediment transport table. This table is generated beforehand by the MIKE 21 Toolbox utility program ‘Generation of Q3D Sediment Tables’. The scientific background behind the calculation of the values in the sediment transport table is given in Section 3.

1.2 Input Velocity

The sand transport in a flow will mainly take place near the bed, even the part of the sand transport that takes place as suspended load.

The sand transport calculations in MIKE 21 and MIKE 3 Flow Model FM, Sand Transport Module, are carried out using a mean horizontal velocity component, assuming the vertical velocity profile to be logarithmic. In cases where the vertical velocity profile differs significantly from a logarithmic velocity profile the findings from a 3D model setup may give considerably different results compared to a 2D model setup.

The sand transport calculations in MIKE 3 Flow Model FM are thus not truly three-dimensional, but carried out in two dimensions in the horizontal direction. However, the findings that a more detailed 3D model can give of the hydrodynamic conditions are included.

In MIKE 21 Flow Model FM the mean horizontal velocity component is set to the depth-averaged velocity from the hydrodynamic module.

In MIKE 3 Flow Model FM the mean horizontal velocity component may be calculated in one of two ways:

- Depth-averaged velocity calculated from the 3D flow field from the hydrodynamic module
- Mean velocity derived from the bottom stress value from the hydrodynamic module

In the first case the mean velocity component is found from the 3D flow field by integration over depth:

$$\overline{V} = \int_0^h \overline{V}(z)dz \tag{1.1}$$

Where *V(z)* is the velocity component at distance *z* above the bed and *h* is the local water depth.

In the latter case the mean velocity component is determined by the bottom stress value:

$$\overline{V} = \sqrt{\tau_b / \rho c_f} \tag{1.2}$$

Where τ_b is the bottom stress value, ρ is the density of water and c_f is the drag coefficient.

The calculation of the drag coefficient depends on the choice of Model Type and, in the case of ‘Pure current’, also the local bed resistance for the sand transport.

For the ‘Pure current’ option, the drag coefficient is taken directly from the hydrodynamic simulation or found by one of the equations below.

$$c_f = \frac{g}{C^2} \tag{1.3}$$

$$c_f = \frac{g}{\left(Mh^{1/6}\right)^2} \tag{1.4}$$

$$c_f = \frac{g}{\left(a \cdot h^b\right)^2} \tag{1.5}$$

Where g is gravity, *C* the Chezy number, *M* the Manning number, *a* the resistance coefficient and *b* the resistance power.

For the ‘Combined current and waves’ option, the drag coefficient is calculated as:

$$c_f = \frac{1}{\left(\frac{1}{\kappa}\left(\ln\left(\frac{30h}{k_s}\right)-1\right)\right)^2} \tag{1.6}$$

Where k_s is derived from the hydrodynamic simulation.

2 Pure Current

2.1 Introduction

For the pure current case (river flow) sediment transport rates are calculated continuously through the simulation based on sediment transport formulae derived from either empirical or deterministic principles. The sediment transport modelling is divided into bed load and suspended load due to their different nature. The bed load, which mainly is controlled by the bed shear stress or stream power per unit area, reacts instantaneously with the flow. In modelling terms this is referred to as an equilibrium transport description. The suspended load on the other hand is characterised by a phase-lag in the transport compared to the flow, because it takes some time or distance to adapt the concentration profile over the vertical to the flow. Model concepts that include the phase-lag effect on the transport of suspended sediment are termed non-equilibrium models and are characterised by a sediment concentration that can differ from the equilibrium concentration. If the actual concentration is greater than the equilibrium concentration, the system will be over-loaded and tend to deposit sediment on the bed; while if under-loaded, it will try to erode the bed.

Both the flow velocity and the concentration profile vary over the water depth. The flow can typically be divided into a logarithmic profile in the main stream direction and a secondary flow profile in the transverse direction. The strength of the secondary flow will mainly be related to the flow curvature and the bed resistance. The concentration profile can typically be approximated with a Vanoni profile. The suspended sediment transport components can be obtained by integrating the product of the velocity components and the concentration over the water depth. However, in order to do so detailed information about the vertical velocity profile is required. The sediment model is therefore extended with a model for the helical flow (secondary flow of the first kind) that includes these effects in the sediment transport through a pseudo 3D description. Furthermore, the bed load is corrected for gravitational bed slope effects.

In the 2D model the helical flow is handled separately in the sediment transport module and does not have any impact on the HD-model. In reality, the secondary flow will have an impact on the flow distribution, because in a river bend the secondary flow will be responsible for moving high-momentum water towards the outside of the bend and low-momentum water towards the inside of the bend. When using 3D HD-models this phenomenon is automatically included and the AD-model for the helical flow becomes irrelevant.

2.2 Hydrodynamics

2.2.1 Helical flow

Mathematical modelling of flow in a river bend requires insight into the physics of the water motion. For this purpose a physical explanation of the flow distribution in a bend is given below.

When water flows into a river bend, an imbalance of centripetal force starts to generate an outward motion near the free surface and an inward motion near the bed. The reason is that the main stream velocities in the upper part of the flow are greater than velocities in the lower part of the flow. Therefore, water particles in the upper part of the water column must follow a path with a larger radius of curvature than water particles in the

lower part to maintain nearly constant centripetal force over the depth. With velocity V and radius of curvature R, centripetal acceleration is V^2/R.

Simultaneously with the generation of helical motion, a lateral free surface slope is created to maintain equilibrium between the lateral pressure force, centripetal force and lateral shear force generated from friction along the bed. The classical analytical solution to this flow problem predicts a single helical vortex, which transports fluid downstream in spiral trajectories. This spiral (or helical) flow pattern can be considered as the sum of a longitudinal flow component (main flow) and a circulation in a plane perpendicular to the main flow direction (secondary flow). The secondary flow is directed towards the centre of curvature near the bottom and outwards in the upper part of the cross-section as illustrated in Figure 2.1.

For changing bend curvature and bed topography, the flow distribution will lag slightly behind the change in topography due to the inertia of the main flow. Analytical expressions for helical flow intensity and the length scale for adaptation of secondary flow to changes in topography are discussed below.

The intensity of the helical flow is the magnitude of the transverse velocity component. This is defined by de Vriend (1981) as:

$$i_s = V \cdot \frac{h}{R_s} \tag{2.1}$$

Where

V	Main flow velocity
R_s	Radius of curvature of streamlines
i_s	Helical flow intensity

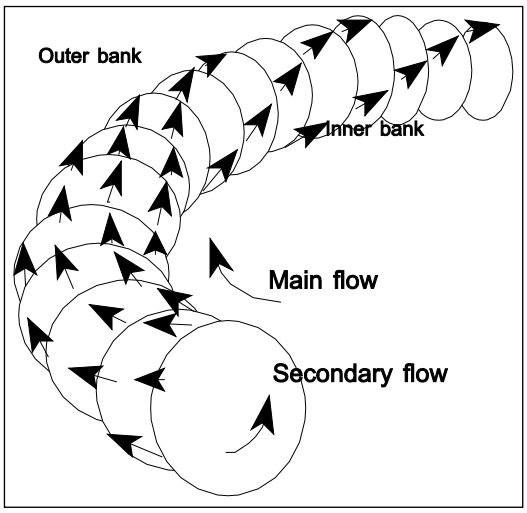

Figure 2.1 Helical flow in river bends

In Section 2.2.2 the vertical distribution of the helical flow is described. Secondary flow due to curving streamlines causes a small deviation δ_s in flow direction near the bed, away from the main stream direction. This also causes deviation in the bed shear stress direction.

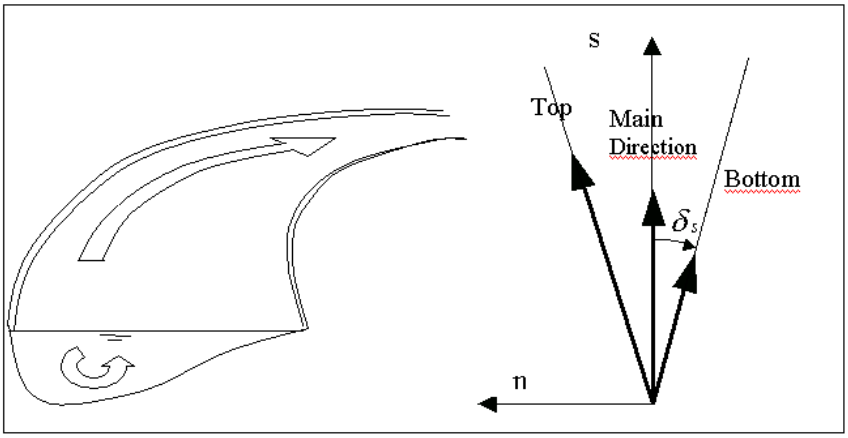

Figure 2.2 Deviation of bed shear stress due to helical flow

The direction of bed shear stress in a curved flow field plays an important role in a bed topography model for river bends. The logarithmic model obtained by Rozovskii (1957), among others, yields a bed shear stress direction given by:

$$\tan\delta_s = \beta \cdot \frac{h}{R_s} \tag{2.2}$$

Where

h	Water depth
R_s	Radius of curvature of flow stream lines
δ_s	Angle between bed shear stress and depth averaged shear stress (or flow)

The parameter β is defined as:

$$\beta = \alpha \cdot \frac{2}{\kappa^2}\left(1 - \frac{\sqrt{g}}{\kappa C}\right) \tag{2.3}$$

Where

κ	Von Kárman's constant, 0.4
g	Acceleration of gravity (9.81 m/s^2)
C	Chezy number
α	Calibration constant

The approximate value of β is 10. Other models for the vertical velocity profile, such as the power model, give slightly different values of β. Increasing flow resistance, represented by a decreasing Chezy number, gives a smaller β-value (i.e. less helical flow intensity and a smaller deviation in the direction of bed shear stress), as discussed by Olesen (1987). In the morphological model, α is specified as an expert user calibration parameter (constant or varying in space). The default value is 1.

In regions with changing curvature of the streamlines, the secondary flow will adapt gradually. The inertia of the secondary flow has been investigated analytically by (among others) Rozovskii (1957) and Nouh & Townsend (1979). De Vriend (1981), Booij & Kalkwijk (1982) and Kalkwijk & Booij (1986) have carried out numerical investigations on this topic. Further investigations are discussed in Olesen (1987).

Modelling of the adaptation of secondary flow is complicated by the fact that (according to numerical experiments) adaptation of the secondary flow profile is considerably faster near the bed (where bed shear stresses act) than higher up in the water column. Strictly speaking, the process of adaptation cannot be characterised by one length scale only. Adaptation length is a function of water depth and friction number. In the present morphological model, the following differential length scale is applied:

$$\lambda_{sf} = \frac{1.2\,h\,C}{\sqrt{g}} \tag{2.4}$$

Where

λ_{sf}	Length scale for secondary flow adaptation
h	Water depth
C	Chezy number
g	Acceleration of gravity

Consequently, the direction of bed shear stress for continuously varying curvature in steady flow conditions can be calculated by:

$$\lambda_{sf}\frac{\partial(\tan\delta_s)}{\partial s_s} + \tan\delta_s = \beta\cdot\frac{h}{R_s} \tag{2.5}$$

Where

s_s	Stream-wise coordinate along the streamline
R_s	Radius of curvature of the streamlines
h	Water depth
λ_{sf}	Length scale for secondary flow adaptation

The equation is transformed into a general Cartesian (x, y) coordinate system through the following equations:

$$\frac{\partial x}{\partial s_s}\frac{\partial \tan\delta_s}{\partial x} + \frac{\partial y}{\partial s_s}\frac{\partial \tan\delta_s}{\partial y} + \frac{\tan\delta_s - \beta\dfrac{h}{R_s}}{\lambda_{sf}} = 0 \tag{2.6}$$

$$\text{Using } \frac{\partial x}{\partial s_s} = \frac{p}{\sqrt{p^2+q^2}} \text{ and } \frac{\partial y}{\partial s_s} = \frac{q}{\sqrt{p^2+q^2}} \tag{2.7}$$

Where p and q are the two Cartesian flux components working in the horizontal plane as shown in Figure 2.3, we get:

$$\frac{p}{\sqrt{p^2+q^2}}\frac{\partial \tan\delta_s}{\partial x} + \frac{q}{\sqrt{p^2+q^2}}\frac{\partial \tan\delta_s}{\partial y} + \frac{\tan\delta_s - \beta\dfrac{h}{R_s}}{\lambda_{sf}} = 0 \tag{2.8}$$

By rearranging the equation and including an unsteady term this finally leads to:

$$\frac{\partial \tan\delta_s}{\partial t} + u\frac{\partial \tan\delta_s}{\partial x} + v\frac{\partial \tan\delta_s}{\partial y} + \frac{\sqrt{p^2+q^2}}{h\cdot\lambda_{sf}}\left(\tan\delta_s - \beta\frac{h}{R_s}\right) = 0 \tag{2.9}$$

The equation is solved time-true numerically with the MIKE-FM AD (advection-dispersion) model. It is seen that that the equation contains no dispersion and the helical flow is generated from the source term.

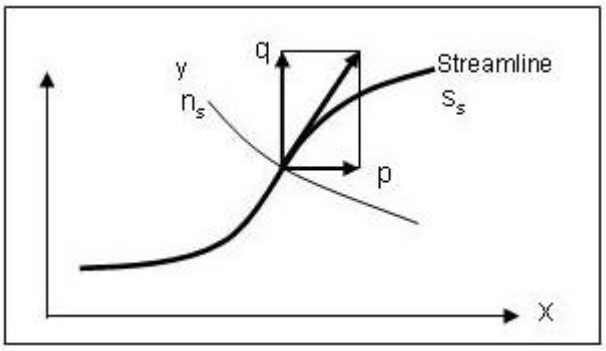

Figure 2.3 Transformation from stream-wise coordinates (s_s, n_s) to general Cartesian coordinates (x, y)

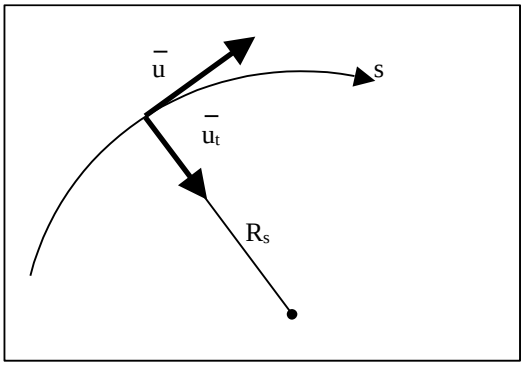

Figure 2.4 Streamline curvature based on velocity vector

The curvature of streamlines is calculated as a cross product between velocity and acceleration vector, as illustrated in Figure 2.4:

$$\frac{1}{R_s} = \frac{|\bar{u} \times \bar{u}_t|}{|\bar{u}|^3} \tag{2.10}$$

In the Cartesian (*x*, *y*) coordinate system, the acceleration vector is (see Figure 2.4):

$$\bar{u}_T = \left(\frac{du}{dt}, \frac{dv}{dt} \right) \tag{2.11}$$

Assuming quasi-steady conditions the Cartesian acceleration components can be reduced to:

$$\frac{du}{dt} = \frac{\partial u}{\partial x}\frac{\partial x}{\partial t} + \frac{\partial u}{\partial y}\frac{\partial y}{\partial t} + \frac{\partial u}{\partial t} \cong u\frac{\partial u}{\partial x} + v\frac{\partial u}{\partial y} \tag{2.12}$$

$$\frac{dv}{dt} = \frac{\partial v}{\partial x}\frac{\partial x}{\partial t} + \frac{\partial v}{\partial y}\frac{\partial y}{\partial t} + \frac{\partial v}{\partial t} \cong u\frac{\partial v}{\partial x} + v\frac{\partial v}{\partial y} \tag{2.13}$$

The cross product between the velocity vector and the acceleration vector can hereafter be obtained as:

$$\vec{u}\times\vec{u}_T=\vec{i}\begin{vmatrix} v & 0 \\ \frac{dv}{dt} & 0 \end{vmatrix}-\vec{j}\begin{vmatrix} u & 0 \\ \frac{du}{dt} & 0 \end{vmatrix}+\vec{k}\begin{vmatrix} u & v \\ \frac{du}{dt} & \frac{dv}{dt} \end{vmatrix}=u^2\frac{\partial v}{\partial x}+uv\left(\frac{\partial v}{\partial y}-\frac{\partial u}{\partial x}\right)-v^2\frac{\partial u}{\partial y} \tag{2.14}$$

Finally, the radius of curvature can be calculated from:

$$\frac{1}{R_s}=\frac{u^2\frac{\partial v}{\partial x}+uv\left(\frac{\partial v}{\partial y}-\frac{\partial u}{\partial x}\right)-v^2\frac{\partial u}{\partial y}}{\left(u^2+v^2\right)^{1.5}} \tag{2.15}$$

Note that the radius of curvature is calculated with a sign, stating that the curvature and helical flow is positive when flow is bending to the left and negative when bending to the right. Note further that the computed deviation in bed shear stress due to helical flow, tan δ_s, is based on the assumption of quasi-steady hydrodynamic conditions. In rapidly varying flow conditions, the expression does not apply.

Once the deviation in bed shear stress is determined, the corresponding helical flow intensity can be estimated from:

$$i_s=\frac{V\cdot h}{R_s}=-\frac{V}{\beta}\tan\delta_s \tag{2.16}$$

The helical flow intensity is of importance for the analysis and parameterisation of the secondary flow velocity profiles.

2.2.2 Vertical velocity profiles

The hydrodynamic model used for sediment transport applications is based on depth-averaged flow equations. However, information about the vertical velocity profiles is required for determining the bed shear stress and for the suspended sediment transport calculations in the morphological model. Even though the sediment model is formulated in general Cartesian coordinates, a local coordinate system (*s*, *n*) aligned with the main streamline is applied for the analysis of the vertical velocity profiles.

Introducing the Reynolds stress concept and the Prandtl mixing length hypothesis, and assuming that viscous (laminar) friction is much smaller than turbulent friction, the shear stresses in the fluid can be expressed by:

$$\tau_s=\rho E\frac{\partial u}{\partial z} \tag{2.17}$$

Where

ρ	Density of water
u	Velocity in main flow direction
z	Vertical coordinate
E	Turbulent (eddy) viscosity coefficient
τ_s	Shear stress in main flow direction

A similar relation for τ_n applies for the transverse direction. Introducing this into the Navier-Stokes equations (see Olesen, 1987) and assuming steady conditions, the

following flow equations for the flow in the longitudinal direction, *s*, and the transverse direction, *n*, emerge:

$$u\frac{\partial u}{\partial s}+v\frac{\partial u}{\partial n}+w\frac{\partial u}{\partial z}+\frac{uv}{R}+\frac{1}{\rho}\frac{\partial P}{\partial s}=\frac{\partial}{\partial z}(E\frac{\partial u}{\partial z})$$

$$u\frac{\partial v}{\partial s}+v\frac{\partial v}{\partial n}+w\frac{\partial v}{\partial z}-\frac{u^2}{R}+\frac{1}{\rho}\frac{\partial P}{\partial n}=\frac{\partial}{\partial z}(E\frac{\partial v}{\partial z}) \quad (2.18)$$

Where

u	Velocity in longitudinal flow direction
v	Velocity in transverse flow direction
w	Velocity in vertical direction
P	Hydrostatic pressure
s	Coordinate in stream wise direction
n	Coordinate in transverse direction
R	Radius of curvature of the main streamline

By assuming a hydrostatic pressure distribution *P* over the vertical, water pressure is simply a function of the water depth.

The vertical distribution of flow velocity can be obtained by asymptotic expansion. First, the zero order approximation of the longitudinal velocity is obtained from the momentum equation in the mainstream direction, assuming *v* and *w* and the gradient of the main velocity (*du/ds*) to be zero (i.e. fully developed flow). Next, the transverse velocity is computed from the momentum equation in the transverse direction with the zero-order longitudinal velocity inserted and disregarding $v + dv/dn$ and $w + dv/dz$.

A first order approximation of the longitudinal velocity can be obtained by introducing the first order secondary flow velocity *v* into the simplified momentum equation in the mainstream direction. De Vriend (1981) and De Vriend & Struiksma (1983) have a thorough description of this. The two listed references show that the form of the first order solution differs slightly from the zero order solution.

The boundary conditions for the momentum equations are zero shear stress at the free water surface and no slip at the bottom (z_0, the roughness height).

The reference level z_b, shown in Figure 2.5, defines the limit between suspended load and bed load transport. In the model the reference level is chosen as the height above the defined bed at which the no-slip condition occurs. Thus, *h* defines the height at which suspended sediment transport occurs, and *H* is the total water depth. In the following the non-dimensional vertical coordinate η is introduced. The η-system is positioned with its origin at the bed and is defined by $\eta = z/H$.

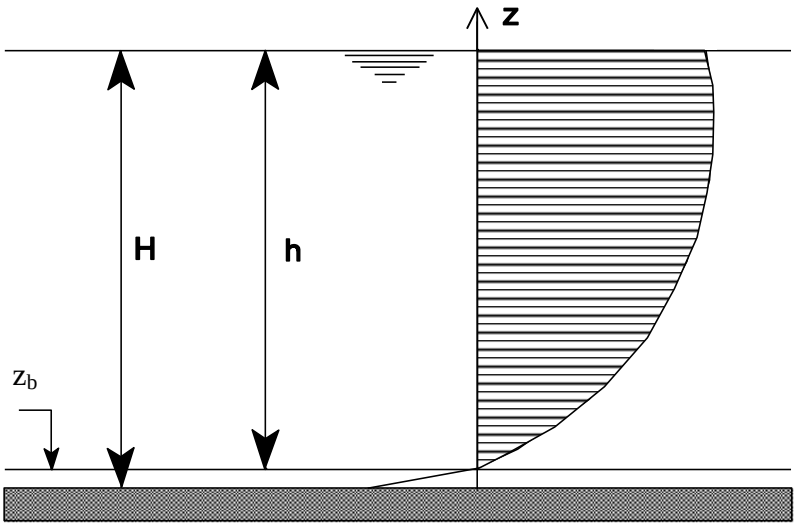

Figure 2.5 Vertical velocity profile in the stream wise direction

The height of the reference is chosen as the height above the defined bed at which the no-slip condition occurs, i.e. η0 = z_b /*H* in order to fit with the theory of Galapatti (1983), who couples suspended sediment transport to the vertical velocity and concentration profiles.

The velocity profile can be related to the depth-averaged velocity by applying a unit profile function $p_1(\eta)$, as shown below.

$$u(z) = V\, p_1(\eta)\ ,\ \eta = \frac{z}{H} \tag{2.19}$$

Solution of the momentum equation in the mainstream direction requires information about the vertical eddy viscosity or the mixing length (using Prandtl's definitions). Applying a logarithmic velocity profile (fully developed rough flow), the unit profile becomes:

$$p_1(\eta) = \frac{u_f}{\kappa V}\ln\left(\frac{\eta}{\eta_0}\right) = \frac{\sqrt{g}}{\kappa C}\ln\left(\frac{\eta}{\eta_0}\right) \tag{2.20}$$

The value of η_0 is obtained from the closure criterion:

$$\int_{\eta_0}^{1} p_1(\eta)\,d\eta = 1 \quad \Rightarrow \quad \eta_0 = Exp\left[\eta_0 - 1 - \frac{\kappa C}{\sqrt{g}}\right] \tag{2.21}$$

The equation for determination of the no-slip level is solved by iteration.

As seen from the unit profile expression, the mainstream velocity profile only depends on the vertical coordinate η and the resistance number, which is convenient for numerical purposes. This means that the mainstream velocity profile for fully developed turbulent flow can be parameterised by the universal function:

$$p_1 = f\left(\eta, \frac{u_f}{V}\right) = f\left(\eta, \frac{\sqrt{g}}{C}\right) \tag{2.22}$$

Where the symbols u_f and C represents the friction velocity and the Chezy number, respectively.

The unit mainstream velocity profile function is evaluated at a number of discrete points located along a vertical logarithmic axis, so that the most intense resolution is obtained near the bottom, where the largest velocity gradients occur. Initially, the discrete vertical points are distributed along the vertical η-coordinate axis by the simple relation:

$$\eta_{j+1} = \eta_j + \Delta \cdot (j+1) \tag{2.23}$$

Where

η	Non-dimensional coordinate $\eta = z/H$
$\Delta = 1.246 \cdot 10^{-5}$	Initial vertical spacing
$n = 400$	Number of numerical points
j	Index for vertical level with η_1=0 and η_n=1

But after the no-slip level, where η_0 has been obtained, the discrete points are redistributed, so that all discrete points are used to resolve the vertical velocity profiles from the no-slip level and up to the free water surface. This is done by the relation:

$$\eta_{j+1}^{new} = \eta_j^{new} + \left(\eta_{j+1}^{old} - \eta_j^{old}\right) \quad (1-\eta_0), \quad with \quad \eta_1^{new} = \eta_0 \tag{2.24}$$

A schematisation of the secondary flow and the vertical velocity profiles are shown in Figure 2.6 and Figure 2.7:

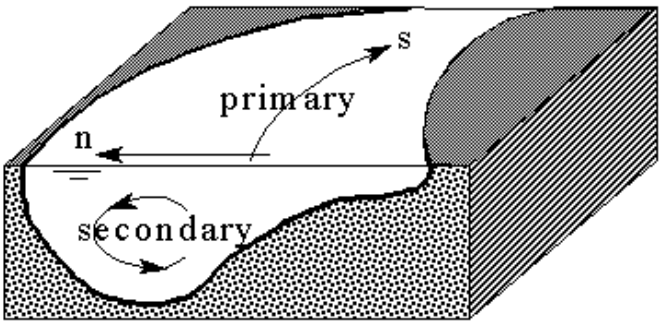

Figure 2.6 Sketch of the river channel

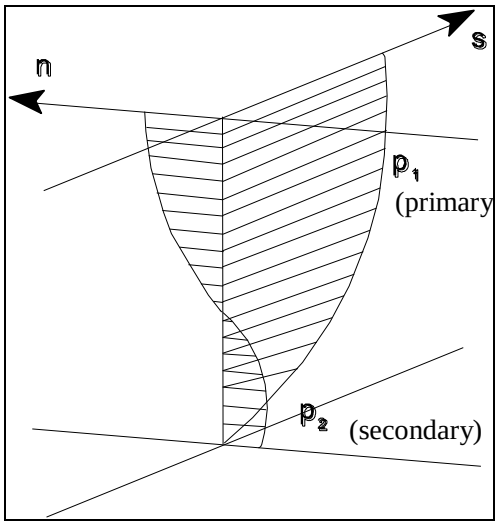

Figure 2.7 Main and secondary velocity profiles

The truncated first order version of the momentum equation in the transverse direction expresses the equilibrium between pressure forces, friction forces and centripetal forces:

$$\frac{1}{\rho}\frac{\partial P}{\partial n} - \frac{1}{\rho}\frac{\partial \tau_n}{\partial z} - \frac{V^2}{R_s} = 0 \tag{2.25}$$

Where the transverse shear stress is given by:

$$\tau_n = \rho E \cdot \frac{\partial v(z)}{\partial z} \tag{2.26}$$

And the symbols represent:

$z = H \cdot \eta$	Vertical coordinate
$P = \rho g \cdot S$	Hydrostatic water pressure
S	Surface elevation
V	Depth-averaged mainstream velocity
v	Transverse (secondary) velocity
R_S	Radius of curvature of stream line
n	Transverse (horizontal) coordinate

The vertical eddy viscosity coefficient is assumed to be parabolic:

$$E = \kappa H u_f \eta(1 - \eta) = \kappa H u_f \varepsilon \tag{2.27}$$

Where

ε	Non-dimensional eddy viscosity
κ	Von Kárman's constant, 0.4
H	Water depth

An equilibrium flow condition is achieved when the sum of the pressure, friction and centripetal force term equals zero.

Likewise the primary flow profile $p1$, a normalised profile $p2$ for the secondary velocity profile v, is applied:

$$v = \frac{V H}{R_s} p_2(\eta) = i_s \cdot p_2(\eta) \tag{2.28}$$

Where i_s, is the helical flow intensity.

Insertion of the three equations above into the equation for the transverse force balance results in the following expression after some re-arranging:

$$\left(\frac{R_s g}{\kappa u_f V}\right)\frac{\partial S}{\partial n} - \frac{\partial}{\partial \eta}\left(\varepsilon \frac{\partial p_2}{\partial \eta}\right) = \frac{1}{\kappa}\frac{V}{u_f} p_1^2 \tag{2.29}$$

Averaged over the depth, the secondary flow is by definition zero. Near the bottom at $\eta = \eta_0$ the velocity vanishes. Thus, the following two conditions must be fulfilled:

$$\int_{\eta_0}^{1} p_2 d\eta = 0 \tag{2.30}$$

and

$$p_2(\eta_0) = 0 \tag{2.31}$$

The first term in the transverse force balance is constant over the depth. This means that the term can be substituted by a constant denoted *A*:

$$A = \left(\frac{R_s g}{\kappa u_f V} \right) \frac{\partial S}{\partial n} \tag{2.32}$$

Integration of the transverse force balance from an arbitrary level in the water column η to the water surface $\eta = 1$ and substituting the constant denoted *A* into the equation results in the following expression:

$$-\varepsilon \frac{\partial p_2(\eta)}{\partial \eta} = -\frac{1}{\kappa} \frac{V}{u_f} \int_{\eta}^{1} p_1^2 d\eta + A(1-\eta) \tag{2.33}$$

Where the shear stress term used on the left side is equal to zero at the free surface, which is due to the fact that no shear forces (like wind) is assumed to act on the free water surface.

The force balance can be rewritten as:

$$\frac{\partial p_2(\eta)}{\partial \eta} = \frac{1}{\varepsilon} \int_{\eta}^{1} \frac{V}{\kappa u_f} p_1^2 d\eta - \frac{A \cdot (1-\eta)}{\varepsilon} \tag{2.34}$$

The secondary velocity profile described by $p_2(\eta)$ can now be obtained by integration from the no-slip level at which $p_2(\eta = \eta_0)$ to a point in the water column η. Hereby, we obtain:

$$p_2(\eta) = \int_{\eta_0}^{\eta} \left(\frac{1}{\varepsilon} \int_{\eta}^{1} \frac{V}{\kappa u_f} p_1^2 d\eta \right) d\eta - A \int_{\eta_0}^{\eta} \frac{1-\eta}{\varepsilon} d\eta \tag{2.35}$$

The function $p_2(\eta)$ is conveniently split up into two functions:

$$p_2(\eta) = p_{21}(\eta) - A \cdot p_{22}(\eta) \tag{2.36}$$

Where the function $p_{21}(\eta)$ is given by

$$p_{21}(\eta) = \int_{\eta_0}^{\eta} \left[\frac{1}{\varepsilon} \int_{\eta}^{1} \left(\frac{V}{\kappa u_f} p_1^2 \right) d\eta \right] d\eta \tag{2.37}$$

and the function $p_{22}(\eta)$ is given by

$$p_{22}(\eta) = \int_{\eta_0}^{\eta} \frac{1-\eta}{\varepsilon} d\eta = \int_{\eta_0}^{\eta} \frac{1-\eta}{\eta(1-\eta)} d\eta = \int_{\eta_0}^{\eta} \frac{1}{\eta} d\eta = \ln\left(\frac{\eta}{\eta_0} \right) \tag{2.38}$$

The integration constant A, representing the transverse surface slope, can now be obtained from the two functions $p_{21}(\eta)$ and $p_{22}(\eta)$ utilizing that the depth-integrated secondary flow velocity is zero:

$$A = \frac{\int_{\eta_0}^{1} p_{21}(\eta) d\eta}{\int_{\eta_0}^{1} p_{22}(\eta) d\eta} \tag{2.39}$$

The function $p_{21}(\eta)$ is singular for $\eta = 1$, which therefore requires special numerical treatment. Furthermore, $p_{21}(\eta)$ consists of integrals with no analytical solution and therefore only can be solved by numerical integration. However, the inner integral in the expression for $p_{21}(\eta)$ can be solved analytically. This results in:

$$\int_{\eta}^{1} p_1^2(\eta) d\eta = \frac{g}{\kappa^2 C^2} \int_{\eta}^{1} \ln^2\left(\frac{\eta}{\eta_0}\right) d\eta = \tag{2.40}$$

$$\frac{g}{\kappa^2 C^2}\left[(1-\eta)\left(2 + 2\ln\eta_0 + \ln^2\eta_0\right) + \eta\left(2\ln\eta + 2\ln\eta_0 \ln\eta - \ln^2\eta\right)\right]$$

Inserting the right hand side into the expression for $p_{21}(\eta)$ yields:

$$p_{21}(\eta) = \frac{\sqrt{g}}{\kappa^3 C} \int_{\eta_0}^{\eta} \frac{2 + 2\ln\eta_0 + \ln^2\eta_0}{\eta} d\eta + \tag{2.41}$$

$$\frac{\sqrt{g}}{\kappa^3 C}\left[2\left(1 + \ln\eta_0\right) \int_{\eta_0}^{\eta} \frac{\ln\eta}{1-\eta} d\eta - \int_{\eta_0}^{\eta} \frac{\ln^2\eta}{1-\eta} d\eta\right]$$

The first integral in the new expression for $p_{21}(\eta)$ has the analytical solution:

$$\int_{\eta_0}^{\eta} \frac{2 + 2\ln\eta_0 + \ln^2\eta_0}{\eta} d\eta = \left(2 + 2\ln\eta_0 + \ln^2\eta_0\right) \ln\left(\frac{\eta}{\eta_0}\right) \tag{2.42}$$

The two remaining integrals in the equation for $p_{21}(\eta)$ do not have any analytical solutions and are evaluated by numerical integration. For $\eta = 1$ some problems can occur due to the singularity. However, by use of the rule of L´Hospital, it can be found that:

$$\frac{\ln^2\eta}{1-\eta} \to 0 \text{ for } \eta \to 1 \text{ and } \frac{\ln\eta}{1-\eta} \to -1 \text{ for } \eta \to 1 \tag{2.43}$$

The shape function for the primary and secondary velocity profiles, which are used for the evaluation of the suspended sediment transport rates, are plotted in Figure 2.8 and Figure 2.9, respectively, for four different Chezy numbers.

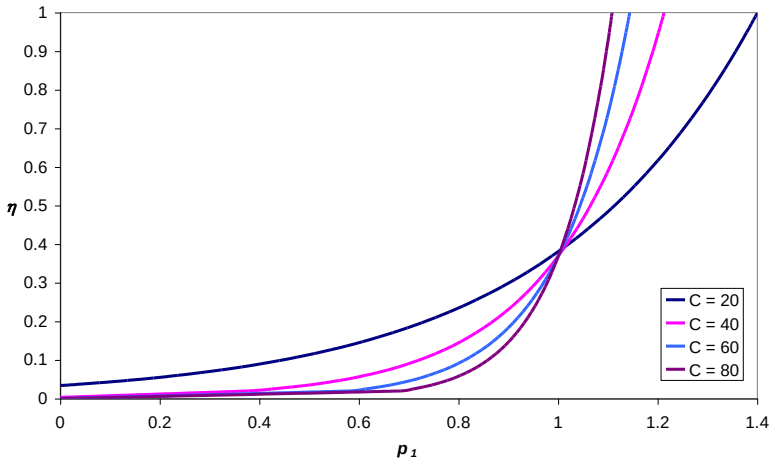

Figure 2.8 Shapes of the primary velocity profile for varying Chezy numbers ($m^{1/2}/s$)

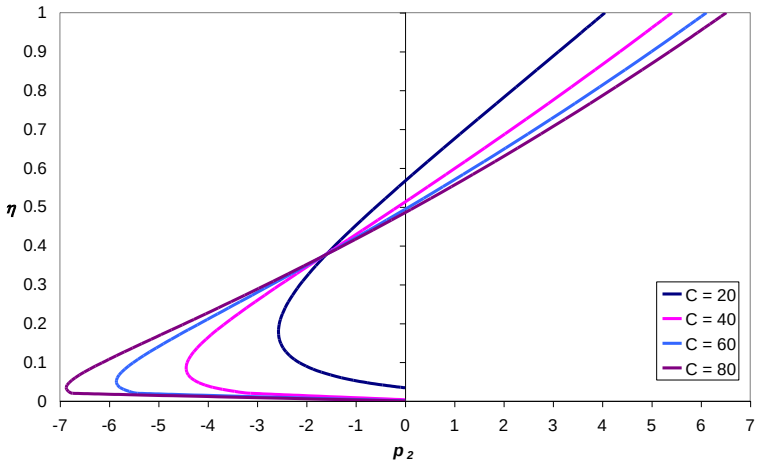

Figure 2.9 Shapes of the secondary velocity profile for varying Chezy numbers ($m^{1/2}/s$)

As shown, the absolute value of the profile functions near the bottom increases for increasing Chezy number, i.e. reduced flow resistance.

The shape of the velocity profiles is also sketched in Figure 2.10 for two Chezy numbers (from Olesen, 1987) and compared with the profiles obtained using a power assumption on the velocity profile instead. Only slight differences between the flow profiles of the different mixing length models (power profile versus logarithmic velocity profile) can be observed in the figure, although the logarithmic model seems to result in a somewhat larger secondary flow.

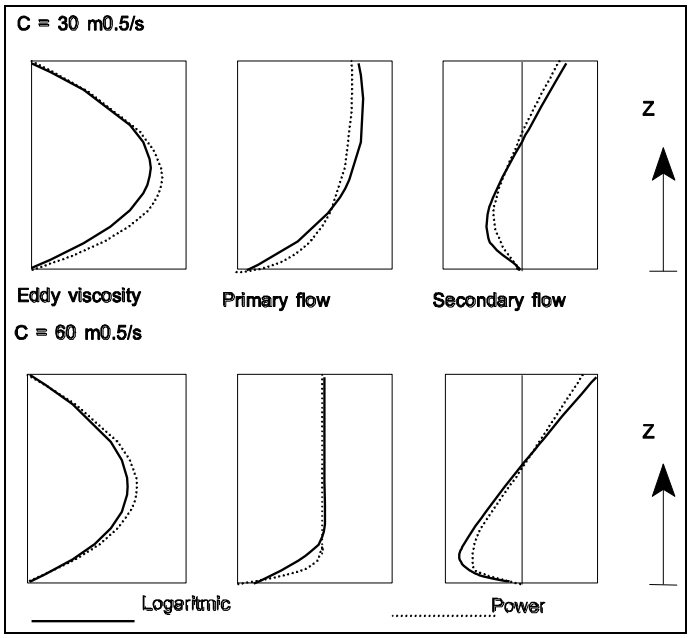

Figure 2.10 Vertical distribution of eddy viscosity and flow velocity profiles for a logarithmic and a power profile assumption, respectively (from Olesen, 1987)

The depth integration of the mathematical model is based on an assumption that the horizontal streamlines are approximately parallel through the water column. This means that the secondary velocity component *v* is much smaller than the main flow component *u*. Due to the non-uniform velocity distribution over the depth, some velocity distribution coefficients on the flow convection terms emerge, as discussed by Olesen (1987). Applying depth integration the momentum equations can be transformed into:

$$\frac{1}{\rho}\frac{\partial P}{\partial s} + k_{uu}\left[\bar{u}\frac{\partial \bar{u}}{\partial s} + \bar{v}\frac{\partial \bar{u}}{\partial n} + \frac{\overline{vu}}{R}\right] + \frac{\tau_{bs}}{h} + \frac{k_{sn}}{h}\left[\frac{\partial \bar{u}\, i_s h}{\partial n} + 2\frac{\bar{u}\, i_s h}{R}\right] = 0 \tag{2.44}$$

and

$$\frac{1}{\rho}\frac{\partial P}{\partial n} + k_{uu}\left[\bar{u}\frac{\partial \bar{v}}{\partial s} - \frac{\overline{u^2}}{R}\right] + \frac{\tau_{bn}}{h} + \frac{k_{sn}}{h}\cdot\frac{\partial \bar{u}\, i_s h}{\partial s} = 0 \tag{2.45}$$

The two velocity distribution coefficients k_{uu} and k_{sn} are defined as:

$$k_{uu} = \int_{\eta_0}^{1} [p_1(\eta)]^2 d\eta \tag{2.46}$$

and

$$k_{sn} = \int_{\eta_0}^{1} p_1(\eta)\cdot p_2(\eta) d\eta \tag{2.47}$$

The coefficient k_{uu} is very close to unity and can in most cases be disregarded (default 1). The k_{sn} coefficient is related to the convection of the main flow momentum by the secondary flow. Kalkwijk et al. (1980) and Olesen (1987) investigated the influence of the secondary flow convection. The latter also compared velocities from flume tests with

numerical experiments using different models of the k_{sn} coefficient. For narrow and smooth channels, the k_{sn} coefficient has some importance, whereas for natural rivers the effect is negligible. Consequently, the convection of momentum by secondary flow is not included in the present model.

2.3 Single-fraction Sediment Transport

For morphological development of alluvial rivers with interaction between bed bathymetry and hydrodynamics, only bed material transport is of interest. Thus, only bed load and the part of the suspended load originating from the bed material is considered. The behaviour of suspended load is fundamentally different from that of bed load, which has to be taken into consideration in the sediment transport modelling.

A description of bed load transport modelling is provided in Section 2.3.1. A description of the suspended load transport modelling is provided in Section 2.3.2. A number of explicit sediment transport formulas for bed load, suspended load and total load have been developed over the years. The formulas implemented in the present modelling system, at the core of the sediment transport modelling, are described in Section 2.3.3.

2.3.1 Bed load transport

The interaction between the bed load and the alluvial bed is one of the most fundamental aspects of the morphological behaviour of a river bend (see Engelund, 1974 and Struiksma et al., 1985).

In contrast to the suspended load, it is assumed that the bed load responds immediately to changes in local hydraulic conditions. Thus, there is no need for advection-dispersion modelling in connection with bed load. However, two important effects must be taken into account:

1. The deviation of the direction of the bed shear stress from the mean flow direction due to helical flow; and
2. The effect of a sloping river bed.

The first issue requires separate modelling of helical flow prior to bed load computations (see Section 2.2.1).

When discussing the local bed load sediment transport capacity of a flow, it is convenient only to consider sediment transport in uniform shear flow. For this schematised case numerous transport relations have been presented during past decades. For a review of this topic, suggested references are Vanoni (1975 and 1984). The transport relations implemented in the present modelling system are presented in Section 2.3.3.

The bed load sediment transport is assumed to be the same as the sediment transport capacity mentioned above (unless supply-limited modelling is applied), except for bed slope effect and helical flow effect. This is illustrated in Figure 2.11.

The bed slope influences the sediment transport rate and direction (the latter being the most important for morphological modelling). Only a few models of the influence of bed slopes on sediment transport rate have been proposed, see Lane (1953), Luque (1976), Koch (1980), Ikeda (1980), and Olesen (1987). In principle, two approaches have been adopted. The first modifies the critical shear stress for initiation of motion:

$$\theta_c = \theta_{c0} \cdot \left(1 + \frac{\partial z_b}{\partial s}\right) \tag{2.48}$$

Where

θ_c	Modified critical Shields parameter
θ_{c0}	Critical Shields parameter in uniform shear flow
z_b	Bed level
s	Stream-wise (horizontal) coordinate

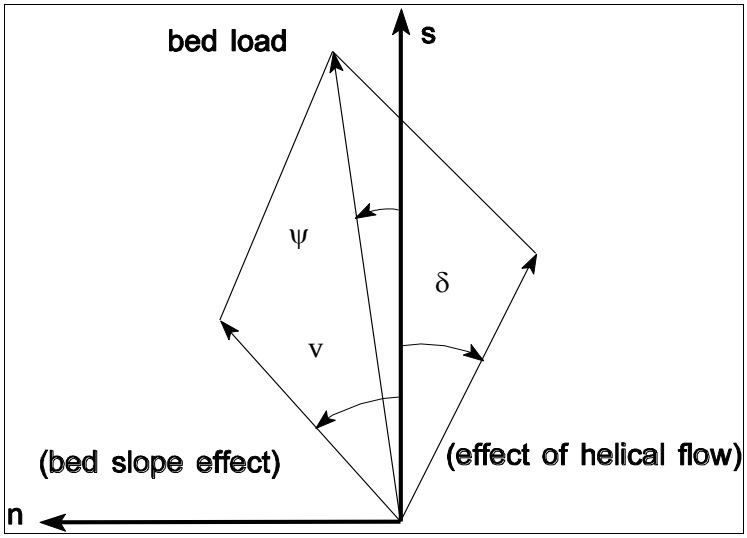

Figure 2.11 Direction of bed load transport influenced by helical flow and transverse bed slope

The slope effect on the sediment transport rate given by the relation above cannot be directly incorporated into a model that does not assume zero bed load transport at a critical shear stress (e.g. the Engelund and Hansen formula). For this kind of formula, the following correction can be applied:

$$S_s = \left(1 - \alpha \cdot \frac{\partial z_b}{\partial s}\right) S_{bl} \tag{2.49}$$

Where

α	Model calibration parameter
S_{bl}	Bed load as calculated from sediment transport formula
S_s	Bed load along streamline, s

This equation is implemented in the present modelling system. In the model the coefficient α is defined as an expert user coefficient, which cannot be changed in the GUI (Graphical user Interface). An estimate of the coefficient can be obtained by estimating the velocity exponent b in the generalised sediment transport formula $\Phi = a \cdot u^b$ (u, is flow velocity, a, a constant factor, and Φ, the non-dimensional sediment transport) by comparison with the Meyer-Peter & Müller (1948) formula $\Phi = 8 \cdot (\theta' - \theta_{c0})^{1.5}$. This gives:

$$b = \frac{3 \cdot \theta'}{\theta' - \theta_c} \tag{2.50}$$

Where

θ'	Effective skin friction
θ_c	Critical Shields parameter

b	Velocity exponent in the transport formula $\Phi = a \cdot u^b$
a	Constant factor
u	Flow velocity
Φ	Non-dimensional sediment transport rate

Using the total load formula of Engelund and Hansen (1967) the velocity exponent *b* is 5 (constant). Using the relation for *b*, it can be seen that *b* varies from infinity at the threshold of motion to 3 for very high shear stresses.

Secondly, the modified critical Shields parameter θ_c is substituted into the Meyer-Peter & Muller (1947) formula. If the relation for θ_c is linearised with respect to the bed slope *dz/ds*, the following expression for the α coefficient is obtained:

$$\alpha = \frac{b}{2} \cdot \frac{\theta_{c0}}{\theta'} \tag{2.51}$$

The coefficient varies from around $\alpha = 1.5$ for $\theta' = 2\theta_{c0}$ down to $\alpha \approx 0.2$ for $\theta' = 9\theta_{c0}$. In the present modelling system however, the α coefficient is specified as a constant throughout the modelling period.

The prediction of transverse depth distribution in alluvial channel bends has had considerable attention from river engineers, as it is essential in investigations of navigability improvement in river bends and in design of optimal channel bank protection. Since the pioneering work of van Bendegom (1947), many models of transverse bed slope have been proposed. Most of these can be reformulated, so that they also predict the direction of sediment transport. Olesen (1987) gives an exhaustive description of the proposed models. Talmon et al. (1995) has carried out extensive bed levelling experiments for verification of mathematical models of the transverse bed slope effect, which in line with Kikkawa et al. (1976), Parker (1983), Odgaard (1981), and Ikeda (1980) suggested the following suitable formula:

$$S_n = \left(\tan\delta_s - G \cdot \theta^{-a} \cdot \frac{\partial z}{\partial n} \right) S_{bl} \tag{2.52}$$

Where

G	Transverse bed slope factor (calibration coefficient)
a	Transverse bed slope exponent (calibration parameter)
tan δ_S	Bed shear direction change due to helical flow strength, see Section 2.2.1

The values of the transverse bed slope factor *G* and the exponent *a*, differ somewhat between the various authors. Especially, when results from laboratory flumes are compared with the results from prototypes. For the laboratory flume case the best fit seems to be obtained by:

$G = 0.6$ and $a = 0.5$ (2.53)

Talmon et al. (1995) conclude from their experiments that a distinction should be made between laboratory conditions and natural rivers. The magnitude of the transverse slope effect (*G*) and the direction coefficient (β) of the secondary flow seem to differ by a factor of two. Also, the distribution between suspended and bed load transport is important. The *G* factor is at least a factor 2 stronger for conditions with prevailing suspended load, indicating that either the transverse slope effect is also acting on the suspended load part or the transverse slope effect is simply stronger. This means that the following values should be used for natural rivers:

$G = 1.25$ and $a = 0.5$ (2.54)

If the angle between flow direction and the *x*-axis is ϕ in a fixed Cartesian coordinate system, the bed slope in the streamline direction can be computed as:

$$\frac{\partial z}{\partial s} = \frac{\partial z}{\partial x}\cos\phi + \frac{\partial z}{\partial y}\sin\phi \tag{2.55}$$

Where

s	The horizontal coordinate along the streamline
n	The horizontal coordinate in the transverse direction
x	The first horizontal coordinate
y	The other horizontal coordinate
z	The bed level
ϕ	Angle of stream line compared to (*x*, *y*) coordinate system

Likewise, the bed slope in the transverse direction is obtained by:

$$\frac{\partial z}{\partial n} = \frac{\partial z}{\partial y}\cos\phi - \frac{\partial z}{\partial x}\sin\phi \tag{2.56}$$

Transformation from streamline coordinates to general Cartesian coordinates results in the following expressions for the transport rates in the two axis-directions:

$$S_{bx} = S_s\cos\phi - S_n\sin\phi$$
$$S_{by} = S_n\cos\phi + S_s\sin\phi \tag{2.57}$$

Finally, the magnitude of the bed load transport is obtained as:

$$S_{bl} = \sqrt{S_{bx}^2 + S_{by}^2} \tag{2.58}$$

The magnitude of the bed load transport rate is mainly relevant for contour plotting of the transport rates.

2.3.2 Suspended load transport

The model for suspended sediment transport is based on the theory of Galapatti (1983). Modelling of non-cohesive suspended sediment in a fluid can be described by a transport equation for the volumetric sediment concentration *c*. If the sediment is treated as a passive scalar in the flow, a transport equation can be established from a mass balance on a rectangular flow element. In the general case the sediment balance contains contributions from the three transport mechanisms: advection, settling, and diffusion. Written as a transport equation for a small water element this can be expressed:

$$\frac{\partial c}{\partial t} + \frac{\partial (uc)}{\partial x} + \frac{\partial (vc)}{\partial y} + \frac{\partial (wc)}{\partial z} = \frac{\partial}{\partial x}\left(\varepsilon\frac{\partial c}{\partial x}\right) + \frac{\partial}{\partial y}\left(\varepsilon\frac{\partial c}{\partial y}\right) + \frac{\partial}{\partial z}\left(\varepsilon\frac{\partial c}{\partial z}\right) + w_s\frac{\partial c}{\partial z} \tag{2.59}$$

Where *c* is the volumetric concentration, *t* is time, *x* and *y* are spatial horizontally coordinates, *z* is a vertical coordinate, *u*, *v*, and *w* are flow velocities in the *x*, *y*, and *z* direction, respectively. ε_x, ε_y, and ε_z are turbulent diffusion coefficients, and w_s is the settling velocity of the suspended sediment.

If we ignore the horizontal diffusion terms, which are assumed small compared to the vertical diffusion terms, and shift the formulation to a coordinate system following the streamline, we obtain the simplified equation:

$$\frac{\partial c}{\partial t}+\frac{\partial(u_s c)}{\partial s}+\frac{\partial(v_n c)}{\partial n}+\frac{\partial(wc)}{\partial z}=\frac{\partial}{\partial z}\left(\varepsilon_z \frac{\partial c}{\partial z}\right)+\frac{\partial(w_s c)}{\partial z} \tag{2.60}$$

Here, *s*, is a streamwise coordinate, *n*, is a transverse coordinate, u_s, is the flow velocity in the main stream direction, and u_n, is a secondary flow velocity normal to the mainstream direction.

The two horizontal flow velocities u_s and u_n can be expressed by the profile functions p_1 and p_2 derived in Section 2.2.2 assuming the flow to be turbulent and fully developed, i.e.:

$$u_s(\eta)=V\cdot p_1(\eta)=\frac{V\sqrt{g}}{\kappa C}\ln\left(\frac{\eta}{\eta_0}\right) \tag{2.61}$$

for the primary flow component, and

$$v_n(\eta)=\frac{Vh}{R_s}p_2(\eta) \tag{2.62}$$

for the secondary flow component.

In order to solve the advection-dispersion equation for the concentration of the suspended load, boundary conditions are needed at the water surface and at the bed. At the free water surface a no flux condition can be applied:

$$w_s\cdot c(\eta=1)+\varepsilon\left.\frac{\partial c}{\partial \eta}\right|_{\eta=1}=0 \tag{2.63}$$

The boundary condition at the bed is simply given as a bottom concentration slightly above the bed at $\eta = \eta_0$:

$$c=c_{bed} \tag{2.64}$$

The method for calculation of c_{bed} depends of the theory applied (transport formula) to describe the transport of the suspended sediment. The level at which c_{bed} is calculated corresponds to the level, where the transport mechanism shifts from bed load to suspended load.

A special asymptotic approximation technique developed by Galappatti (1983) can be used to provide information about the concentration profile. This technique is applicable for conditions, where the vertical diffusion coefficient and the fall velocity term are the dominating terms in the transport equation for the concentration of the suspended sediment), or that non-dimensional parameter *e* is very small. The parameter *e* is defined by:

$$e=\frac{h}{L}\frac{V}{w_s} \tag{2.65}$$

Where h is the height of the water column at which suspended transport occurs, L is a length scale for variations in the mean flow direction, w_s is the settling velocity of the suspended sediment, and V is the depth-averaged flow velocity.

The theory applied to describe the suspended load in the model is based on an extension of the model developed by Galappatti, who did not account for the effects from helical flow. The general solution for slowly varying flow is based on the assumption that the concentration profile can be obtained as a sum of concentration profiles of increasing orders:

$$c = \sum_{i=0}^{n} c_i \tag{2.66}$$

Where c_0 is the zero-order contribution to c, c_1 is the first order contribution, c_2 the second order contribution, etc.

The concentration of different orders is found by solving the advection-dispersion equation for the suspended sediment by an asymptotic technique. First, the c_0 concentration profile is obtained ignoring the temporal and spatial varying terms and only considering the remaining two terms representing equilibrium between settling of suspended sediment and vertical diffusion, i.e.

$$w_s \frac{\partial c_0}{\partial z} + \frac{\partial}{\partial z}\left(\varepsilon \frac{\partial c_0}{\partial z}\right) = 0 \tag{2.67}$$

Secondly, the zero-order concentration c_0 profile, which can be obtained by solving the equation, is substituted into the left side of the advection-dispersion equation, while the right side now is represented by the first order concentration profile terms. Hereby, we obtain rearranging the terms:

$$w_s \frac{\partial c_1}{\partial z} + \frac{\partial}{\partial z}\left(\varepsilon \frac{\partial c_1}{\partial z}\right) = \frac{\partial c_0}{\partial t} + u\frac{\partial c_0}{\partial s} + v\frac{\partial c_0}{\partial n} w\frac{\partial c_0}{\partial z} \tag{2.68}$$

This procedure is repeated for the first order concentration c_1, so that the equation for the second order concentration c_2 now becomes:

$$w_s \frac{\partial c_2}{\partial z} + \frac{\partial}{\partial z}\left(\varepsilon \frac{\partial c_2}{\partial z}\right) = \frac{\partial c_1}{\partial t} + u\frac{\partial c_1}{\partial s} + v\frac{\partial c_1}{\partial n} + w\frac{\partial c_1}{\partial z} \tag{2.69}$$

Equations for the higher order concentration profile can be found in the same manner, but usually one stops with the first or second order contribution assuming the higher order contributions to be extremely small.

The following non-dimensional parameters are introduced:

Suspension time scale τ:

$$\tau = \frac{w_s}{h} \cdot t \tag{2.70}$$

Two horizontal length scales ξ and ψ for suspended sediment in the stream-wise and transverse direction, respectively:

$$\xi = \frac{w_s}{Vh} \cdot s$$

$$\psi = \frac{w_s}{Vh} \cdot n \tag{2.71}$$

Finally, the vertical length scale is defined by:

$$\eta = \frac{z}{h} \tag{2.72}$$

Furthermore, the differential operator D is introduced:

$$D = \frac{\partial}{\partial \eta} + \frac{\partial}{\partial \eta}\left(\varepsilon' \frac{\partial}{\partial \eta}\right) \tag{2.73}$$

Where ε' is a non-dimensional turbulent diffusion coefficient $\varepsilon/(w_s h)$
Applying the differential operator and the non-dimensional parameters the equation for the zero order concentration profile c_0 can be expressed as:

$$D[c_0] = 0 \tag{2.74}$$

For the higher order concentration profiles the following general expression can be obtained:

$$D[c_i] = \frac{\partial c_{i-1}}{\partial \tau} + p_1(\eta)\frac{\partial c_{i-1}}{\partial \xi} + p_2(\eta)\frac{Vh}{R_s}\frac{\partial c_{i-1}}{\partial \psi} + \frac{w}{w_s}\frac{\partial c_{i-1}}{\partial \eta} \tag{2.75}$$

Where *i,* represents orders greater than or equal to 1. In the further analysis the last term on the right side is ignored assuming that the vertical velocities are much smaller than the settling velocity of the suspended sediment w_s. The boundary condition at the free water surface must be valid for all orders of the concentration, i.e.

$$c_i + \varepsilon' \frac{\partial c_i}{\partial \eta} = 0 \tag{2.76}$$

Furthermore, it is assumed that higher order concentration profiles do not contribute to the depth-integrated concentration, i.e.

$$\int_0^1 c_i \, d\eta = 0 \ , \text{for } i \geq 1 \tag{2.77}$$

As for the velocity profiles, it is convenient to operate with unit concentration profiles. Thus, the zero order concentration profile is the product between the depth-averaged concentration and a unit profile function $\Phi_0(\eta)$:

$$c_0 = \bar{c}(\eta, \tau) \cdot \Phi_0(\eta) \tag{2.78}$$

The following discussion considers concentration terms of higher order:

Galappatti (1983) shows that a differential equation of the type $D[F(\eta)] = G(\eta)$, with a free surface ($\eta = 1$) boundary condition $F + \varepsilon' \cdot dF/d\eta$ and a restriction that F is zero when integrated from $\eta = \eta_0$ to $\eta = 1$, has the solution:

$$F(\eta) = D^{-1}[G(\eta)] = -\int_{\eta}^{1} G(\eta)d\eta + \Phi_0(\eta) \cdot \int_{\eta}^{1} \frac{G(\eta)}{\Phi_0(\eta)} d\eta + B \cdot \Phi_0(\eta) \tag{2.79}$$

Where the constant B is obtained from the requirement:

$$\int_{\eta_0}^{1} F(\eta)d\eta = 0 \tag{2.80}$$

Higher order concentrations c_i ($i > 0$) can be obtained using this solution technique once the zero order concentration c_0 is known. For the first order profile we obtain:

$$c_1(\eta) = D^{-1}[\Phi_0(\eta)] \cdot \frac{\partial \bar{c}}{\partial \tau} + D^{-1}[p_1(\eta) \cdot \Phi_0(\eta)] \cdot \frac{\partial \bar{c}}{\partial \xi} + D^{-1}[p_2(\eta) \cdot \frac{Vh}{R_s} \cdot \Phi_0(\eta)] \cdot \frac{\partial \bar{c}}{\partial \psi} \tag{2.81}$$

Thus, if we determine the vertical concentration profile of the suspended sediment as the sum of zero order profile at the first order profile, we obtain the following expression:

$$c(\eta) = \Phi_o(\eta) \cdot \bar{c} + \Phi_t(\eta) \cdot \frac{h}{w_s} \frac{\partial \bar{c}}{\partial t} + \Phi_1(\eta) \cdot \frac{Vh}{w_s} \frac{\partial \bar{c}}{\partial s} + \Phi_2(\eta) \cdot \frac{V h^2}{R_s w_s} \frac{\partial \bar{c}}{\partial n} \tag{2.82}$$

Where the higher order concentration profiles Φ_t , Φ_1 , and Φ_2 are obtained by solving:

$$\begin{aligned} \Phi_t(\eta) &= D^{-1}[\Phi_0(\eta] \\ \Phi_1(\eta) &= D^{-1}[p_1(\eta) \cdot \Phi_0(\eta)] \\ \Phi_2(\eta) &= D^{-1}[p_2(\eta) \cdot \Phi_0(\eta)] \end{aligned} \tag{2.83}$$

If we assume quasi-steady conditions so that the spatial changes are dominant compared to the temporal changes, the expression for the vertical concentration profile of the suspended sediment can be further simplified to:

$$c(\eta) = \Phi_o(\eta) \cdot \bar{c} + \Phi_1(\eta) \cdot \frac{Vh}{w_s} \frac{\partial \bar{c}}{\partial s} + \Phi_2(\eta) \cdot \frac{V h^2}{R_s w_s} \frac{\partial \bar{c}}{\partial n} \tag{2.84}$$

The zero order solution for the concentration profile is in the model based on an exponential profile with modified Rouse parameter Z (Galappatti 1983, who refers to Delft Hydraulics Laboratory, 1980):

$$\Phi_0(\eta) = \exp[Z \cdot f(\eta)] \tag{2.85}$$

Where the function $f(\eta)$ is defined by the following two expressions for the lower and upper part of the fluid, respectively:

$$f(\eta) = \ln\left[\frac{1-\eta}{\eta}\right] \quad \text{for } \eta < \frac{1}{2} \tag{2.86}$$

and

$$f(\eta) = -4\eta + 2 \quad \text{for } \eta \geq \frac{1}{2} \tag{2.87}$$

The modified Rouse number is defined by:

$$Z = \frac{w_s}{4u_f} \cdot \frac{1}{0.13 + 0.20\left(\frac{w_s}{u_f}\right)^{2.12}} \tag{2.88}$$

Where u_f is the friction velocity and w_s is the settling velocity of the suspended sediment. The settling velocity is obtained from the following relations:

The fall velocity w for any grain fraction with a diameter d is found by Eq. (2.89), Rubey's formula (1933):

$$w = \sqrt{g(s-1)d} \cdot \left(\left(\frac{2}{3} + \frac{36\nu^2}{g(s-1)d^3} \right)^{½} - \left(\frac{36\nu^2}{g(s-1)d^3} \right)^{½} \right) \tag{2.89}$$

Where s is the relative sediment density, g is gravity and ν is kinematic viscosity.

Near the bed at $\eta = \eta_0$ the concentration will adapt instantaneous to the equilibrium conditions, so that:

$$c(\eta = \eta_0) = c_e(\eta = \eta_0) = \bar{c}_e \Phi_o(\eta_0) \tag{2.90}$$

Inserting this into the equation obtained for the vertical concentration profile Eq. (2.84), we get the following relation:

$$\Phi_1(\eta_0)\bar{u}\frac{\partial \bar{c}}{\partial s} + \Phi_2(\eta_0)\frac{\bar{u}h}{R}\frac{\partial \bar{c}}{\partial n} = \Phi_o(\eta_0)\frac{w_s}{h}\left(\bar{c}_e - \bar{c}\right) \tag{2.91}$$

By analysing the terms it can be seen that the right hand side expresses the suspended sediment flux contribution from/to the bed, while the two terms on the left side expresses spatial changes due to erosion or deposition of suspended sediment. When $\bar{c}_e > \bar{c}$ the system is under-loaded and will try to pick up loose sediment from the bed, while if $\bar{c}_e < \bar{c}$ the system is overloaded and will deposit sediment on the bed.

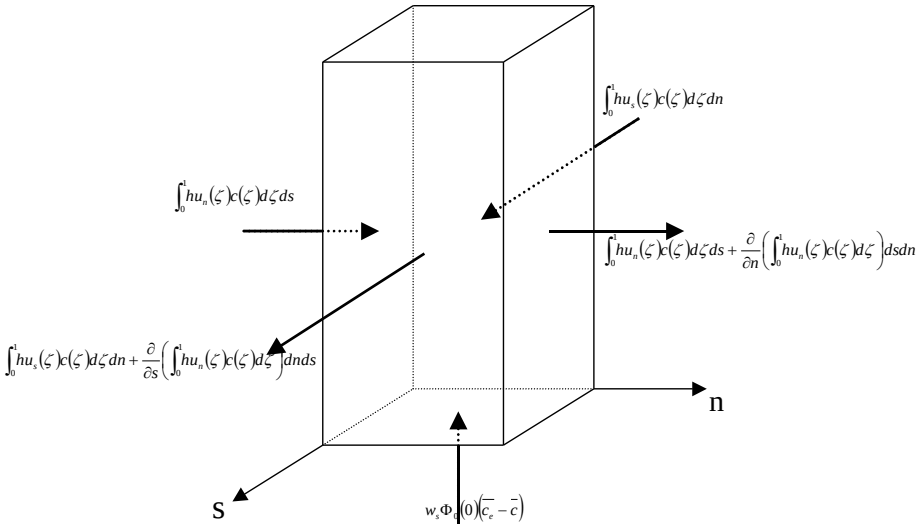

Figure 2.12 Mass balance of suspended sediment on a vertical water column

The knowledge of the vertical flux of sediment from the bed and into the water column can be used in combination with the knowledge of the vertical concentration profile and the primary and secondary velocity profile to establish a mass balance for the transport of suspended sediment. If we look at the vertical water column shown in Figure 2.12 with faces parallel to the (*s*,*n*)-coordinate system, we find that:

$$\frac{\partial\left(h\overline{c}\right)}{\partial t}dsdn + \frac{\partial}{\partial s}\left(\int_{\eta_0}^{1} hu_s(\eta)c(\eta)d\eta\right)dsdn + \frac{\partial}{\partial n}\left(\int_{\eta_0}^{1} hu_n(\eta)c(\eta)d\eta\right)dsdn = \tag{2.92}$$

$$w_s\Phi_0(\eta_0)\left(\overline{c}_e - \overline{c}\right)dsdn$$

Where the physical interpretation of the terms from the left to the right is as follows: temporal change of sediment volume in suspension, spatial variation of depth-integrated sediment fluxes across the water column, and sediment flux deposited or eroded from the bed covered by the water column.

If we insert the previously obtained expressions for the concentration profile and the mainstream and secondary velocity profile into the mass balance equation, we get the following expression:

$$\frac{\partial\left(h\overline{c}\right)}{\partial t} + \frac{\partial}{\partial s}\left(\int_{\eta_0}^{1} Vhp_1(\eta)\left[\Phi_0(\eta)\overline{c} + \Phi_1(\eta)\frac{Vh}{w_s}\frac{\partial\overline{c}}{\partial s} + \Phi_2(\eta)\frac{Vh^2}{w_sR}\frac{\partial\overline{c}}{\partial n}\right]d\eta\right) + \tag{2.93}$$

$$\frac{\partial}{\partial n}\left(\int_{\eta_0}^{1}\frac{Vh^2}{R}p_2(\eta)\left[\Phi_0(\eta)\overline{c} + \Phi_1(\eta)\frac{Vh}{w_s}\frac{\partial\overline{c}}{\partial s} + \Phi_2(\eta)\frac{Vh^2}{w_sR}\frac{\partial\overline{c}}{\partial n}\right]d\eta\right) = w_s\Phi_0(\eta_0)\left(\overline{c}_e - \overline{c}\right)$$

By introduction of the coefficients α_{ij} this mass balance can be further simplified to:

$$\frac{\partial\left(h\bar{c}\right)}{\partial t}+\frac{\partial}{\partial s}\left(\alpha_{01}Vh\bar{c}+\alpha_{11}\frac{V^2h^2}{w_s}\frac{\partial\bar{c}}{\partial s}+\alpha_{21}\frac{V^2h^3}{w_sR}\frac{\partial\bar{c}}{\partial n}\right)+$$

$$\frac{\partial}{\partial n}\left(\alpha_{02}\frac{Vh^2\bar{c}}{R}+\alpha_{12}\frac{V^2h^3}{w_sR}\frac{\partial\bar{c}}{\partial s}+\alpha_{22}\frac{V^2h^4}{w_sR^2}\frac{\partial\bar{c}}{\partial n}\right)=w_s\Phi_0\left(\eta_0\right)\left(\bar{c}_e-\bar{c}\right) \tag{2.94}$$

The coefficients α_{ij} are obtained by numerical integration of the integrals:

$$\alpha_{01}=\int_{\eta_0}^{1}\Phi_0(\eta)p_1(\eta)d\eta$$

$$\alpha_{11}=\int_{\eta_0}^{1}\Phi_1(\eta)p_1(\eta)d\eta$$

$$\alpha_{21}=\int_{\eta_0}^{1}\Phi_2(\eta)p_1(\eta)d\eta$$

$$\alpha_{02}=\int_{\eta_0}^{1}\Phi_0(\eta)p_2(\eta)d\eta$$

$$\alpha_{12}=\int_{\eta_0}^{1}\Phi_1(\eta)p_2(\eta)d\eta$$

$$\alpha_{22}=\int_{\eta_0}^{1}\Phi_2(\eta)p_2(\eta)d\eta$$

So far the analysis has mainly been carried out based on a coordinate system coinciding with the streamlines. A transformation to the general Cartesian coordinate system (see Figure 2.13) can be obtained by:

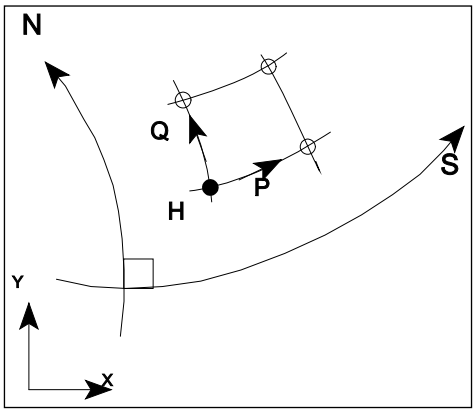

Figure 2.13 Transformation from stream wise (s,n) coordinates to fixed (x,y) coordinate system

$$\frac{\partial\bar{c}}{\partial s}=\frac{\partial\bar{c}}{\partial x}\frac{\partial x}{\partial s}+\frac{\partial\bar{c}}{\partial y}\frac{\partial y}{\partial s}=\frac{u}{V}\frac{\partial\bar{c}}{\partial x}+\frac{v}{V}\frac{\partial\bar{c}}{\partial y} \tag{2.95}$$

and

$$\frac{\partial\bar{c}}{\partial n}=\frac{\partial\bar{c}}{\partial x}\frac{\partial x}{\partial n}+\frac{\partial\bar{c}}{\partial y}\frac{\partial y}{\partial n}=-\frac{\mathrm{v}}{\mathrm{V}}\frac{\partial\bar{c}}{\partial x}+\frac{u}{V}\frac{\partial\bar{c}}{\partial y} \tag{2.96}$$

Where *u* and *v* represents the depth-averaged flow velocity in the *x* and *y* direction, respectively.

Based on these two expressions, the transport equation for the suspended sediment can now be transformed to Cartesian coordinates, which yields:

$$\frac{\partial\left(h\bar{c}\right)}{\partial t}+\frac{\partial}{\partial x}\left(\alpha_{01}uh\bar{c}\right)+\frac{\partial}{\partial y}\left(\alpha_{01}vh\bar{c}\right)+\frac{\partial}{\partial x}\left(\alpha_{11}\frac{u^2h^2}{w_s}\frac{\partial\bar{c}}{\partial x}\right)+\frac{\partial}{\partial y}\left(\alpha_{11}\frac{v^2h^2}{w_s}\frac{\partial\bar{c}}{\partial y}\right)+$$

$$\frac{\partial}{\partial x}\left(\alpha_{11}\frac{uvh^2}{w_s}\frac{\partial\bar{c}}{\partial y}\right)+\frac{\partial}{\partial y}\left(\alpha_{11}\frac{uvh^2}{w_s}\frac{\partial\bar{c}}{\partial x}\right)-\frac{\partial}{\partial x}\left(\alpha_{21}\frac{uvh^3}{w_sR}\frac{\partial\bar{c}}{\partial x}\right)+\frac{\partial}{\partial y}\left(\alpha_{21}\frac{uvh^3}{w_sR}\frac{\partial\bar{c}}{\partial y}\right)+$$

$$\frac{\partial}{\partial x}\left(\alpha_{21}\frac{u^2h^3}{w_sR}\frac{\partial\bar{c}}{\partial y}\right)-\frac{\partial}{\partial y}\left(\alpha_{21}\frac{v^2h^3}{w_sR}\frac{\partial\bar{c}}{\partial x}\right)-\frac{\partial}{\partial x}\left(\alpha_{02}\frac{vh^2}{R}\bar{c}\right)+\frac{\partial}{\partial y}\left(\alpha_{02}\frac{uh^2}{R}\bar{c}\right)- \tag{2.97}$$

$$\frac{\partial}{\partial x}\left(\alpha_{12}\frac{uvh^3}{w_sR}\frac{\partial\bar{c}}{\partial x}\right)+\frac{\partial}{\partial y}\left(\alpha_{12}\frac{uvh^3}{w_sR}\frac{\partial\bar{c}}{\partial y}\right)-\frac{\partial}{\partial x}\left(\alpha_{12}\frac{v^2h^3}{w_sR}\frac{\partial\bar{c}}{\partial y}\right)+\frac{\partial}{\partial y}\left(\alpha_{12}\frac{u^2h^3}{w_sR}\frac{\partial\bar{c}}{\partial x}\right)+$$

$$\frac{\partial}{\partial x}\left(\alpha_{22}\frac{v^2h^4}{w_sR^2}\frac{\partial\bar{c}}{\partial x}\right)+\frac{\partial}{\partial y}\left(\alpha_{22}\frac{u^2h^4}{w_sR^2}\frac{\partial\bar{c}}{\partial y}\right)-\frac{\partial}{\partial x}\left(\alpha_{22}\frac{uvh^4}{w_sR^2}\frac{\partial\bar{c}}{\partial y}\right)-\frac{\partial}{\partial y}\left(\alpha_{22}\frac{uvh^4}{w_sR^2}\frac{\partial\bar{c}}{\partial x}\right)=$$

$$w_s\Phi_0\left(\eta_0\right)\left(\bar{c}_e-\bar{c}\right)$$

This equation can be further simplified by collecting the terms and changing the formulation from velocities to fluxes. The Cartesian flux components *p* and *q* are defined by:

p = uh
q = vh

Substitution of the fluxes into the transport equation leads to:

$$\frac{\partial\left(h\bar{c}\right)}{\partial t}+\frac{\partial}{\partial x}\left(\left(\alpha_{01}p-\alpha_{02}q\frac{h}{R}\right)\bar{c}\right)+\frac{\partial}{\partial y}\left(\left(\alpha_{01}q+\alpha_{02}p\frac{h}{R}\right)\bar{c}\right)+$$

$$\frac{\partial}{\partial x}\left(\frac{1}{w_s}\left(\alpha_{11}p^2-\left(\alpha_{21}+\alpha_{12}\right)pq\frac{h}{R}+\alpha_{22}q^2\frac{h^2}{R^2}\right)\frac{\partial\bar{c}}{\partial x}\right)+$$

$$\frac{\partial}{\partial y}\left(\frac{1}{w_s}\left(\alpha_{11}q^2+\left(\alpha_{21}+\alpha_{12}\right)pq\frac{h}{R}+\alpha_{22}p^2\frac{h^2}{R^2}\right)\frac{\partial\bar{c}}{\partial y}\right)+ \tag{2.98}$$

$$\frac{\partial}{\partial x}\left(\frac{1}{w_s}\left(\alpha_{11}pq+\left(\alpha_{21}p^2-\alpha_{12}q^2\right)\frac{h}{R}-\alpha_{22}pq\frac{h^2}{R^2}\right)\frac{\partial\bar{c}}{\partial y}\right)+$$

$$\frac{\partial}{\partial y}\left(\frac{1}{w_s}\left(\alpha_{11}pq-\left(\alpha_{21}q^2-\alpha_{12}p^2\right)\frac{h}{R}-\alpha_{22}pq\frac{h^2}{R^2}\right)\frac{\partial\bar{c}}{\partial x}\right)$$
$$=w_s\Phi_0\left(\eta_0\right)\left(\bar{c}_e-\bar{c}\right)$$

Even though the transport equation looks complicated, it is in reality a standard advection-dispersion equation for the transport of sediment containing terms for temporal change, advection, dispersion, and source or sink. The complexity of the terms is only a result of taking the variation of the vertical concentration profile and the primary and secondary flow velocity distribution into account.

If we define the modified fluxes:

$$p_{\mathrm{mod}} = \alpha_{01} p - \alpha_{02} q \frac{h}{R}$$

$$q_{\mathrm{mod}} = \alpha_{01} q + \alpha_{02} p \frac{h}{R} \tag{2.99}$$

and the dispersion coefficients:

$$k_{xx} = -\frac{1}{h w_s}\left(\alpha_{11} p^2 - (\alpha_{12} + \alpha_{21}) pq \frac{h}{R} + \alpha_{22} q^2 \frac{h^2}{R^2}\right)$$

$$k_{yy} = -\frac{1}{h w_s}\left(\alpha_{11} q^2 + (\alpha_{12} + \alpha_{21}) pq \frac{h}{R} + \alpha_{22} p^2 \frac{h^2}{R^2}\right)$$

$$k_{xy} = -\frac{1}{h w_s}\left(\alpha_{11} pq + (\alpha_{12} q^2 + \alpha_{21} p^2)\frac{h}{R} - \alpha_{22} pq \frac{h^2}{R^2}\right) \tag{2.100}$$

$$k_{yx} = -\frac{1}{h w_s}\left(\alpha_{11} pq - (\alpha_{12} p^2 - \alpha_{21} q^2)\frac{h}{R} - \alpha_{22} pq \frac{h^2}{R^2}\right)$$

The transport equation can be rewritten as:

$$\frac{\partial\left(h\bar{c}\right)}{\partial t}+\frac{\partial\left(p_{\mathrm{mod}}\bar{c}\right)}{\partial x}+\frac{\partial\left(q_{\mathrm{mod}}\bar{c}\right)}{\partial y}-\frac{\partial}{\partial x}\left(k_{xx}h\frac{\partial\bar{c}}{\partial x}\right)-\frac{\partial}{\partial y}\left(k_{yy}h\frac{\partial\bar{c}}{\partial y}\right)$$
$$-\frac{\partial}{\partial x}\left(k_{xy}h\frac{\partial\bar{c}}{\partial y}\right)-\frac{\partial}{\partial y}\left(k_{yx}h\frac{\partial\bar{c}}{\partial x}\right)=w_s\Phi_0\left(\eta_0\right)\left(\bar{c}_e-\bar{c}\right) \quad (2.101)$$

From the expressions for the dispersion coefficients it is seen that dispersion is anisotropic. Furthermore, it is seen that the advective transport is controlled by a modified flux field, which is different due to the inclusion of pseudo three-dimensional effects.

2.3.3 Sediment transport formulae

Sediment transport capacity in uniform shear flow has been extensively investigated over the years. For instance, reviews are given in Vanoni (1984). This section discusses the sediment transport formulas used for calculation of bed load and suspended load transport capacity (equilibrium concentration at the riverbed), which are implemented in the present modelling system.

The following symbols are applied.

Symbols

S_{bl}	Bed load	<m²/s>
k_b	Bed load calibration factor	< - >
S_{sl}	Suspended load	<m²/s>
k_s	Suspended load calibration factor	< - >
s	Relative density of the sediment	< - >
S_{tl}	Total load	<m²/s>
c_e	Equilibrium mass concentration	<g/m³>
C	Chezy number	<m½/s>
V	Velocity	<m/s>

All sediment transport formulas described herein exclude the effect of riverbed porosity, which is included in the continuity equation for update of bed level instead.

Some of the formulas only predict total load (bed load + suspended load), whereas information about both bed load and suspended load is required. The total load formulas can still be applied by using the calibration factors k_b and k_s for bed load and suspended load, respectively, in order to differentiate between the two modes of transport. Assume for instance a total load formula. By specifying $k_b = 0.1$ and $k_s = 0.9$, it is understood that 10% of the transport takes place as bed load.

Due to the non-uniform vertical distribution of the suspended sediment concentration, the effective fall height of grains will be different from the mean fall height $h/2$ (where h is water depth). For a uniform vertical concentration profile, the time scale for settling is defined as h/w_s (w_s is the settling velocity). With information about the Rouse number Z, the actual concentration profile can be predicted and therefore a better estimate for the settling time scale t_s can be obtained if using the height of the centroid. However, the time scale effect on the settling has already been included in the modelling using the described profile functions, and the $\Phi(\eta_0)$ factor on the sink/source term in the advection-dispersion equation for the concentration of the suspended sediment.

The Shields parameter θ is defined as:

$$\theta = \frac{\tau}{\rho g (s-1) d_{50}} \tag{2.102}$$

Where

τ	The flow shear stress
ρ	Density of water, approx. 1000 kg/m^3
g	Acceleration of gravity, 9.81 m/s^2
s	ρ/ρ_s relative density of the sediment
ρ_s	Density of sediment, for quartz sand 2650 kg/m^3

Flow shear stress is divided into form drag τ'' and skin friction τ'. The total shear stress $\tau = \tau' + \tau''$ is estimated from the local flow velocity u and the local Chezy number C:

$$\tau = \rho g \frac{V^2}{C^2} \tag{2.103}$$

For skin friction the following approximate friction formula (Engelund & Hansen, 1967) is applied unless otherwise calculated (i.e. in the model of van Rijn or the model of Engelund and Fredsøe, where more sophisticated models are used to describe the physical processes):

$$\theta' = 0.06 + 0.4 \cdot \theta^2 \tag{2.104}$$

The non-dimensional sediment transport rate is defined as:

$$\Phi = \frac{S}{\sqrt{(s-1) g d^3}} \tag{2.105}$$

Where

S	Sediment transport (bed load, total or suspended load)
d	Characteristic grain size
Φ	Non-dimensional sediment transport

Engelund and Hansen model

The model by Engelund and Hansen (1967) is a total load model that needs user-specified information in order to divide the sediment transport into bed load and suspended load. The transport rates are obtained from the relations:

$$S_{bl} = k_b \cdot S_{tl}$$
$$S_{sl} = k_s \cdot S_{tl} \tag{2.106}$$

Where the total sediment transport is obtained by:

$$S_{tl} = 0.05 \frac{C^2}{g} \theta^{\frac{5}{2}} \sqrt{(s-1) g d_{50}^3} \tag{2.107}$$

The equilibrium concentration is simply specified as the suspended load divided by the water flux and converted from volumetric concentration to mass concentration:

$$c_e = \frac{S_{sl}}{V \cdot h} \cdot s \cdot 10^6 \tag{2.108}$$

Van-Rijn model

Van-Rijn (1984) proposed the following models for sediment transport of bed load and suspended load:

$$S_{bl} = 0.053 \frac{T^{2.1}}{D_*^{0.3}} \sqrt{(s-1) g \cdot d_{50}^{\ 3}} \tag{2.109}$$

Where T is the non-dimensional transport stage parameter and given by:

$$T = \left(\frac{u_{f'}}{u_{fc}} \right)^2 - 1 \tag{2.110}$$

The critical friction velocity $u_{f,c}$ is determined as:

$$u_{fc} = \sqrt{\theta_c (s-1) g \, d_{50}} \tag{2.111}$$

The effective friction velocity is estimated from:

$$u'_f = V \frac{\sqrt{g}}{C'} \tag{2.112}$$

Where the resistance (Chezy number) originating from skin friction is based on a logarithmic velocity profile assuming a certain bed roughness:

$$C' = 18 \log \left(\frac{4h}{d_{90}} \right) \tag{2.113}$$

The non-dimensional particle parameter D_* in the van Rijn bed load transport formula is defined as:

$$D_* = d_{50} \left(\frac{(s-1) g}{\nu^2} \right)^{\frac{1}{3}} \tag{2.114}$$

Where ν, is the kinematic viscosity and approximately equal to 10^{-6} m^2/s for water.

Instead of using a constant critical Shields parameter θ_c (approximately equal to 0.06), van Rijn assumes the following variation as a function of D_*, see Table 2.1.

Table 2.1 Relations for determination of critical Shields stress

Range of D_*	θ_c
$D_* < 4$	$0.24/D_*$
$4 < D_* < 10$	$0.14D_*^{-0.64}$
$10 < D_* < 20$	$0.04D_*^{-0.1}$
$20 < D_* < 150$	$0.013D_*^{0.29}$
$D_* > 150$	0.055

Suspended sediment transport occurs only if one of the following criteria is satisfied:

$$u_f > \frac{4w_s}{D_*} \quad \text{for} \quad D_* < 10 \tag{2.115}$$

$$u_f > 0.4w_s \quad \text{for} \quad D_* > 10 \tag{2.116}$$

The reference level, at which the bed concentration is determined, is expressed as:

$$a = \max\begin{pmatrix} 0.01h \\ 2\,d_{50} \end{pmatrix} \tag{2.117}$$

The volumetric bed concentration is obtained from the relation:

$$c_a = 0.015 \cdot \frac{d_{50}\,T^{1.5}}{a\,D_*^{0.3}} \tag{2.118}$$

In Figure 2.14 the reference level and the bed concentration are sketched.

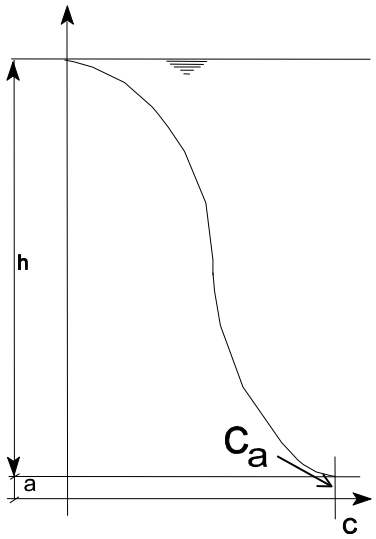

Figure 2.14 Definition of the reference level a for the bed concentration C_a

A correction coefficient, denoted β is applied to the hydrodynamic diffusion coefficient in order to transform the coefficient into a diffusion coefficient for the suspended sediment:

$$\beta = 1 + 2\left(\frac{w_s}{u_f}\right)^2 \tag{2.119}$$

Van Rijn defines a correction factor φ for the concentration profile, which is determined by:

$$\varphi = \frac{5}{2}\left(\frac{w_s}{u_f}\right)^{0.8}\left(\frac{c_a}{c_o}\right)^{0.4} \tag{2.120}$$

Where c_o (if expressed as volumetric concentration) is the concentration corresponding to firm packing of the sediment, i.e.:

$$c_o = 0.65\frac{m^3}{m^3} \tag{2.121}$$

When applying the correction coefficients defined above, a Rouse suspension parameter Z can be obtained by:

$$Z = \frac{w_s}{\beta\kappa u_f} + \varphi \tag{2.122}$$

Finally, the depth-integrated transport of suspended load is computed as:

$$S_{sl} = f \cdot c_a \cdot V \cdot h \tag{2.123}$$

Where the correction factor for suspended load is obtained from:

$$f = \frac{\left(\frac{a}{h}\right)^Z - \left(\frac{a}{h}\right)^{1.2}}{\left(1 - \frac{a}{h}\right)^Z (1.2 - Z)} \tag{2.124}$$

The equilibrium concentration c_e is calculated from the approximation formulas given in Table 2.2 below:

Table 2.2 Polynomial approximations for determination of the equilibrium concentration

Condition	Corresponding value of C_e and h_*
$Z \leq 1$	$c_e = c_a$[[(2.21Z - 6.41)Z + 7.21)Z - 3.95]Z + 0.97]
$1 \leq Z \leq 3$	$c_e = c_a$ [[(0.007Z – 0.06)Z + 0.220)Z - 0.347]Z + 0.22]
$Z > 3$	$c_e = c_a$ [[(4·10-6 Z - 1.2·10-4)Z + 1.4·10-3)Z - 7.67·10-3]Z + 0.018]

Engelund and Fredsøe model

The probability of a moving sediment grain can, according to Engelund and Fredsøe (1976), be determined by the expression:

$$p = \left[1 + \left(\frac{\frac{\pi}{6}\mu_d}{\theta' - \theta_c} \right)^4 \right]^{-\frac{1}{4}} \quad , \theta' > \theta_c \tag{2.125}$$

The dynamic friction coefficient μ_d is assumed to be equal to μ_d = 0.51 = tan27°. The non-dimensional skin shear stress is defined by:

$$\theta' = \frac{u_f'^{\,2}}{(s-1)\, g\, d_{50}} \tag{2.126}$$

Where the friction velocity related to skin friction is calculated from the assumption of a logarithmic velocity profile:

$$u_f' = \frac{V}{6 + 2.5 \ln\left(\frac{h}{2.5 d_{50}} \right)} \tag{2.127}$$

The bed load transport rate is estimated from:

$$S_{bl} = 5\, p \cdot (\sqrt{\theta'} - 0.7\sqrt{\theta_c})\sqrt{(s-1)\, g\, d_{50}^3} \tag{2.128}$$

The reference concentration near the bed is calculated from an empirical relation obtained by Zyserman and Fredsøe (1994):

$$c_b = \frac{0.331(\theta - \theta_c)^{1.75}}{1 + \frac{0.331}{0.46}(\theta - \theta_c)^{1.75}} \tag{2.129}$$

The empirical relation was established from analysis of the experimental data sets of Guy et al. (1966) and covers a range from pure bed load to dominant suspended transport. The influence of lateral bed slope is included in the relation through a reduced critical Shields stress for onset of motion.

Numerical integration is performed along a logarithmic vertical scale, because a greater density of computational points is required close to the bottom, where the largest velocity gradients occur. The non-dimensional vertical coordinate is obtained from the relation:

$$\eta_j = \eta_{j-1} + \Delta \cdot 1.06^{j-1} \tag{2.130}$$

Where the step height Δ is determined by:

$$\Delta = \frac{1}{\left(\frac{1 - 1.06^{99}}{1 - 1.06} \right) - 1} \tag{2.131}$$

Due to the specific value of the exponent, it is seen that the depth is divided into 99 segments. The velocity profile is assumed to be:

$$u(\eta) = \frac{\sqrt{g}}{0.4C} \ln\left(\frac{\eta}{\eta_0}\right) \tag{2.132}$$

Where the no-slip level η_0, is obtained from:

$$\eta_o = \exp\left(\eta_o - 1 - \frac{0.4\,C}{\sqrt{g}}\right) \tag{2.133}$$

and solved by iteration.

The normalised vertical concentration profile is specified in the following way:

$$c(\eta) = \left(\frac{1-\eta}{\eta} \cdot \frac{a}{1-a}\right)^Z \tag{2.134}$$

Where the reference level a, is defined by:

$$a = \frac{2 \cdot d_{50}}{h} \tag{2.135}$$

The Rouse suspension parameter Z, is defined as:

$$Z = \frac{w_s}{\kappa u_f} \tag{2.136}$$

The suspended load transport rate S_{sl}, is obtained from:

$$S_{sl} = c_b V h \cdot \int_{\eta_0}^{1} u(\eta) \cdot c(\eta) d\eta \tag{2.137}$$

The equilibrium mass concentration c_e, is determined from:

$$c_e = \frac{S_{sl}}{V h} s \cdot 10^6 \tag{2.138}$$

Meyer-Peter and Müller model

The Meyer-Peter and Müller model (1948) relates the non-dimensional bed load transport Φ to the dimensionless shear stress acting on the grains through the relation:

$$\Phi_{bl} = 8(\theta' - \theta_c)^{1.5} \tag{2.139}$$

or expressed as a transport rate:

$$S_{bl} = 8(\theta' - \theta_c)^{1.5}\sqrt{(s-1)gd_{50}^3} \tag{2.140}$$

Where θ' is the part of the Shields stress related to skin friction. The relation is only valid for fluvial systems with dominating bed load and slopes ranging from 0.0004 to 0.02.

2.4 Multi-fraction Sediment Transport

The above version of MIKE 21 FM Sand Transport (ST) model allows a single set of sediment characteristics (i.e. a single fraction) and a single bed layer. This means that important transport processes such as bed armouring by coarser fractions and stratification of the subsurface bed cannot be described by the model; thus limiting the applicability of the model to locations where such effects are not important.
In many places these effects are important and therefore a multi-fraction, multi-bed layer sand transport model has been developed. The new model combines a transport formulation by Wilcock and Crowe (2003) for sand and gravel mixture with a multi-layered model for bed-stratification.
The following explains the theoretical background of the multi-fraction sand transport formulation (Wilcock and Crowe, 2003), and how it has been implemented in MIKE 21 FM framework. Validation cases are conducted to illustrate the capabilities of the new model.

2.4.1 Background

The single-fraction model is capable of calculating the transport capacity (or transport rate) based on simulated hydrodynamic condition and given sediment properties (e.g. relative density, grain size and bed thickness), and updating the morphology with optional feedback to the hydrodynamics. The single-fraction model only calculates the transport potential based on a given initial sediment bed condition. The single bed layer description put a constraint on describing the continuous sorting process within the sediment bed. As soon as the finer sediments are being transported away, the local sediment composition becomes coarser, which reduces the transport rate because the coarser sediments act as shelters for the finer parts. This phenomenon is called “bed armouring effect”. Thus, for a natural graded sediment bed subjected to erosion, the transport rate may eventually decrease to zero if there is no supply of new sediment, leaving only coarse material on the bed, effectively armouring the bed and the sediment beneath it from further transport. On the other hand, if a sediment bed is subjected to accretion, the newly deposited sediments will form the new surface layer and directly affect the local transport rate. Therefore, to describe the transport phenomenon more precisely, more than one bed layer is necessary to resolve the vertical bed stratification.
Apart from the bed layer, the single-fraction model describes the sediment properties using only one fraction, which is characterized by a constant grain size d_{50} and geometric spreading factor σ. To incorporate the bed armouring effect, the sediment composition needs to be updated in a transient manner. One way is to allow the updates of d_{50} and σ. However, to avoid making assumptions on the shape of sediment distributions, the multi-fraction model describes the sediment composition discretely by allowing multiple

fractions, each of which is represented by a unique grain size. The composition is dynamically updated and book-kept for all fractions in all bed layers. This approach is similar to the one used MIKE 21 FM Mud Transport model to describe cohesive sediment transport.

2.4.2 Transport Formulation for Mixed-Size Sediment

With the new multi-bed layer and multi-faction features, the transient armouring effect and transport rate are described by implementing Wilcock and Crowe (2003)'s surface-based transport formulation for mixed-size sediment. As shown in Figure 2.15, the normalized critical/reference bed shear stress of sediment motion is plotted against the normalized sediment sizes. The diagonal line represents Shields relationship for non-cohesive sediment, along which the reference shear stress increases linearly with the sediment size in a log-log scale. The experiments conducted by Wilcock and Crowe (2003) reveal that in a sediment mixture, the coarse sediments act as shelters for finer sediments, while the finer ones act as lubricants to the coarser parts. This leads to the deviation between the actual data and the Shields relationship; i.e. a larger critical shear stress for the sediment fractions with a grain size smaller than the mean grain size and smaller critical shear stress for the sediment fractions with a grain size larger than the mean grain size.

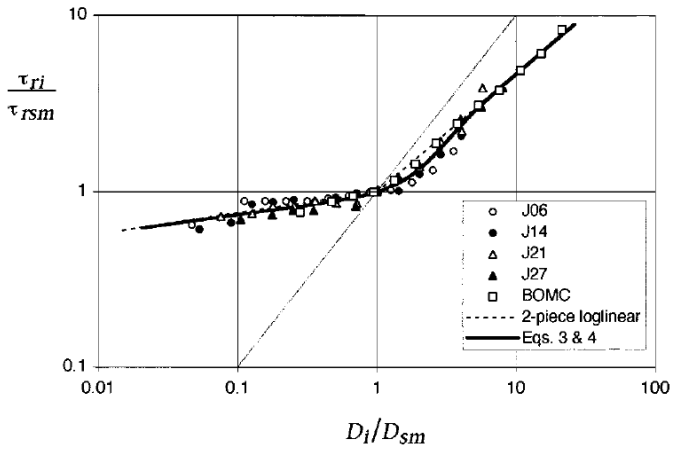

Figure 2.15 Normalized reference bed shear stress of erosion vs. normalized sediment size; Figure 4 of Wilcock and Crowe (2003)

Wilcock and Crowe established an empirical correlation based on laboratory experiments on sand (0.5 to 2.0 mm) and gravel (2.0 to 64 mm) mixture with a range of sand contents (from 6.2% to 34.3%). It is described as a hiding function defined in Eq. (2.141):

$$\frac{\tau_{ri}}{\tau_{rsm}} = \left(\frac{D_i}{D_{sm}}\right)^b \tag{2.141}$$

with

$$b = \frac{0.67}{1 + e^{\left(1.5 - \frac{D_i}{D_{sm}}\right)}} \tag{2.142}$$

$$\tau_{rsm} = (0.021 + 0.015e^{-20F_s}) \cdot (s-1)\rho_a g \tag{2.143}$$

where,

- b is an empirical parameter from curve fitting
- D_i is the grain size of fraction i
- D_{sm} is the geometric mean grain of bed surface
- F_s is the proportion of sand in bed surface
- s is the relative density of sediment
- ρ_a is the density of ambient water
- g is the gravitational acceleration

The ratio between the reference shear stress of each sediment size/fraction (τ_{ri}) and the reference shear stress of mean size of bed surface (τ_{rsm}) is correlated with the size ratio through a power-law relationship. Wilcock and Crowe (2003) also found that τ_{rsm} generally decreased with the sand fraction (F_s) and tended to reach a constant value (0.021) when F_s was large (refer to Eq. (2.143)). Although only tested up to F_s = 34.4%, Wilcock and Crowe (2003) suggested that Eq. (2.143) is likely to be valid for even larger sand fraction based on analysis of additional laboratory and field transport data (Wilcock 1998, Wilcock and Kenworthy 2002).

Therefore, with knowledge of the surface sediment composition, the reference shear stress (τ_{ri}) for each sediment fraction can be calculated through Eq. (2.141). The fractional transport rate can then be calculated based on the following empirical relationship Eq. (2.144), as visualized in Figure 2.16.

$$W_i^* = \begin{cases} 0.002\phi^{7.5} & for\ \phi < 1.35 \\ 14\left(1 - \frac{0.894}{\phi^{0.5}}\right)^{4.5} & for\ \phi \geq 1.35 \end{cases} \quad (2.144)$$

With

$$W_i^* = \frac{(s-1)gq_{bi}}{F_i u_*^3} \quad (2.145)$$

where,

- W_i^* is the dimensionless transport rate of fraction i
- $\phi = \tau/\tau_{ri}$ is a staging parameter (or normalized bed shear stress)
- τ is the bed shear stress
- q_{bi} is the transport rate of fraction i per unit width
- F_i is the proportion of fraction i in bed surface
- $u_* = \sqrt{\tau/\rho}$ is the shear velocity

Thus, the fractional transport rate can be calculated from Eqs. (2.141) to (2.145). Kwan (2009) implemented Wilcock and Crowe (2003)'s formulation in a coupled hydrodynamics and sand transport model, and highlighted that Eq. (2.144) is simply the best fit of all available data (in Figure 2.16) and the variation in transport rate can be as large as two to three orders of magnitude. Thus, Kwan (2009) introduced a scaling factor (k_T = 0.1 to 10) to the calculated transport rate from Eq. (2.144). The same scaling factor is implemented in the present model as a calibration parameter.

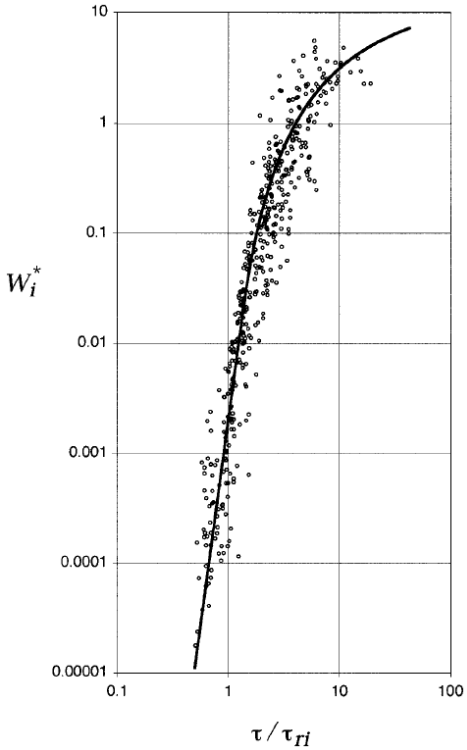

Figure 2.16 Normalized transport rate vs. normalized bed shear stress; Figure 6 of Wilcock and Crowe (2003)

2.4.3 Bed Stratification Model

To resolve bed armouring effects, at least two bed layers are necessary to allow vertical exchange and sorting of grain size composition. Kwan (2009) implemented the vertical sorting process by defining an active surface layer with a constant thickness, and a substrate layer with a varying thickness during erosion and accretion. The concept is illustrated using the schematics below in Figure 2.17 which represents a typical condition of accretion, i.e. the net sediment flux into the element is positive. With the surface layer thickness assumed as a constant L_s, newly deposited sediment will form part of the surface layer, and an equivalent portion of the existing surface layer will join the substrate layer. On the contrary during erosion, part of the substrate layer will be exposed and join the surface layer as illustrated in Figure 2.18. Eventually, after most fine sediments are eroded away, the surface layer is filled up by coarser sediments, limiting the sediment transport and thereby armouring the bed.

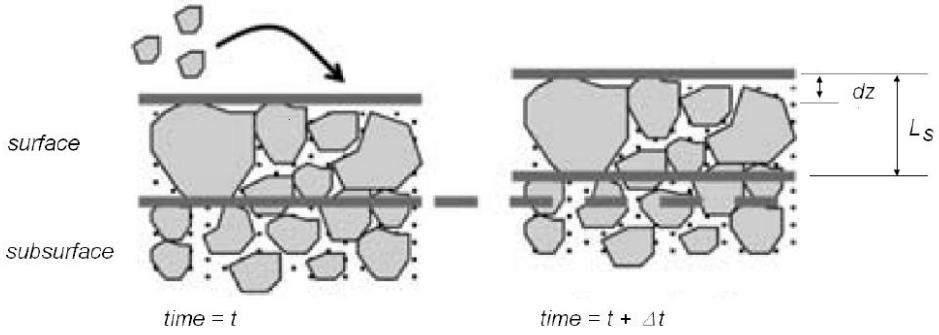

Figure 2.17 Conceptual model during accretion. The bed load mixes with the surface layer to form a new grain size distribution. The surface layer thickness is assumed to be a constant thickness L_s; Figure 23 of Kwan (2009).

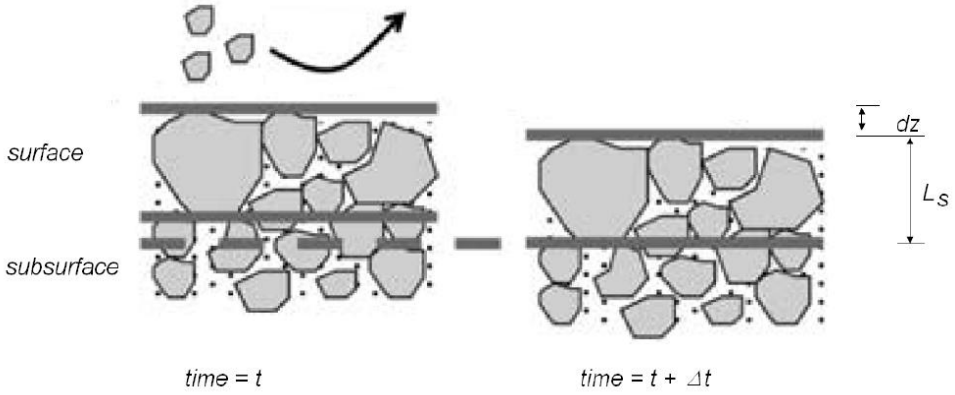

Figure 2.18 Conceptual model during erosion. The surface layer mixes with the sub-surface layer to form a new grain size distribution. The surface layer thickness is assumed to be a constant thickness L_s; Figure 24 of Kwan (2009).

Kwan (2009) provided a clear demonstration on the feasibility and procedures to book-keep the sediment exchange between two bed layers. The main limitation is the assumption of a single well-mixed substrate layer. This is not critical for areas with either pure accretion or pure erosion. However, for areas with frequent switch between the two transport modes, one substrate layer is insufficient to describe the vertical bed stratification. This shortcoming is illustrated using schematics comparing two-layer with three-layer systems, as shown in Figure 2.19. At time = t_0, the sediment bed is divided into surface and substrate layers. Assuming there is accretion during this time, the surface layer will receive the additional sediment (as marked in yellow colour) and update its composition. With the surface layer being assumed to have a constant thickness (or equivalently constant mass if the sediment density and porosity are assumed to be similar), the extra sediment will be transferred into the substrate layer(s). As illustrated by the top branch of Figure 2.19, within a two-layer system, the extra sediment transferred downwards becomes well-mixed within the only substrate layer (at time = t_1). Thus, during the following erosion process, a portion of the mixed substrate layer is supplied back to the surface layer to maintain its constant thickness (time = t_2), and the composition within substrate layer remains the same as time = t_1. In contrast, if a three-layer system is utilized as illustrated in the bottom branch of Figure 2.19, the extra sediment after accretion process will be book-kept as a new substrate layer (labelled as “Substrate 1”), with the “Substrate 2” layer below unchanged. During the subsequently erosion, only the sediments in “Substrate 1” layer is suppled back to the surface layer and suppressed. By comparing the end states at time = t_2, it is clear that artificial vertical mixing can be alleviated by introducing more bed layers during the book-keeping. Depending on the targeted level of details, the new multi-fraction ST model provides the flexibility of defining an arbitrary number of substrate bed layers.

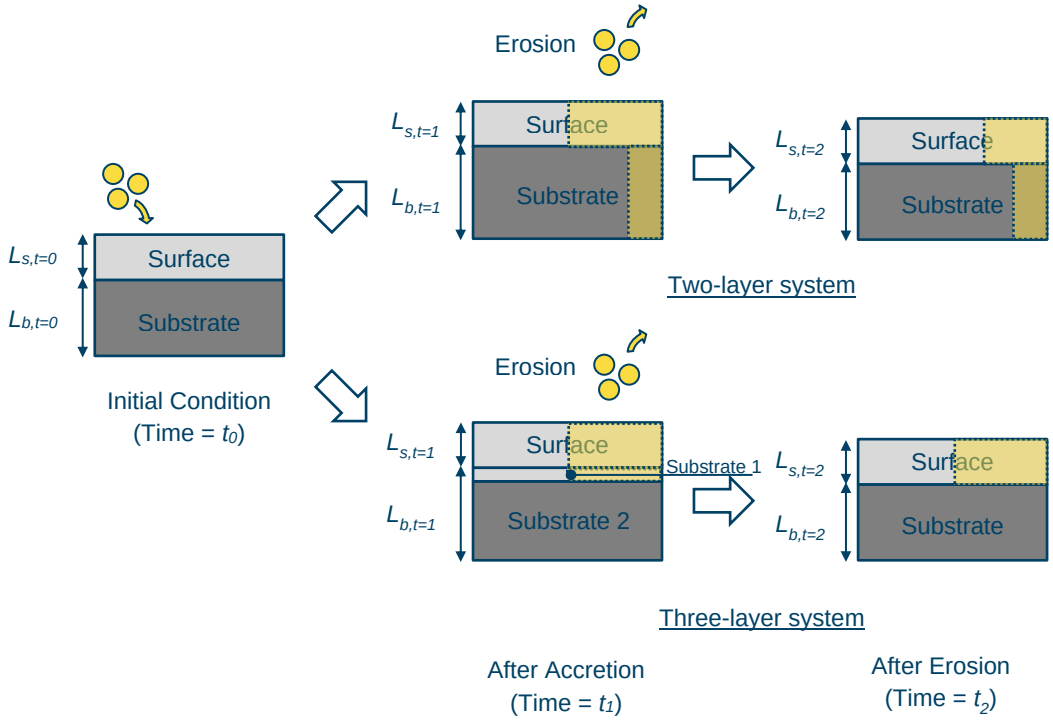

Figure 2.19 Schematic of book-keeping systems: two-layer vs. three-layer (top vs. bottom). All sediments are assumed to have the same physical properties.

2.4.4 General Work-Flow

The Implementation of the multi-fraction formulation is illustrated by a flow chart as shown in Figure 2.20. At each computational time step, the flow field is solved in the hydrodynamic model, and used to derive the instantaneous bed shear stress. To determine the transport rate for each sediment fraction in the surface layer, the percentage of sand in the surface layer (F_s) (defined as sediment with grain size < 2mm) is first determined, and then Eqs. (2.141) to (2.145) are utilized in a sequence as shown inside the dashed rectangular box. After all the fractional transport rates have been determined, the bed thicknesses for all fractions and all bed layers are updated according to mass conservation.

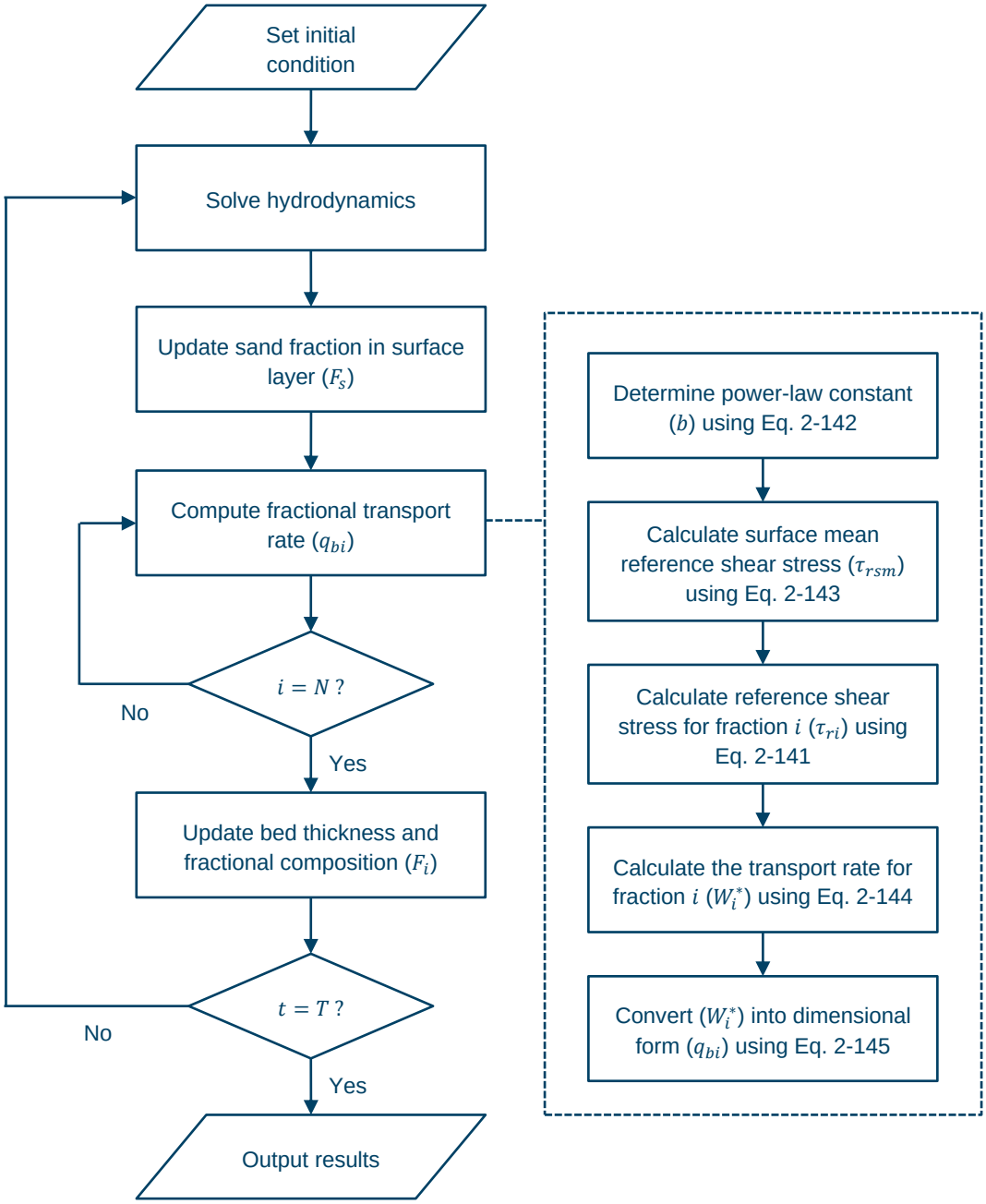

Figure 2.20 Work-flow of non-capacity model implementation (steps for computing fractional transport rate are described in the dashed box on the right-hand-side).

3 Combined Wave and Current

3.1 Introduction

For the case of combined current and waves (coastal application) sediment transport rates are derived by linear interpolation in a sediment transport table. The values in the table are calculated by the MIKE 21 Toolbox utility program 'Generation of Q3D Sediment table'. The core of this utility program is a quasi three-dimensional sediment transport model (STPQ3D).

The model (STPQ3D) calculates instantaneous and time-averaged hydrodynamics and sediment transport in two horizontal directions. As the model calculates the bed load and suspended load separately, the values in the sediment transport table are total load.

The essence of the Quasi-3D hydrodynamics model is the solution of the force balance across the water column

$$\tau = \rho \nu_t \left| \frac{\partial \overline{U}}{\partial z} \right| \tag{3.1}$$

from which the time averaged flow velocity $\overline{U}$ is found by integration.

The temporal and vertical variations of shear stress, turbulence, flow velocity and sediment concentrations are resolved. The time evolution of the boundary layer due to combined wave/current motion is solved by means of the integrated momentum approach of Fredsøe (1984). The force balance includes contributions from the near bed wave orbital motion, forces associated with wave breaking (gradients of radiation stresses) and the sloping water surface.

In the following the different aspects of the STPQ3D model are described.

3.2 Hydrodynamics

3.2.1 Mean flow

Prior to the sediment transport calculations the hydrodynamic flow conditions must be calculated. The mean horizontal velocity component is input parameter to the model. For two-dimensional flow this value is defined as the depth-averaged current velocity and for three-dimensional flow the value can be calculated on basis of either the 3D flow field or from the bottom stress value. The pre-defined mean discharge is obtained by superposing the wave motion by a steady current driven by a gradient in the water surface elevation and solving the turbulent boundary layer for the combined wave/current motion. The interaction of the undertow, the longshore current and the waves are automatically taken into account. The wave induced mass transport and the discharge in the surface rollers are included in the calculation of the mean flow. The gradients in the water surface elevations in the x and y directions are not known beforehand and are found through iteration to obtain the prescribed fluxes.

The time-averaged flow velocity distribution is calculated from the vertical distribution of the driving forces and the mean eddy viscosity. By using the no slip condition at the bed, the mean velocity profile is solved by integrating Eq.(3.1).

Figure 3.1 shows an example of the time varying velocity profiles across the vertical in the current direction.

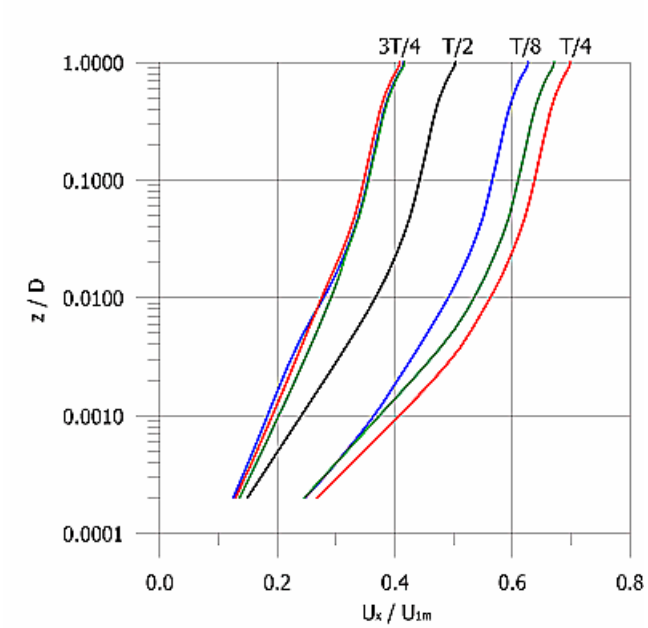

Figure 3.1 Example of velocity profiles in the current direction during one wave period. Test conditions are: Cnoidal 5th order wave theory, H_{rms}=1.0 m, T_z=6 s, Angle=10 deg., D=2 m, V=0.5 m/s. No wave breaking

Figure 3.2 shows the corresponding velocity profiles perpendicular to the current direction.

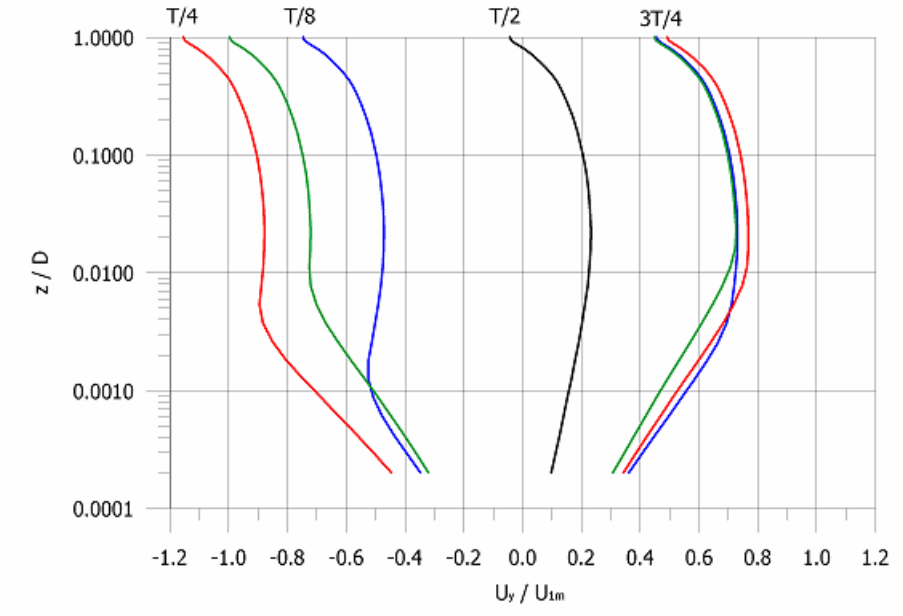

Figure 3.2 Example of velocity profiles perpendicular to the current direction during one wave period. Test conditions as in Figure 3.1

3.2.2 Wave motion

In the model, the wave motion is defined through a number of general wave parameters such as wave height H (or H_{rms}), wave period T (or T_z) and angle of incidence α (or MWD). The values in parentheses refer to an irregular wave description.

In shallow water the wave motion becomes non-linear, e.g. the velocities under the wave crest are higher than under the wave trough. This phenomenon is very important in the calculation of cross-shore sediment transport. The time varying water surface and orbital velocities can be calculated from various wave theories.

The wave motion outside the boundary layer is assumed to be inviscid (potential flow). In order to fulfil the requirements of potential theory, the mean bed shear stress due to the wave motion must be zero for pure oscillatory flow. In case of progressive waves, a small but significant mean bed shear stress occurs due to the non-uniformity of the wave boundary layer.

In the model, a small additional constant velocity is added to the wave orbital motion. This velocity is not known beforehand, but must be found by iteration, such that the mean bed shear stress, calculated from the turbulent boundary layer model, corresponds to the pre-defined value. The concept of the additional potential velocity is described in Brøker (1985).

In case of breaking waves, energy is extracted from the organized wave motion and is converted into turbulence. The turbulent energy generated at the water surface is transported downwards into the water column. The amount of turbulence produced at the water surface is calculated from general wave parameters such as wave height and period and the water depth. The production of energy can be calculated according to a regular or an irregular wave description.

Near bed orbital velocities

The wave motion outside the bottom boundary layer can be calculated from a number of wave theories. Both classical wave theories as well as semi-empirical theories are available.

The use of non-linear wave theory is important to resolve higher order velocity moments (skewness, asymmetry), which are important for sediment transport. Unfortunately, no wave theory exists today that covers all hydrodynamic conditions satisfactorily. Therefore, a number of the existing ones are included in the model. Each of them is valid in a limited range of hydrodynamic conditions.

The available wave theories and their area of application are listed below.

Classic theories:

- Stokes theory 1st, 3rd and 5th Order (Fenton 1985).
  Deep water/ Non-breaking waves
- Cnoidal theory (1st, 3rd and 5th Order (Fenton 1990).
  Shallow water/ Non-breaking waves
- Vocoidal theory (Swart 1982).
  All water depths/Non breaking waves

Semi-empirical theories:

- Isobe and Horikawa (1982).
  All water depths/Breaking and Non-breaking waves

- Doering and Bowen (1995).
  All water depths/Breaking and Non-breaking waves

Detailed descriptions of the wave theories can be found in the referred literature. Figure 3.3 shows an example of the near bed velocity, u_0, during a wave period.

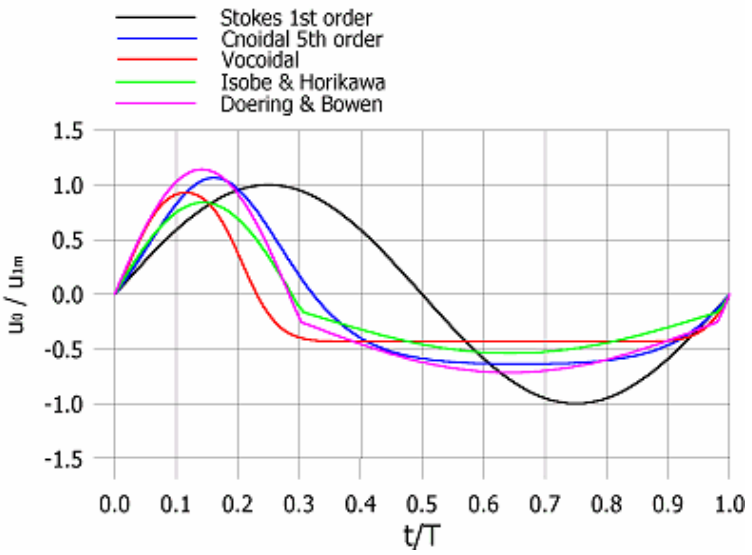

Figure 3.3 Example of near bed velocity u_0 for 5 different wave theories

The terms 'shallow' and 'deep' water refer to the Ursell number, U_s, which is defined as:

$$U_s = \frac{HL^2}{D^3} \tag{3.2}$$

Where is the wave height, L is the wave length and D is the water depth.

Deep water corresponds to $U_s < 25$, shallow water corresponds to $U_s > 25$.

Stokes' and Cnoidal wave theories descriptions of orbital velocities can be used for $U_s < 25$ and $U_s > 25$, respectively. In the model an option is available that automatically applies either Stokes' or Cnoidal wave theory, according to the above mentioned validity range. In some cases it is desirable to use linear wave theory regardless of the Ursell number. The model also provides an option for this.

Vocoidal wave theory has the advantage that it is applicable in all water depths, which means that the same theory is used in both deep and shallow water.

The model of Isobe and Horikawa (1982) includes the effect of the bed slope on the time varying orbital velocity. The model is semi-empirical and has not been tested for applications including breaking and broken waves.

The model of Doering and Bowen (1995) relates the skewness of the wave orbital motion to general wave parameters (H,T,D), but does not describe time varying near bed orbital velocities. The description of velocity skewness is valid for both breaking and non-

breaking waves. In order to calculate the velocity variation, the semi-empirical description of Isobe and Horikawa (1982) is used in the model, where the ratio between the maximum velocities at wave crest and wave trough are found by iteration such that the skewness of the velocity distribution corresponds to the model of Doering and Bowen (1995).

Mass transport

For progressive waves a net mass transport (drift) occurs between the wave trough and the wave crest (Eulerian definition). Under uniform conditions in the longshore direction the net cross-shore discharge must be zero. The mass flux is calculated from the applied wave theory. For the semi-empirical wave theories the mass flux is estimated by using linear wave theory, as no descriptions of mass flux exist for these wave theories.

The mass transport can be included or excluded from the calculation when generating the sediment transport table.

Surface roller area

In case of breaking waves a surface roller is present at the water surface. The mass flux in the surface roller and the shear stress exerted on the water surface by the roller are important in the calculation of the undertow. In the present model the surface roller area is calculated according to the model of Dally and Brown (1995), in which the surface roller area *A* is related to the energy dissipation through:

$$\rho A = \frac{Diss}{\beta_d} \tag{3.3}$$

Where *Diss* is the dissipation of wave energy through breaking and β_d is an empirical constant between 0.1 and 0.2, which is an input parameter to the model. The default value is 0.15 according to Deigaard (1986). The surface roller area is thus defined in the model by the parameter β_d and the energy dissipation, which is calculated either from a regular or an irregular wave description.

3.2.3 Bottom boundary layer

The development in time of the boundary layer in combined wave-current motion is described by the following first-order differential equation, Fredsøe (1984).

$$\frac{\partial z}{\partial t} = \frac{z\left(1+z-e^z\right)}{e^z\left(z-1\right)+1}\frac{1}{U_0}\frac{dU_0}{dt} + \frac{30\kappa}{k}\frac{\sqrt{\kappa^2 U_0^2 + z^2 U_{f0}^2 + 2\kappa z U_{f0} U_0 \cos\gamma}}{e^z\left(z-1\right)+1} \tag{3.4}$$

Where

κ	is von Kármán constant
t	is time
z	is a parameter related to the boundary layer thickness δ, see Eq. (3.6)
U_0	is the near-bed wave orbital velocity

U_{f0}	is the friction velocity due to the current inside the wave boundary layer
γ	is the angle between the current and the waves
k	is the bed roughness, taken to be equal to 2.5 d_{50} for a plane bed, and 2.5 d_{50} + k_R for a ripple-covered bed
d_{50}	is the median grain size, and
k_R	is the ripple-related roughness, see Eq. (3.34)

The near-bed wave-induced velocity U_0 varies in time according to Eq. (3.5):

$$U_0(t) = U(0,t) \tag{3.5}$$

Equation (3.4) is solved by the application of a fourth-order Runge-Kutta method over the wave period. The time step is defined by dividing the wave period T into two times $n/2$ (defining $n/2+1$ evenly spaced calculation points in one half period). It is assumed that a new boundary layer begins to develop each time the flow reverses.

Once $z(t)$ is known, the boundary layer thickness δ is calculated for every time step:

$$\delta = \frac{k}{30}\left(e^z - 1\right) \tag{3.6}$$

Figure 3.4 shows an example of the boundary layer thickness during a wave period applying Cnoidal wave theory.

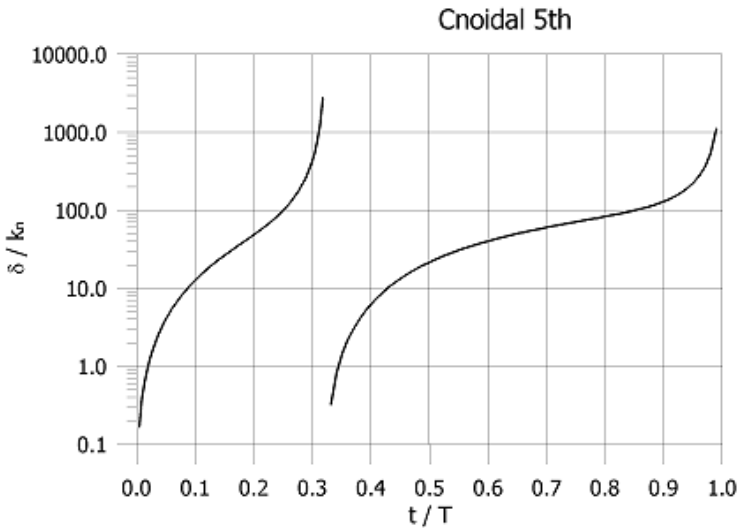

Figure 3.4 Example of boundary layer thickness δ, using Cnoidal wave theory

The friction velocity $U_f(t)$ is derived from the boundary condition for the velocity at the top of the boundary layer.

$$\left[\frac{U_f}{\kappa}\ln\left(\frac{\delta + k/30}{k/30}\right)\right]^2 = \left[\frac{U_{f0}}{\kappa}\ln\left(\frac{\delta + k/30}{k/30}\right) + U_0\cos\gamma\right]^2 + \left[U_0\sin\gamma\right]^2 \tag{3.7}$$

$$\cos\phi = \frac{U_0\kappa\cos\gamma + U_{f0}z}{U_f z} \tag{3.8}$$

$$\sin\phi = \frac{U_0 \kappa \sin\gamma}{U_f z} \tag{3.9}$$

Figure 3.5 and Figure 3.6 show examples of the friction velocity U_f in the cross-shore and longshore direction, respectively, for the 5 different wave theories.

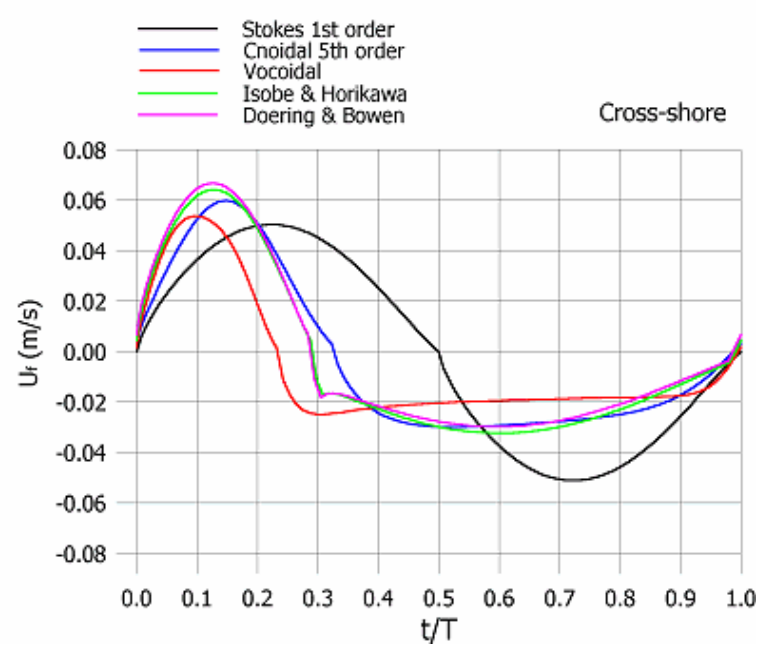

Figure 3.5 Example of friction velocity U_f in the cross-shore direction

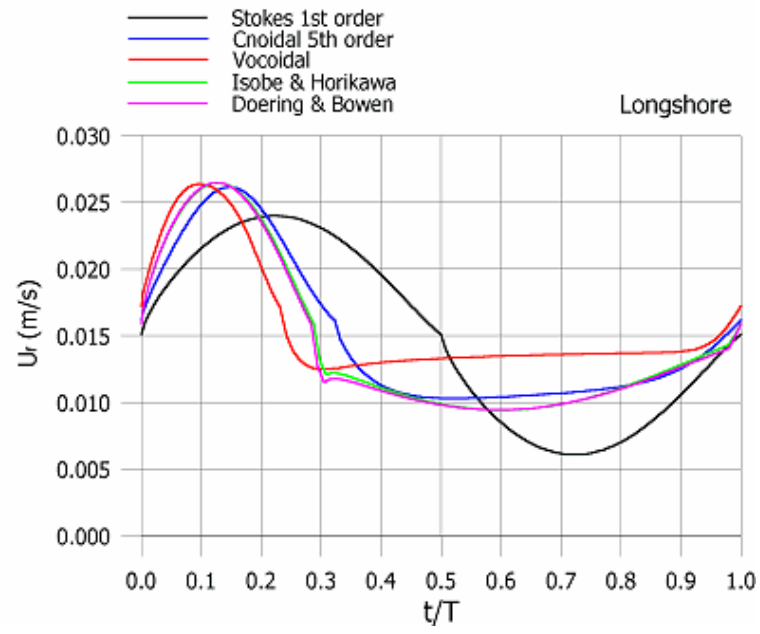

Figure 3.6 Example of friction velocity U_f in the longshore direction

Additional parameters determined by the model are:

$$U_{fc} = \sqrt{\frac{1}{T}\int_0^T U_f^2 \cos\phi \, dt} \tag{3.10}$$

$$\delta_m = \frac{1}{2}\left(\delta\left(t = \frac{T}{4}\right) + \delta\left(t = \frac{3T}{4}\right)\right) \tag{3.11}$$

$$k_w = k\left(\frac{30\delta_m}{k}\right)^{1-\frac{U_{f0}}{U_{fc}}} \tag{3.12}$$

Where

δ	is the instantaneous thickness of the boundary layer
δ_m	is the mean boundary layer thickness
U_f	is the friction velocity
U_{fc}	is the friction velocity of the mean current V
D	is the local water depth
k_w	is the apparent bed roughness
ϕ	is the angle between the instantaneous flow in the boundary layer and the mean current.

The value of the friction velocity of the current inside the boundary layer U_{f0} is not known beforehand and is found by iteration.

The calculations are repeated until the difference between the value of U_{fc} is given and the value determined through Eq. (3.10) becomes smaller than the chosen tolerance ε.

3.2.4 Turbulence

The turbulence originates from 3 different sources:

1. The wave boundary layer
2. The energy dissipation due to wave breaking
3. The mean flow

The three contributions to the eddy viscosity are calculated more or less independently from each other. The contribution from the wave boundary layer is calculated from the boundary layer model of Fredsøe (1984). The contribution from the mean flow is modelled by applying a mixing length concept, see Elfrink et al. (1996) and the eddy viscosity due to wave breaking is calculated from the transport equation for turbulent kinetic energy, see Deigaard et al. (1986). The total instantaneous eddy viscosity is calculated by summing the three contributions at the energy level:

$$\nu_t^2 = \nu_{bl}^2 + \nu_c^2 + \nu_{br}^2 \tag{3.13}$$

Where ν_t is the total instantaneous eddy viscosity, ν_{bl} the eddy viscosity in the bottom boundary layer, ν_c the eddy viscosity due to the mean current and ν_{br} the eddy viscosity due to wave breaking.

Figure 3.7 shows an example of the mean total eddy viscosity distribution across the depth for a non-breaking and breaking wave, respectively.

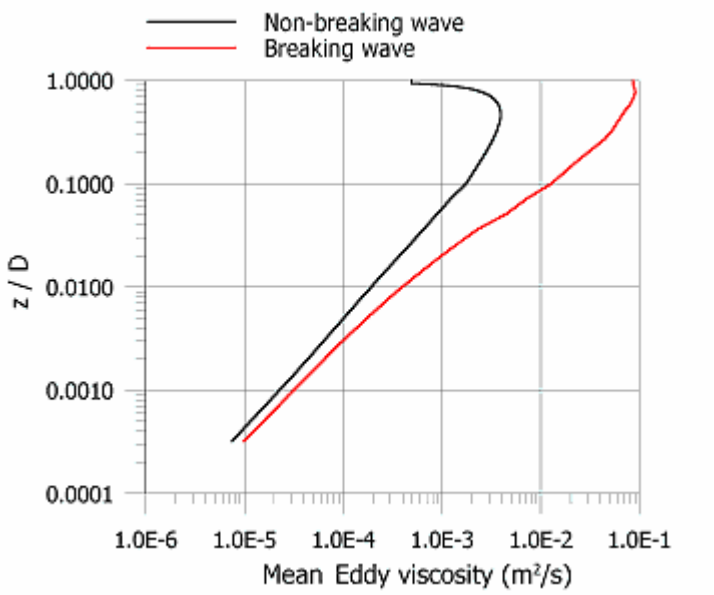

Figure 3.7 Example of mean total eddy viscosity for a non-breaking and breaking wave

Eddy viscosity in bottom boundary layer

Inside the bottom boundary layer the eddy viscosity is calculated as:

$$\nu_{bl} = \kappa U_f z \left(1 - \frac{z}{\delta}\right) \tag{3.14}$$

Where δ is the instantaneous boundary layer thickness, U_f the instantaneous shear velocity due to the combined wave-current motion and z is the height above the bed.

The shear velocity U_f and the boundary layer thickness δ are calculated from the model of Fredsøe (1984).

In the case of a ripple-covered bed, an extra contribution to the eddy viscosity ν_{bl} is added according to Eq. (3.37).

Eddy viscosity due to mean current

Outside the boundary layer the eddy viscosity due to the mean current is calculated from the mixing length concept:

$$\nu_c = l^2 \frac{d\overline{U}}{dz} \tag{3.15}$$

Where l is the mixing length defined as $l = k\ z\ (1 - z/D)$ and U is the mean current velocity

Eddy viscosity due to wave breaking

The time-averaged production of turbulent kinetic energy at the water surface is calculated from a regular or an irregular wave description. For regular waves the production of turbulent energy is defined at the input level as a dimensionless factor f_{br} , which is defined as the ratio of the actual energy dissipation and the energy dissipation in a steady hydraulic jump, $Diss_j$, which yields:

$$\overline{Diss_j} = \frac{\rho g D}{T}\left(\frac{H^3}{4D^2 - H^2}\right) \tag{3.16}$$

The energy dissipation in the model can thus be varied gradually from $f_{br} = 0$ for non-breaking waves to $f_{br} = 1$ for fully developed breaking waves.

For irregular waves the production of turbulent energy is calculated according to the model of Battjes and Janssen (1978), which yields:

$$Diss = 0.25\alpha Q_b H_{\max}^2 \cdot \frac{\rho g}{T} \cdot \frac{H_{\max}}{D} \tag{3.17}$$

Where H_{max} is the maximal wave height, Q_b the fraction of breaking waves and α the dimension less parameter, taken as 1.

The maximal wave height is:

$$H_{\max} = \frac{\gamma_1}{k}\tanh\left(\frac{\gamma_2 kD}{\gamma_1}\right) \tag{3.18}$$

Where k is the wave number and D the water depth.

In case $kD > 2\pi$, the eddy viscosity due to wave breaking is omitted from the calculations.

The fraction of breaking waves Q_b is:

$$\frac{1 - Q_b}{\ln Q_b} = -\left(\frac{H_{rms}}{H_{\max}}\right)^2 \tag{3.19}$$

The two parameters γ_1 and γ_2, which describe the maximum wave steepness H/L and height/depth ratio H/D, respectively, are input parameters to the model. As default, the theoretical value of $\gamma_1 = 0.88$ is used. The second parameter, γ_2 is calculated from the expression as presented in Battjes and Stive (1984):

$$\gamma_2 = 0.5 + 0.4\tanh\left(33 s_0\right) \tag{3.20}$$

Where s_0 is the deep-water wave steepness, H/L_0, where L_0 is the deep-water wave length.

The eddy viscosity due to wave breaking is calculated from the diffusion equation for turbulent kinetic energy according to the model of Deigaard et al. (1986):

$$\frac{\partial k}{\partial t} = \frac{\partial}{\partial z}\left(\frac{\nu_t}{\sigma_n}\frac{\partial k}{\partial z}\right) + \frac{1}{\rho}PROD - c_1\frac{k^{2/3}}{l} \tag{3.21}$$

$$\nu_t = l\sqrt{k} \tag{3.22}$$

Where *PROD* is the production of turbulent kinetic energy due to wave breaking, i.e. total production of turbulent energy equals the dissipation of energy. The 'production' is

assumed to take place during the time T_{diss} after passage of the crest and limited to above the trough level.

In case of irregular waves, the time scale T_{diss} over which the turbulent energy is produced, diffused and dissipated is taken as: $T_{diss} = T_p/Q_b$.

3.2.5 Shear stress

The driving forces for the mean flow basically consist of three contributions:

1. The time averaged shear stress associated with the wave motion
2. The shear stress associated with wave breaking
3. The shear stress due to gradients in the water surface

The vertical distribution of the time mean shear stress is illustrated in Figure 3.8.

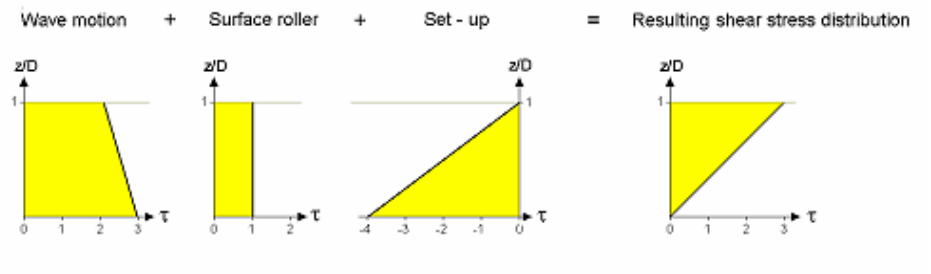

Figure 3.8 Illustration of vertical distribution of mean shear stress

For details reference is given to Fredsøe and Deigaard (1992).

Wave motion

Asymmetric wave orbital motion

The non-linear wave motion will give rise to a mean bed shear stress in the wave direction. In order to fulfil the requirements of potential theory, a small additional velocity is added to the oscillatory wave motion such that the mean bed shear stress becomes zero.

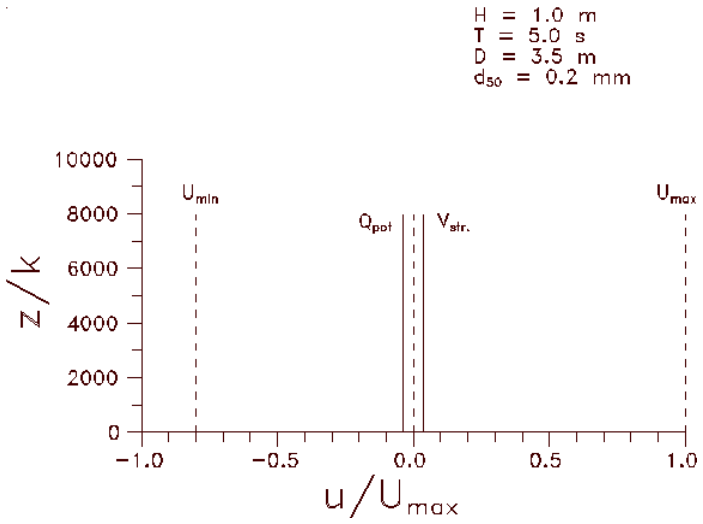

Figure 3.9 Sketch of components in asymmetric wave motion

Streaming in the boundary layer

In case of progressive waves, a small net shear stress is generated due to the non-uniformity of the wave boundary layer. Brøker (1985) showed that this streaming induced shear stress at the bed can be expressed as:

$$\tau_{str} = \frac{\rho}{c}\overline{U_0 U_f \left|U_f\right|} \tag{3.23}$$

The user can turn the effect of streaming on or off.

Radiation stresses

Deigaard and Fredsøe (1989) determined the time mean shear stress necessary to balance the gradients in the radiation stresses. It was found that the vertical transfer of horizontal momentum gives a significant contribution to the momentum balance. Deigaard (1994) derived expressions for time mean shear stress at the wave trough level in case of oblique waves by considering the momentum balance for the surface rollers. The shear stress is constant over the water column. In the wave direction it yields:

$$\frac{\overline{\tau_s}}{\rho} \approx -\frac{\overline{Diss}}{c} \tag{3.24}$$

Where *c* is the wave celerity and *Diss* is the time averaged energy dissipation due to wave breaking.

Water level gradients

On uniform beaches the mean flow in the cross shore direction must balance the mass transport associated with the wave motion and the discharge in the surface roller. In the longshore direction the mean flow corresponds to the time averaged longshore current velocity. In the model the predefined mean flow discharge is obtained by superposing a shear stress arising from a sloping water surface to the shear stress associated with the wave motion (radiation stress, surface roller, streaming). It is noted that this water level gradient not automatically corresponds to the gradient in radiation stress.

This shear stress due to the sloping water surface is zero at the water surface and varies linearly through the water column (hydrostatic pressure). In this model, the pre-defined current may have any magnitude and direction.

3.2.6 Ripples

Wave-generated ripples exist for values of the Shield's parameter θ_{max} less than approximately 1, Nielsen (1979):

$$\theta_{\max} = \frac{U_{f,\max}^2}{(s-1)gd_{50}} \tag{3.25}$$

Where s is the relative density of the bed material, g is the acceleration of gravity and d_{50} is the mean grain size.

For similar values of θ_{max} the ripples are the largest for pure wave motion and are smoothed out when current superposes the wave motion.

The ripples act on the flow as large roughness elements. The influence of ripples on the sediment transport is considered by calculating:

- The dimensions of the ripples as a function of the characteristics of the waves and the current
- The increased roughness experienced by the flow due to the presence of ripples
- The contribution to the eddy viscosity due to ripples
- The mean concentration at the level of the ripple crest

Ripple dimensions

In pure wave motion the ripple dimensions are determined according to Nielsen (1979):

$$h_r = 21 \cdot \psi^{-1.85} \cdot a \tag{3.26}$$

$$\lambda = h_r / \left(0.342 - 0.34 \cdot \theta^{0.25}\right) \tag{3.27}$$

Where

ψ	is $U_{1m}^2 / (s-1)gd_{50}$
h_r	is ripple height
λ	is ripple length
θ'	is Shield's parameter for plane bed case (k = 2.5 d_{50})
a	is amplitude of wave orbital motion near the bed
U_{1m}	maximum orbital velocity

In the estimates of ripple dimensions θ'_{pn} is calculated using Swart's formula for the friction factor (1982):

$$f_w = \exp\left(5.213\left(\frac{2.5d_{50}}{a}\right)^{0.194} - 5.977\right) \tag{3.28}$$

$$\theta'_{pn} = \frac{U_f^2}{(s-1)gd} = \frac{1}{2} f_w \psi \tag{3.29}$$

In cases where current superposes the wave motion, the ripple height is decreased. In the model the effect of current is included by introduction of a 'reduced ripple height'.

The reduced ripple height in combined wave-current motion is estimated as:

$$h_r(wave, current) = h_r(wave) \cdot R_f\left(\frac{U_{fc}}{U_{fw}}\right) \tag{3.30}$$

The reduction factor, R_f, is given as follows:

$$R_f = \begin{cases} 1 & for \quad \frac{U_{fc}}{U_{fw}} \le C_1 \\ 0.5 + 0.5 \cdot \cos\left(\left(\frac{U_{fc}}{U_{fw}} - C_1\right) \cdot \frac{\pi}{C_2 - C_1}\right) & for \quad C_1 < \frac{U_{fc}}{U_{fw}} \le C_2 \\ 0 & for \quad \frac{U_{fc}}{U_{fw}} \ge C_2 \end{cases} \tag{3.31}$$

Where C_1 and C_2 are user-defined constants, having default values of C_1 = 0.1 and C_2 = 2.

When C_2 is set to zero, the influence of ripples on the transport is neglected.

In Eqs. (3.30) and (3.31), U_{fc} is estimated as:

$$U_{fc} = \frac{V}{6 + 2.5 \cdot \ln\left(\frac{D}{k_r + 2.5 d_{50}}\right)} \tag{3.32}$$

Where k_r is ripple roughness corresponding to ripples in pure wave motion. U_{fw} is found from:

$$U_{fw} = \sqrt{\frac{1}{2} \cdot f_w \cdot U_{1m}^2} \tag{3.33}$$

Roughness due to ripples

The roughness due to ripples according to Raudkivi (1988) is given by:

$$k_r = \frac{C_3 \cdot h_r^2}{\lambda} \tag{3.34}$$

Where C_3 is a constant and the default value is 16.

Eddy viscosity from ripples

In the case of a ripple-covered bed, an extra contribution ν_r to the eddy viscosity is added according to the empirical formulation of Nielsen (1979).

$$\nu_r(0) = h_r \cdot \alpha\omega \exp\left(1.5 - 4500 d_{50} - 1.21 n\left(\frac{\alpha\omega}{w}\right)\right) \tag{3.35}$$

It is assumed that the eddy viscosity related to the presence of wave ripples decreases with the distance above the bed according to:

$$\nu_r(y) = \nu_r(0) \cdot \cos\frac{\pi y}{4 h_r C_4} \tag{3.36}$$

Where C_4 is an empirical constant and the default value is 3.

The eddy viscosity near the bed is corrected for the presence of ripples according to

$$\nu_{bl}(z,t) = \nu_{bl}(z,t) + \nu_r(z) \tag{3.37}$$

For $y > 2+C_4 h_r$ the ripples have no effect on the eddy viscosity.

3.3 Sediment Transport

The sediment transport is calculated as:

$$q_t = q_b + q_s \tag{3.38}$$

Where q_t is the total sediment transport, q_b the bed load transport and q_s is the sediment transport in suspension.

In the STPQ3D model the bed load transport model of Engelund and Fredsøe (1976) is used, where the bed load transport is calculated from the instantaneous Shields parameter.

In case of shingle sized material only bed load is considered to exist and the calculation of the bed load is different from the default description for sand.

The vertical variation of the suspended sediment concentration is calculated from the vertical diffusion equation for suspended sediment, according to Fredsøe et al. (1985).

The omission of the convective terms in the diffusion equation is compensated by adding the Lagrangian flow velocity times the mean concentration to the time averaged product of instantaneous velocity and concentrations.

The suspended sediment transport is calculated as the product of the instantaneous flow velocities and the instantaneous sediment concentration:

$$q_s = \frac{1}{T}\int_0^T \int_{2d}^D (uc)\, dz dt \tag{3.39}$$

The time integration of the diffusion equation for suspended sediment is repeated until a periodic solution is obtained.

3.3.1 Bed load transport

The dimensional bed load transport Φ_b is found by a deterministic approach:

$$\Phi_b = 5p\left(\sqrt{\theta'} - 0.7\sqrt{\theta_c}\right) \tag{3.40}$$

Where p is found from Eq. (3.48).

From Φ_b the following time-averaged quantities are calculated:

$$\Phi_{b1} = \frac{1}{T}\int_0^T \Phi_b(t)\cos\left(\phi(t)\right)dt \tag{3.41}$$

$$\Phi_{b2} = \frac{1}{T}\int_0^T \Phi_b(t)\sin\left(\phi(t)\right)dt \tag{3.42}$$

$$q_{b1} = \Phi_{b1}\cdot\sqrt{(s-1)gd_{50}^3} \tag{3.43}$$

$$q_{b2} = \Phi_{b2}\cdot\sqrt{(s-1)gd_{50}^3} \tag{3.44}$$

Where

$\phi(t)$	is the direction of the instantaneous flow
Φ_{b1}	is the dimension less bed load in the mean current direction
Φ_{b2}	is the dimension less bed load normal to the mean current direction
q_{b1}	is the bed load in the mean current direction
q_{b2}	is the bed load normal to the mean current direction

The presence of ripples does not influence the bed transport. This is the reason why Φ_b, p and λ are evaluated based on θ'.

Effect of sloping bed

The bed load transport is influenced by the effect of both a longitudinal slope, β_L and a transverse slope, β_T on the bed-load transport and on the critical value of the Shields parameter θ_c. The effect on the suspended load is attained indirectly through the inclusion of θ_c, which accounts for the effect of a sloping bed, in the expression for the bed concentration of suspended sediment, c_b.

All the equations presented in the following are valid for small bed slopes, either transverse or longitudinal.

For the general case where the flow is at an angle ψ to the slope β, the critical Shields parameter is given by:

$$\theta_c = \theta_{c,0}\cdot\left(\frac{-\cos\psi\sin\beta + \sqrt{\mu_s^2\cos^2\beta - \sin^2\psi\sin^2\beta}}{\mu_s}\right) \tag{3.45}$$

Where μ_s is a static friction coefficient ($\mu_s = \tan\phi_s$, ϕ_s = angle of repose) and $\theta_{c,0}$ is the critical Shields parameter for a plane bed.

The influence of a transversal slope on the bed-load transport is exhibited through a deflection of the transport direction, i.e. that a down-slope component of the transport will appear. This component can be expressed as:

$$q_{by} = \frac{\tan\beta_T}{1.6\sqrt{\theta'}} q_{bx} \tag{3.46}$$

Where θ' is the dimension less bed shear stress related to skin friction, and q_{bx} is the rate of bed-load transport in the x direction, which is along the strike of the slope.

The influence of a longitudinal slope on the bed-load transport is simply accounted for by modifying the threshold value θ_c according to Eq. (3.45) and then using this modified value in the bed transport formulation. See Fredsøe and Deigaard (1992) for more details.

3.3.2 Suspended load transport

Reference bed concentration

Once the variation of the friction velocity U_f over the wave period has been determined by the boundary layer module over a flat bed, the following properties may be derived for every time step, see Engelund and Fredsøe (1976).

Shield's parameter:

$$\theta' = \frac{U_f^2}{(s-1)gd_{50}} \tag{3.47}$$

The deterministic description of the bed concentration is given by Eqs. (3.48) - (3.50):

$$p = \left[1 + \left(\frac{\frac{\pi}{6}\beta}{\theta' - \theta_c}\right)^4\right]^{-0.25} \tag{3.48}$$

$$\lambda = \sqrt{\frac{\theta' - \theta_c - \frac{\pi}{6}\beta p}{0.027 s\theta'}} \tag{3.49}$$

$$c_b = \frac{0.65}{(1 + 1/\lambda)^3} \tag{3.50}$$

Where

ρ	is the relative density of the sediment
g	is the acceleration of gravity
d_{50}	is the median grain diameter
θ'	is Shield's parameter determined for a plane bed

θ_c	is its critical value
p	is the probability that all the particles of a layer are moving
λ	is the linear concentration
c_b	is the bed concentration.

Eq. (3.51) gives an alternative empirical description of the bed concentration by Zyserman & Fredsøe (1994):

$$c_b = \frac{0.331(\theta' - 0.045)^{1.75}}{1 + \frac{0.331}{0.46}(\theta' - 0.045)^{1.75}} \tag{3.51}$$

The empirical description of the bed concentration was developed based on a critical Shields parameter θ_{c0} for plane bed to be equal to 0.045. This value is set automatically by the model and overrules any other input of θ_{c0}, if an empirical description is chosen for C_b.

In Figure 3.10 the bed concentration C_b versus Shield's parameter θ' for both the deterministic approach and the empirical approach is shown.

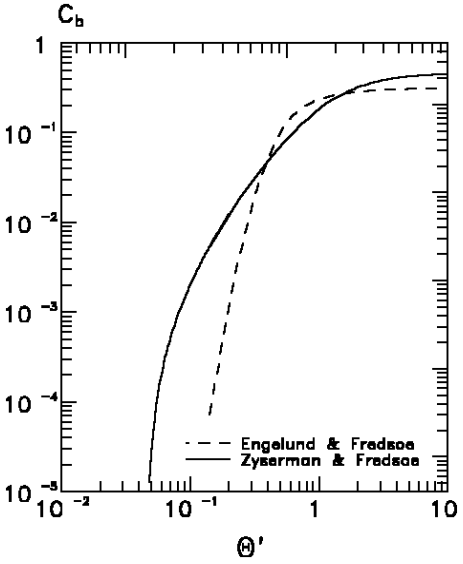

Figure 3.10 Bed concentration c_b versus θ'.

Bed concentration in case of ripples

The contribution from the ripples to c_b is included according to:

$$c_b(t) = \left(2 \cdot d_{50} \cdot c_b(t) + c_o \cdot h_r\right) / \left(h_r + 2 \cdot d_{50}\right) \tag{3.52}$$

In Eq. (3.52) h_r the ripple height is calculated as described in Section 3.2.6. The contribution from the ripples to the bed concentration c_0 is given by

$$c_0 = 0.028\left(\theta'_{pn} - \theta_c\right) \cdot \frac{2}{\pi} \cos^{-1} \sqrt{\frac{\theta_c}{\theta'_{pn}}} \tag{3.53}$$

with θ'_{pn} determined by Eq. (3.29).

Concentrations of suspended sediment

The present section describes the calculation of the concentration varying in time and over the depth. The program iterates over several wave cycles until a periodic solution is found, i.e. until the time variation of the concentration is repeated from one wave cycle to another at any position above the bed.

At the bottom the time-averaged bed concentration c_b is used as a boundary condition for the initial profile:

$$c(0) = \overline{c_b} \tag{3.54}$$

The time varying concentration is calculated from the diffusion equation:

$$\frac{\partial c}{\partial t} = \frac{\partial}{\partial y}\left(\varepsilon_s \frac{\partial c}{\partial y}\right) + w\frac{\partial c}{\partial y} \tag{3.55}$$

The turbulent diffusion coefficient for the sediment ε_s is taken equal to the eddy viscosity ε.

The boundary condition at the bottom is given by the instantaneous bed concentration:

$$c(i+1) = c_b(i+1) \qquad at \quad y = 0 \tag{3.56}$$

At the top the second boundary condition demands zero sediment flux through the water surface:

$$\varepsilon\frac{\partial c}{\partial y} + wc = 0 \qquad at \quad y = D \tag{3.57}$$

The determination of the concentration over the wave period is continued until a periodic solution is reached. In order to speed up the convergence towards periodic conditions, the initial concentration profile is determined by over-relaxation, using the previous initial profile *c'(0,j)* and the profile determined at the end of the previous calculation period *c'(n,j)*, according to:

$$c(0,j) = \frac{3}{2}c'(n,j) - \frac{1}{2}c'(0,j) \tag{3.58}$$

The primes indicate concentration values determined from the previous wave cycle.

The process of accelerating the convergence is stopped when the number of periods calculated reaches 0.75 times the *maximum number of wave cycles* prescribed. The initial concentration profile is taken as:

$$c(0,j) = c'(n,j) \tag{3.59}$$

The iteration is stopped when the relative deviation in the suspended transport in the mean current direction q_s at time $t = T/4$ is less than equal to the prescribed tolerance ν. q_s is calculated as:

$$q_s = \int_{2d}^{D} c\left(\frac{T}{4}, y\right) \cdot U_1\left(\frac{T}{4}, y\right) dy \tag{3.60}$$

U_1 is the instantaneous total velocity in the direction of the mean current.

The relative deviation is determined with respect to the transport q'_{s1} determined at $t = T/4$ in the previous wave cycle

$$\frac{q_{s1} - q_{s'1}}{q_{s'1}} \leq \nu \tag{3.61}$$

Mean concentration profile and centre of gravity

Having determined the variation of the concentration over time and depth as described in Eq. (3.56), the time-averaged concentration over the vertical is found as:

$$\bar{c}(y) = \frac{1}{T} \cdot \int_0^T c(y,t)\,dt \tag{3.62}$$

Figure 3.11 shows an example of the time-averaged concentration over the vertical for a non-breaking and breaking wave, respectively.

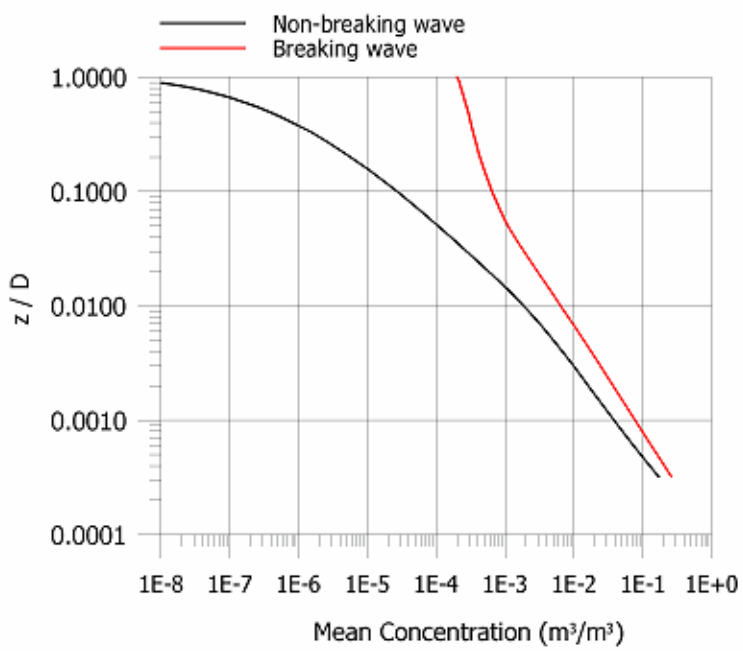

Figure 3.11 Example of time-averaged concentration profile for a non-breaking and breaking wave, respectively

The centre of concentration y_c is calculated as the height of the centre of gravity of the mean concentration profile above the bottom

$$y_c = S / A \tag{3.63}$$

with

$$A = \int_{2d_{50}}^{D} \bar{c}(y)\,dy \tag{3.64}$$

$$S = \int_{2d_{50}}^{D} \bar{c}(y)\, y\, dy \tag{3.65}$$

Where A is the total amount of suspended material per unit width, and S is the first-order moment of the mean concentration profile with respect to the bed level.

Time averaged transport

The instantaneous suspended load transport in the x and y direction is defined as:

$$\phi_x(t) = \int_{2d}^{D} U_x(z,t) \cdot c(z,t)\, dz \tag{3.66}$$

$$\phi_y(t) = \int_{2d}^{D} U_y(z,t) \cdot c(z,t)\, dz \tag{3.67}$$

Where U_x and U_y are the instantaneous resulting velocities in the x and y direction, respectively.

The resulting suspended transport over the wave period in both directions is calculated as:

$$\bar{q}_{sx} = \frac{1}{T} \int_0^T \left[\int_{2d}^{D} U_x(z,t) \cdot c(z,t)\, dz \right] dt \tag{3.68}$$

$$\bar{q}_{sy} = \frac{1}{T} \int_0^T \left[\int_{2d}^{D} U_y(z,t) \cdot c(z,t)\, dz \right] dt \tag{3.69}$$

The dimension less suspended transport is calculated as:

$$\Phi_{sx} = \bar{q}_{sx} / \sqrt{(s-1) g d_{50}^3} \tag{3.70}$$

$$\Phi_{sy} = \bar{q}_{sy} / \sqrt{(s-1) g d_{50}^3} \tag{3.71}$$

3.3.3 Graded sediment description

For a 'uniform' sediment description the geometrical characteristics of the bed material are represented through the median grain size d_{50} when calculating the concentration of suspended sediment and the sediment transport numerically.

By using a 'graded' sediment description, it is possible to describe the effect that the presence of different grain size fractions have on the amount of bed load and suspended material and on the total rate of sediment transport. (Zyserman et. al. 1996).

In the following it is described how the graded sediment description is included in the calculations.

Grain curve

The sediment distribution is described by a log-normal grain curve, which is calculated on basis of the mean grain size, d_{50} and the geometrical deviation or spreading σ_g defined as $(d_{84}/d_{16})^{½}$.

Where d_{84} and d_{16} express the weight percentages 84% and 16%, respectively, by which the material is finer. Figure 3.12 shows the grading curves for d_{50} = 0.2 mm and different values of σ_g.

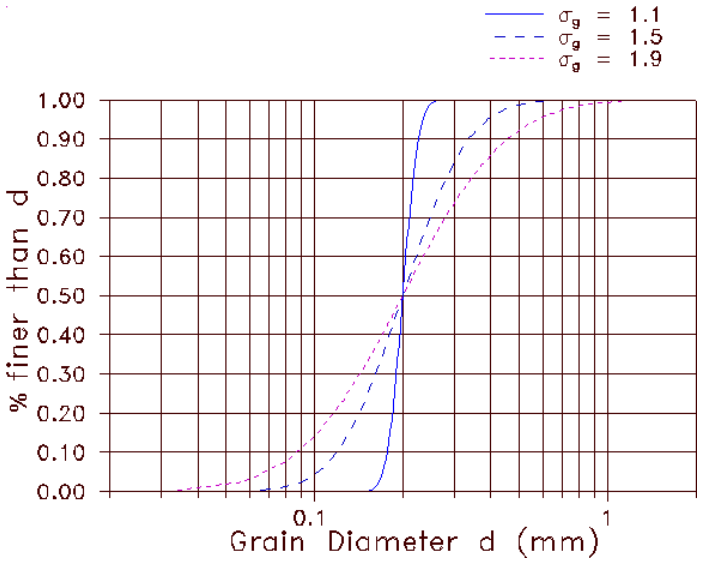

Figure 3.12 Grading curve on basis of d_{50} and σ_g

The fall velocity w for any grain fraction with a diameter d is found by Eq. (3.72), Rubey's formula (1933):

$$w = \sqrt{g(s-1)d}\cdot\left(\left(\frac{2}{3}+\frac{36\nu^2}{g(s-1)d^3}\right)^{½}-\left(\frac{36\nu^2}{g(s-1)d^3}\right)^{½}\right) \quad (3.72)$$

Where s is the relative sediment density, g is gravity and ν is kinematic viscosity found by Eq. (3.73):

$$\nu = \left(1.78 - 0.0570812T + 0.00106177T^2 - 8.27141 \cdot 10^{-6} T^3\right) \cdot 10^{-6} \quad (3.73)$$

Where T is the water temperature in degrees Celsius.

Bed concentration

The limiting grain size that can be brought into suspension by the flow is found using the criterion:

$$w_s \leq 0.80 U'_{f,\max} \quad (3.74)$$

Where $U'_{f,max}$ is the maximum value attained by the instantaneous skin friction velocity over the wave period. The criterion simply states that only the particles having a fall velocity w_s less than the threshold value given by Eq. (3.74) will be picked up from the bed. The critical diameter for suspension is indicated as d_{crit}, and the associated probability is called f_{crit}.

The value of f_{crit} is then divided in N equal parts, where N is the selected number of suspended fractions, and a representative grain diameter d_i $(i=1,...,N)$ is related to every suspended fraction, see Figure 3.13.

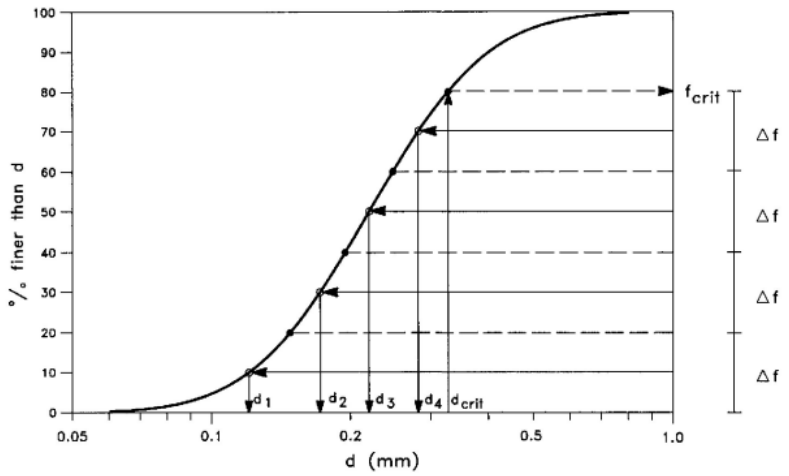

Figure 3.13 Definition of fractions of suspended sediment for N=4, d_{50}=0.22 mm, σ_g=1.60, f_{crit}=80% and d_{crit}=0.33 mm. $D_f=f_{crit}/N$

Next, the diffusion equation for suspended sediment is solved for each of the N fractions, with the settling velocity w_i and the bed concentration $c_{b,i}$ calculated on the basis of d_i. Two conditions are applied to the concentration values and should be calculated as follows:

a. The composition of the sediment in suspension is assumed to be equal to the composition of the original bed material (i.e. for that part finer than d_{crit}). If f_i is a proportionality factor for fraction ***i***, this results in the following requirement for each of the N fractions in suspension:

$$\phi_1 M_1 = \phi_2 M_2 = \phi_3 M_3 = \ldots = \phi_N M_N \quad (3.75)$$

M_i is the time-averaged total amount of sediment in suspension for fraction ***i***, defined as:

$$M_i = \int_{2d_{50}}^{D} \overline{c_i} dz \tag{3.76}$$

Where D is the local water depth, c is concentration, z is the vertical co-ordinate measured upwards from the bed and the over bar indicates time average. By making $\phi_N = 1$ in Eq. (3.75), the remaining ϕ_i can be readily calculated.

b. At $z=2d_{50}$, the bed concentration must be equal to the one determined on the basis of d_{50} and taking into account the gradation of the sediment, i.e.:

$$Kc_b \left(\sum_{i=1}^{N} \overline{c_{b,i}} \phi_i \right) = \overline{c_{b,50}} \tag{3.77}$$

Where K_{c_b} is a constant, and c_{b50} is the value of c_b based on d_{50}.

Condition (a) is a reasonable assumption under equilibrium situations, because the dispersive stresses associated with the coarser suspended fractions, which are kept in suspension closer to the bed than the finer ones, limit the capacity of the flow to pick up large amounts of fine sediment from the bed.

If the empirical description of c_b is chosen, c_{b50} is found directly by calculating θ' on the basis of d_{50} and using Eq. (3.51).

If the deterministic description of c_b is chosen, c_{b50} is calculated taken into account the fact that the different grain fractions d_i cover different % of the area of the bed, using Eqs. (3.47) - (3.61) where d_{50} is replaced by d_i.

Once Kc_b has been found, the bed concentration c_b for each representative grain diameter d_i is found by

$$c_b = Kc_b \cdot c_{b,i} \cdot \phi_i \tag{3.78}$$

Concentration of suspended material

The concentration of suspended sediment for each of the representative grain diameters, c_i, is found by inserting the bed concentration c_b from Eq. (3.78) into Eqs. (3.54) and (3.56).

The different contributions of the suspended concentration $c_i(z,t)$ are added directly without additional weighting by ϕ_i.

$$c(z,t) = \sum_{i=1}^{N_{frac}} c_i(z,t) \tag{3.79}$$

4 Morphology

A morphological model is a combined hydrodynamic/sediment transport model. The hydrodynamic flow field is updated continuously according to the changes in bed bathymetry.

In case of a combined wave/current simulation, the wave field may be updated as well to reflect the changes in bed bathymetry.

Morphological models are traditionally divided into coupled and uncoupled models. In coupled models, the governing equations for flow and sediment transport are merged into a set of equations, which are solved simultaneously. In uncoupled models, the solution of the hydrodynamics is solved at a certain time step prior to the sediment transport equations. Subsequently, a new bed level is computed and the hydrodynamic model proceeds with the next time step. The latter approach is applied in the present modelling system.

4.1 Sediment Continuity Equation

The key parameter for determination of the bed level changes is the rate of bed level change $\frac{\partial z}{\partial t}$ at the element cell centres. This parameter can be obtained in a number of ways, but in general all methods are based on the Exner equation (sediment continuity equation), which can be written:

$$-(1-n)\frac{\partial z}{\partial t} = \frac{\partial S_x}{\partial x} + \frac{\partial S_y}{\partial y} - \Delta S \tag{4.1}$$

Where

n	Bed porosity
z	Bed level
t	Time
S_x	Bed load or total load transport in the x direction
S_y	Bed load or total load transport in the y direction
x, y	Horizontal Cartesian coordinate
ΔS	Sediment sink or source rate

For an equilibrium description of the sediment transport, the sink/source term is zero unless lateral sediment supply is included in the model, for example from bank erosion processes (see Section 4.3). The description of the sediment transport rates for a combined wave/current model is always an equilibrium description.

For a non-equilibrium description, i.e. solution of an advection-dispersion equation for the suspended load, the sediment sink/source term can be written:

$$\Delta S = \Phi_0(\eta_0) w_s (c - c_e) \tag{4.2}$$

Where

η_0	Normalised no slip level above the bed
Φ_0	Unit profile function for the sediment concentration
w_s	Settling velocity for the suspended sediment
c	Depth-averaged sediment concentration
c_e	Depth-averaged equilibrium concentration

The term expresses that sediment deposits at the bed if the actual concentration in the water column is larger than the equilibrium concentration, and the opposite if it is lower.

After having solved the advection-dispersion equation, the term can be calculated directly at all the element cell centres such that only the contribution from the bed load needs to be included in order to find the bed level rate.

4.2 Morphological Bed Update

The bed is updated continuously through a morphological simulation (at every HD-time step) based on the estimated bed level change rates. New values for the bed level change rates are estimated at every N^{th} HD-time step, where N is a user defined time step factor. The new bed levels are obtained with a forward in time difference scheme stating:

$$z_{new} = z_{old} + \frac{1}{1-n}\frac{\partial z}{\partial t}\Delta t_{HD} \tag{4.3}$$

For this reason, it is only necessary to calculate the bed load transport at the same time step as $\frac{\partial z}{\partial t}$, while the advection-dispersion equation for the concentration of the suspended sediment needs to be calculated at every time step.

The contribution from the bed load transport to the bed level change rate is obtained by taking the divergence of the sediment fluxes on the element faces. The divergence can be obtained by summing up all the fluxes crossing the element faces, as shown in Figure 4.1. Hereby, we obtain:

$$\frac{\partial S_x}{\partial x} + \frac{\partial S_y}{\partial y} = \sum_{i=1}^{m} S_{in}\, ds_i \tag{4.4}$$

Where

S_{in}	Sediment flux normal to the element face (positive outward)
ds_i	Element face length
m	Number of faces on element

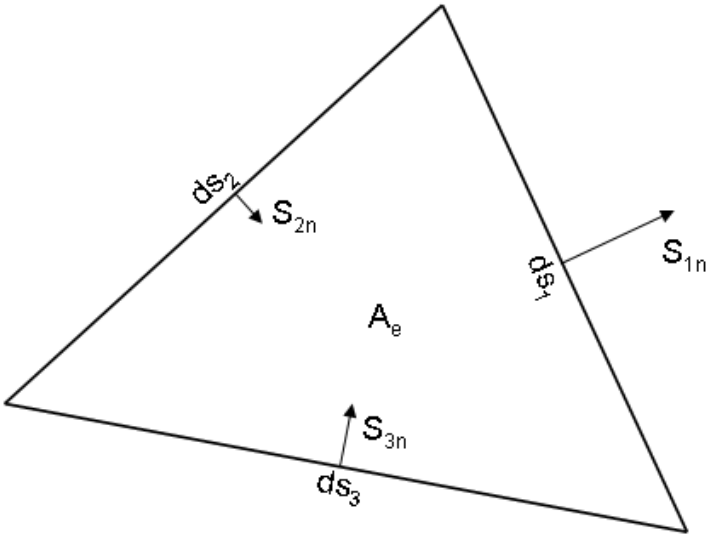

Figure 4.1 Normal sediment fluxes at the cell faces used to obtain the divergence

The model is based on a cell centred formulation, so some sort of weighting scheme is needed to obtain the sediment fluxes at the element faces. The following approach is applied: First the upwind and downwind elements are identified from the sum of the two flux components normal to the element face, as shown in Figure 4.2.

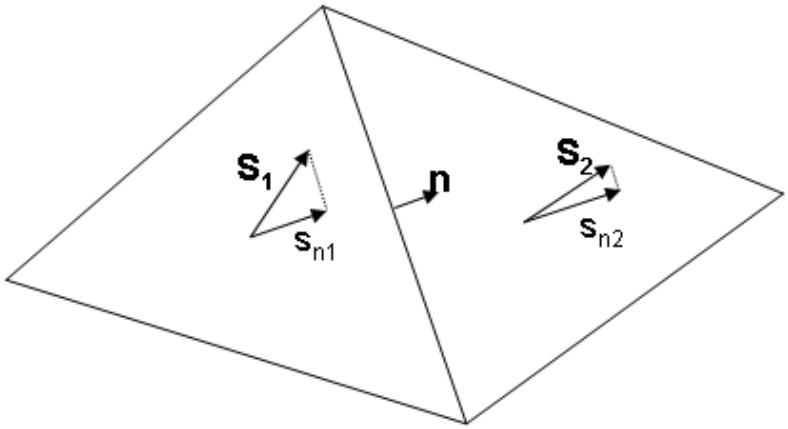

Figure 4.2 Sediment fluxes used to identify the upwind and downwind elements

If the sediment flux S_n obtained by Equation (4.5) is greater than zero, element 1 (left element in Figure 4.2) is located upwind compared to element 2, while located downwind if the flux is less than zero. Equation (4.5) reads:

$$S_n = S_{1x} n_x + S_{1y} n_y + S_{2x} n_x + S_{2y} n_y \tag{4.5}$$

After having identified the upwind element, the sediment flux normal to the element face is calculated by the weighting scheme:

$$S_{in} = \alpha S_{n1} + (1-\alpha) S_{n2} \tag{4.6}$$

Where α is a weighting coefficient depending on the ratio between the two sediment fluxes S_{n1}/S_{n2}. The value α is obtained from the expression:

$$\alpha = \tanh\left(0.5493 \max\left(\left(\frac{S_{n1}}{S_{n2}}\right)^2, \left(\frac{S_{n2}}{S_{n1}}\right)^2\right)\right) \tag{4.7}$$

From Equation (4.7) it is seen that the expression converges against an upwind formulation whenever there is a relative large difference in magnitude between the two transport rates.

4.2.1 Speedup factor

It is possible to speed-up the morphological evolution by multiplying the derived bed level change by a dimensionless speedup factor.

$$Z^{n+1} = Z + \Delta z^n \cdot Speedup \tag{4.8}$$

Note that the calculated sediment transport rates (both bed load and suspended load) and the amount of suspended sediment are unaffected by this. Only the bed is affected. The layer thickness is updated in the same way.

4.3 Slope Failure

4.3.1 Simple bank erosion

In addition to the general morphological update of the bed, it is possible to include bank slope failure effects acting on elements in the region from flooded (real wet) elements to dry elements.

The criterion for activation of slope failure is determined by a user defined angle of repose, which can be specified either as a constant or with spatially variations through a map. In the case where a map is prescribed the critical angle is determined as the average value of the angle of repose in two adjacent elements. In Figure 4.3 a part of a mesh where bank slope failure might occur is shown. If bank slope failure is included in the model, bank slope should be calculated at all adjacent elements covering transition from flood to dry. The bank slope α in the present model is obtained as:

$$\tan(\alpha) = \left|\frac{z_d - z_f}{ds}\right| \tag{4.9}$$

Where z_d and z_f are bed levels at the dry and flooded element, respectively. If the bank slope is larger than the critical angle (angle of repose), a land slide adjusting the slope to the angle of repose φ takes place - otherwise nothing happens. The new bed levels z´ in the elements are obtained as:

$$if\ \ \tan(\alpha) > \tan(\varphi) \quad \Rightarrow \quad \begin{cases} z_d' = z_d - \dfrac{A_f}{A_f + A_d}\left(z_d - z_f - \tan(\varphi)ds\right) \\ z_f' = z_f + \dfrac{A_d}{A_f + A_d}\left(z_d - z_f - \tan(\varphi)ds\right) \end{cases} \tag{4.10}$$

Where A_f and A_d are the areas of the flooded and dry element, respectively, and *ds* the distance between the two cell centres.

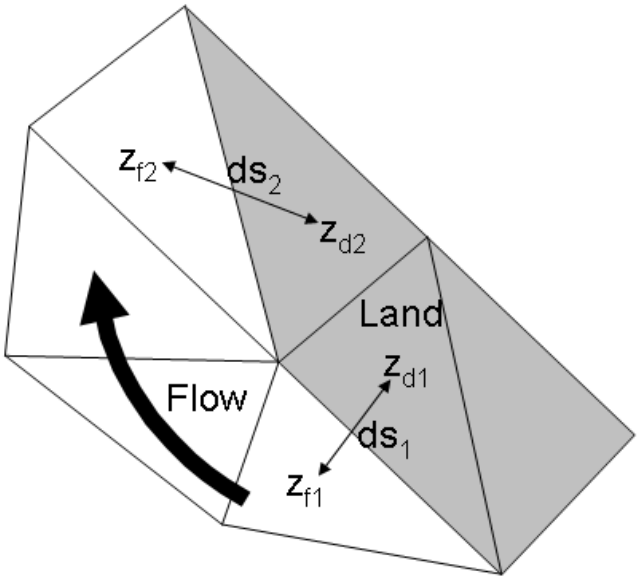

Figure 4.3 Sketch showing principles for calculation of bank slope failure

Please note that a correct behaviour of the bank slope failure is only obtained if the bank area is satisfactorily resolved. A too coarse mesh resolution implies that locally steep slopes are not resolved and thereby that the bank slope failure never becomes activated. The module has shown to be useful for modelling of the development of breach failure through sand barriers.

4.3.2 Extended bank erosion

The bank erosion is calculated by the same process as described above for simple bank erosion however the region is extended to consider both real wet elements and wet elements next to dry elements.

4.3.3 General slope failure

The slope failure is calculated by the same process as described above for simple bank erosion however all elements in the domain are considered. I.e. slope failure can occur in totally flooded regions as well as near dry elements.

5 Shoreline Morphology

5.1 Introduction

The Shoreline Morphology (SM) module for FM combines a one-line model description for the shoreline with a 2D description of the wave, current and sediment transport field to create a flexible and robust shoreline model capable of handling shorelines with large curvature, off-shore reefs, breakwaters, seawalls, groins, rocky outcrops and much more. The model can be used to describe long term shoreline evolution ranging from days to centuries and more.

Without the SM module, the morphology in the Sand Transport Module simply updates the bed level in each mesh element according to the local sediment continuity equation as described in the previous section. This strategy works well in the short term, say on the timescale of a single storm, but for long-term simulations the coastal profile tends to degenerate to a non-realistic shape. With the SM module, the sediment volume deposited during each time step is integrated across the shoreface and the morphology is updated according to the continuity equation for the shoreline using a predefined coastal profile. Thereby the effect of the cross-shore transport is eliminated from the morphology allowing for long term simulations.

5.2 Model Description

The model solves a modified version of the one-line equation for the shoreline (see Kaergaard and Fredsoe, 2013):

$$\frac{\Delta \mathrm{n}}{\Delta \mathrm{t}} = -\frac{vol}{\Delta A_z} \tag{5.1}$$

Where Δn is the distance the shoreline is moved perpendicular to the local shoreline orientation, Δt is the time step, vol is the volume of sediment deposited on the shoreface in front of the shoreline edge and dA_z is the area of the strip of shoreface in front of the shoreline edge projected onto the plane defined by the shoreline edge and the vertical axis, see also Figure 5.1.

The direction the shoreline is moved is perpendicular to the local orientation of a baseline. The baseline is defined by a set of points forming a polyline. The position of the baseline points is fixed during the simulation.

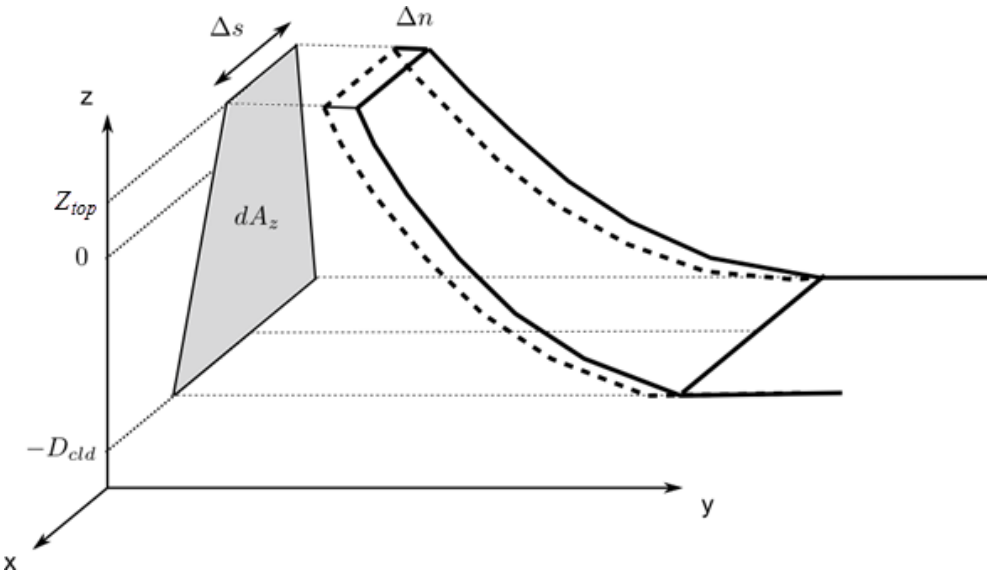

Figure 5.1 Sketch of a strip of shoreface with definitions of model parameters

5.3 Model Inputs

A number of input files are required for the SM module. These can be prepared in the Mesh Generator using the tools under the *Shoreline* menu.

5.3.1 Initial bathymetry

The initial bathymetry specified by the mesh will only be used outside the shoreline model domain, inside the shoreline model domain; the bathymetry is set by the combination of the initial shoreline position and the coastal profiles. At the edges of the shoreline model domain large jumps may therefore be seen in the bathymetry after the shoreline model has set the bathymetry inside its domain. This should be avoided by setting the bathymetry in the mesh to match the bathymetry specified by the shoreline model as accurate as possible.

5.3.2 Baseline and coastline

The local orientation of the baseline determines the direction in which the coastline points are moved on-shore and off-shore. The coastline points are always moved perpendicular to the local orientation of the baseline; the positions of the baseline points remain fixed throughout a simulation.

The coastline and baseline points are staggered as shown in Figure 5.2. Furthermore the coastline has two boundary points outside the shoreline model domain these are used for boundary condition purposes. The boundary condition in the model is zero gradient in the littoral drift across the boundary; it means that the orientation of the shoreline at the boundary remains constant throughout the simulation.

The staggered grid and coastline boundary points mean that there is one more coastline point than baseline points.

The baseline is specified as an xyz file while the coastline can be specified as either a xyz file or as a dfs1 file.

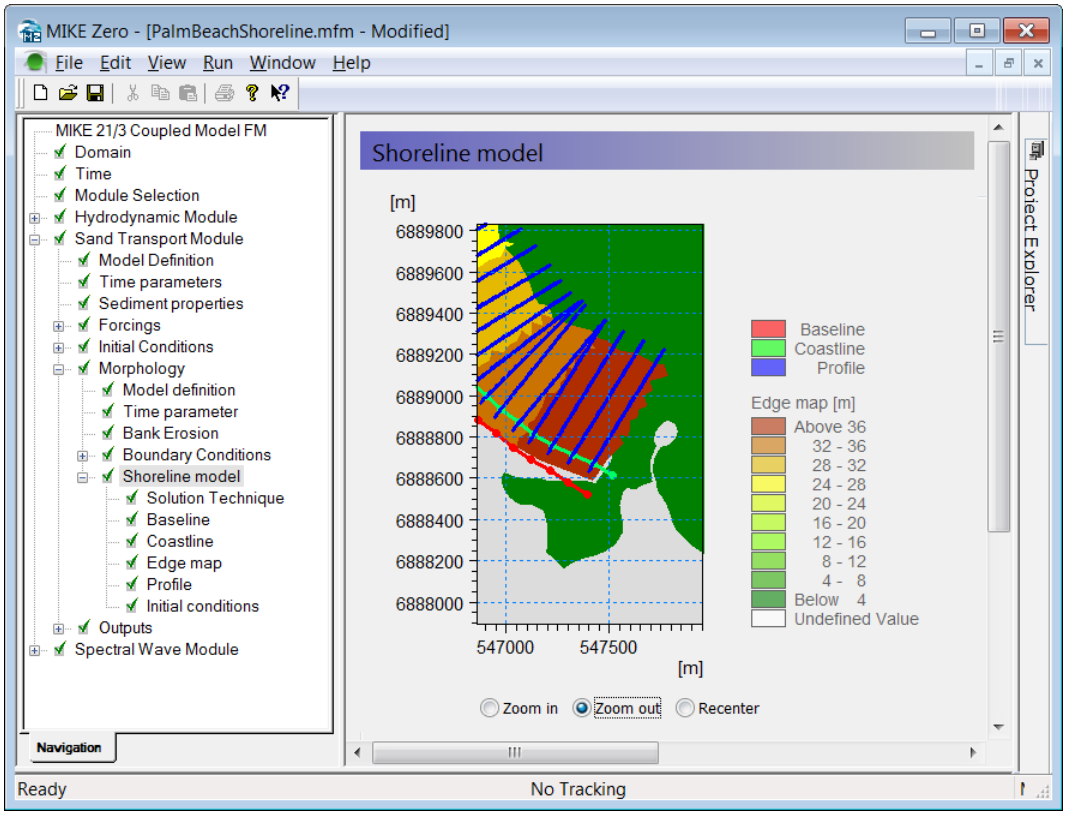

Figure 5.2 Coastline points and baseline points are staggered

5.3.3 Edge Map

The edge map defines the baseline edge to which each mesh element belongs. It is a dfsu file with the same structure as the mesh. Baseline edge #1 is the edge going from point 1 to point 2 in the baseline. The coastline position of edge #1 is point #2 in the coastline due to the boundary ghost point, see Figure 5.3.

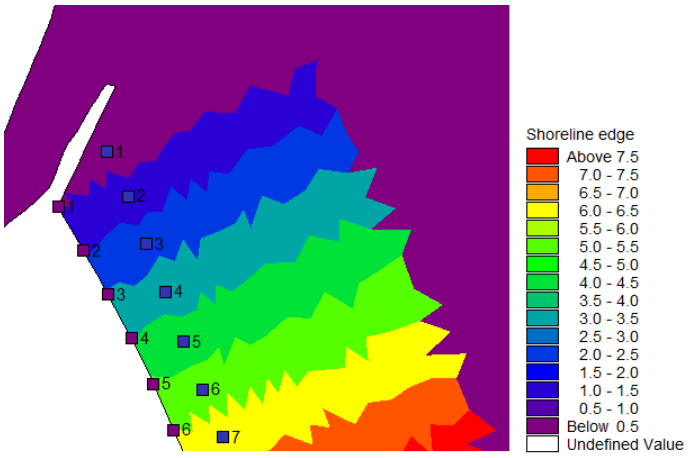

Figure 5.3 Edge Map with baseline points (purple squares) and coastline points (dark blue squares)

5.3.4 Coastal Profile

The coastal profile is one of the most important inputs in the shoreline model and choosing it or them correctly is usually part of the calibration process for the model.

Because the coastal profile usually varies a lot in time in the real world, but must be pre-defined in the model, the specified coastal profile has to represent the bathymetry in such a way that the desired sediment transport / coastal morphology is obtained in the model. E.g. in case the winter and summer profile differs significantly it may be advantageous to specify a time series of profiles that reflects this behaviour.

The closure depth and top level are also important factors for the coastal profile:

- Closure depth, D_{cld}. Distance from mean sea level to bottom of the active profile.
- Top level, Z_{top}. Distance from mean sea level to top of the active profile.

The closure depth specifies the off-shore boundary for the active profile and the top level specifies the on-shore boundary for the active profile. Together they define the active height of the coastal profile as shown in Figure 5.4, which also shows how the model handles the case where the initial bathymetry is not perfectly flat seaward of the position of the closure depth or landward of the position of the dune height.

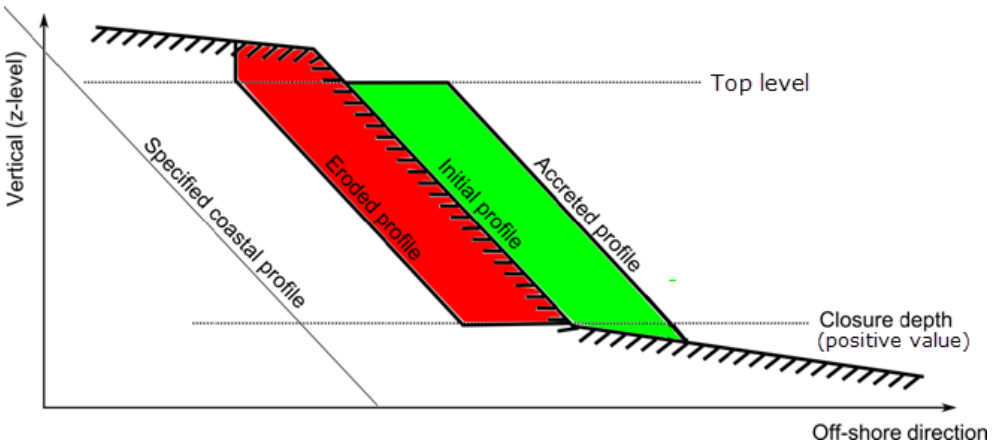

Figure 5.4 Accreted and eroded coastal profile.

It is seen that the specified coastal profile extends below the closure depth and above the top level. At the off-shore boundary the specified profile is used to specify the water depth in the area between the initial bathymetry and the closure depth, so the specified closure depth is actually only used when eroding the initial bathymetry. At the inshore boundary the specified profile is used to determine the bathymetry between the top level and the original bathymetry when the profile erodes, while this part of the specified coastal profile is ignored when the profile accretes.

The above behaviour should be taken into account when constructing the coastal profile to use in the model: The slope of the profile below the closure depth and above the top level should be relatively large and larger than the slope of the initial bathymetry in the respective areas.

If the specified coastal profile is too short, a sharp edge will occur at the inshore and off-shore boundaries as shown in Figure 5.5. If the steps at either boundary become too large, it can cause convergence problems in the iteration of the sediment volume when new elements are entering the active profile at either boundary.

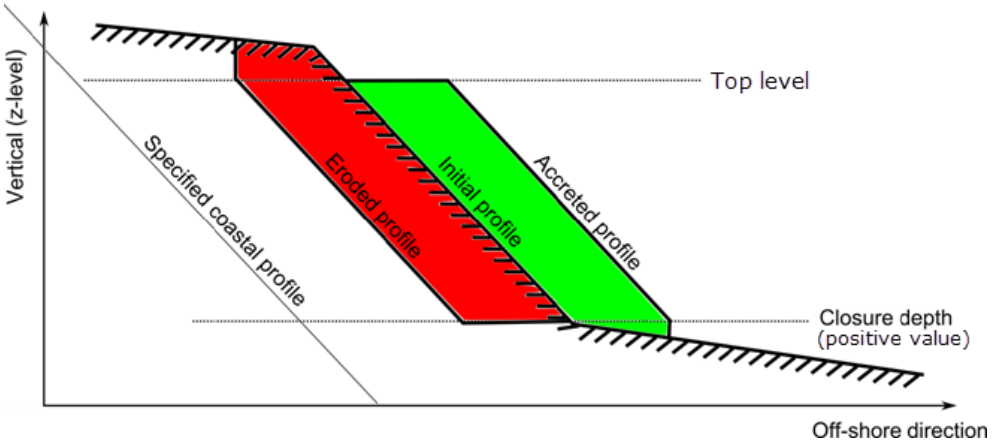

Figure 5.5 Accreted and eroded coastal profile for a specified coastal profile, which is too short compared with the initial bathymetry and the morphological changes

The coastal profile is defined as a combination of
- The distance to the shoreline
- The bed level

The profile can be specified as a xyz file if a single profile is used along the shoreline, or as a dfs2 file with one row per shoreline node if the profile varies along the shoreline. A pre-defined time varying profile can be specified using a time varying dfs2 file.

5.4 Dune Erosion

The erosion of the dune is described as an irreversible process; the dune front moves only back as result of the erosion by the waves running up the beach.

The modelling of the dune erosion consists of two parts:

1. a description of the retreat of the dune front, notably the variation in the dune foot level as the dune front is eroded, and
2. an assessment of the rate of sediment loss from the dune front under given conditions in the form of morphology, water level and wave conditions.

The dune geometry is described by the following parameters (see Figure 5.2):
- Dune crest level: H_{dune}
- Dune foot level: FL
- Coastline position, the position of the contour at the MWL: Y
- Dune front position, the position of the dune foot: Y_{dune}
- Dune angle of repose: α

The dune crest level H_{dune} is an input parameter, while the other parameters vary in time, determined by the model starting from given initial conditions. The slope of the dune front given by α_{re} .

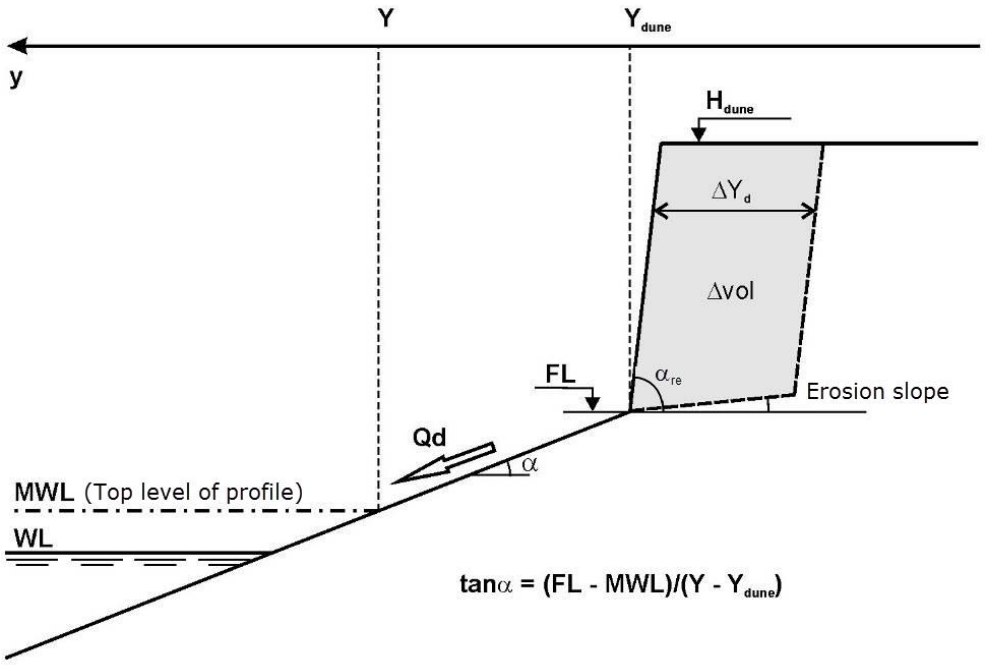

Figure 5.6 Definition sketch for the dune erosion model

5.4.1 Retreat of dune front

The rate of retreat of the dune front is determined by the continuity equation from the rate of loss of sediment from the dune front, Q_d. During the time step of Δt the dune front retreats the distance ΔY_{dune} which is determined so that the change in volume equals the rate of loss

$$\Delta vol = Q_d \Delta t \tag{5.2}$$

The onshore movement of the foot of the dune, Δn_{dune}, during each time step is calculated as

$$\Delta n_{dune} = Q_d / A_{z,dune} \tag{5.3}$$

Where $A_{z,dune}$ is the area of the face of the dune projected onto the vertical plane parallel to the baseline edge. The minimum active area, $A_{z,min}$, is used to stabilize the dune erosion model in cases where the entire dune has been eroded, i.e. $A_{z,dune} = \max(A_{z,dune}, A_{z,min})$.

As the dune front retreats, the dune foot increases its level by moving back along a defined erosion slope. The profile levels from the dune foot level *FL* to the dune crest level H_{dune} is defined via $\tan(\alpha_{re})$, where α_{re} is the angle of repose.

The actual beach slope $\tan(\alpha)$ is determined from the foot level, FL, and the difference in the position of the coastline and the dune foot:

$$\tan(\alpha) = \frac{FL - MWL}{Y - Y_{dune}} \tag{5.4}$$

If the coastline retreats faster than the dune front the beach slope tan(α) increases correspondingly. A maximum beach slope, tan(α_{be}) is defined. If the beach slope reaches tan(α_{be}), as (Y-Y_{dune}) is decreasing, the dune foot level FL is reduced, maintaining the beach slope at tan(α_{be}). If the actual beach slope is found to be larger than tan(α_{be}), the dune foot level is reduced to make the beach slope equal to the maximum beach slope.

5.4.2 The rate of loss from the dune front

The rate of sediment loss from the dune front is caused by erosion of sand from the dune front and is therefore associated with the intensity of the wave run-up impinging on the front. The formulation of the erosion rate is based on Larson et al. (2004).

The run-up height above the instantaneous water level WL is determined from the model by Van der Meer and Janssen (1994). The run-up height at a dike exceeded by 1 in 50 waves, $R_{2\%}$, is estimated as:

$$\frac{R_{2\%}}{H_{m0}} = 1.77 \cdot \gamma_f \gamma_b \gamma_\beta \xi_0 = 1.77 \gamma \frac{\tan\alpha}{\sqrt{H_{m0} / L_0}} \tag{5.5}$$

Where γ_f, γ_b and γ_β are reduction factors due to the presence of a berm, roughness of the slope and the wave angle. No attempt is made to assess the individual reduction factors, instead all these factors have been lumped into a single γ− factor. ξ_0 is the Irribarren number (or surf-similarity parameter) giving a measure of the steepness of the beach compared to the wave steepness.

H_{m0} is the significant wave height near the toe of the dike and L_0 is the deep water wave length based on the spectral wave period (approximately $0.9T_p$).

Adjustment to other run-up values may be obtained by changing the coefficient in eq.(5.5). For example, $R_{1/3}$ is found with a coefficient of 1.31 instead of 1.77. A simple estimate of the run-up is therefore obtained from the offshore wave height H_s as

$$R = 1.77 \gamma_r \tan\alpha \sqrt{H_s L_0} \tag{5.6}$$

with γ_r as a single calibration factor.

The rate of loss of sediment from the dune is calculated from the run-up with formulae based on Larson et al. (2004). The maximum loss, corresponding to a situation with the dune foot level at the water level is found as

$$Q_{d0} = 4 C_s \frac{R^2}{T} \tag{5.7}$$

Where C_s is a calibration factor normally found to be in the range 1×10^{-3} to 3×10^{-3} . As the dune foot level is higher than the water level, the actual rate of sediment loss is found by applying a reduction factor:

$$R_{ed} = \exp\frac{-2\left(Fl - WL\right)}{R} \tag{5.8}$$

Giving a rate of dune loss of

$$Q_d = \exp\frac{\left(-2\left(FL - WL\right)/R\right)4C_s R^2}{T} \tag{5.9}$$

Q_d is always positive corresponding to a retreating dune front. If the dune foot moves so far back and up that it reaches the level of the dune crest the rate of loss Q_d is put to zero. If the coastline is eroded the beach becomes more narrow and steep, if the beach slope becomes equal to the maximum tan(α_{be}), and the coastline continues to move back, a new dune front will be formed in the model as the foot level moves down to maintain the beach slope at the maximum. The new dune front can then again be subject to erosion if the run-up reaches the dune foot level.

The loss Q_d is eroded from the dune and is transferred to the coastline model as a source term so that the coastline advances correspondingly.

5.5 Conserving Sediment

The conservation of sediment in the hybrid model is ensured by an iterative procedure. Small errors in the sediment balance are induced by the curved baseline as well as the way the model treats the regions around the closure depth and dune height.

The iterative procedure works on the change in shoreline position. After each iteration the actual sediment volume deposited/eroded on each strip of shoreface is compared with the sediment volume available for deposition/erosion due to gradients in the sediment transport and sediment availability. The error in the sediment volume is thereby determined and the corrected shoreline position is then found as:

$$dn_{i+1} = dn_i + 0.5 \cdot \frac{vol_{error}}{dA_z} \tag{5.10}$$

Where dn is the change in shoreline position. vol_{error} is the error in the deposited volume and dA_z is the vertical area of the strip of shoreface in question. The index i indicates the number in the iteration.

The tolerance is the iteration criteria which is based on rms(volume error) in m^3. A suitable criteria depends on the individual case; criteria between 0.001 and 0.1 have been used in practical projects, it is recommended to make a few tests to find a suitable value. The calculated error can be output in the coastline output and based on this output the overall sediment conservation for the shoreline model can be estimated.

The difference between using 0.1 and 0.001 is evident in Figure 5.7, which shows the cumulative sediment conservation error for two different tolerances. It is noted that during the simulation more than 500,000 m^3 of sediment passes through the system, with a significant amount being eroded and accreted during different times, so even the 12,000 m^3 error is not critical for the results which is seen in the bottom plot of Figure 5.7, which compares the total change in shoreline position for the two runs, only minor differences are observed.

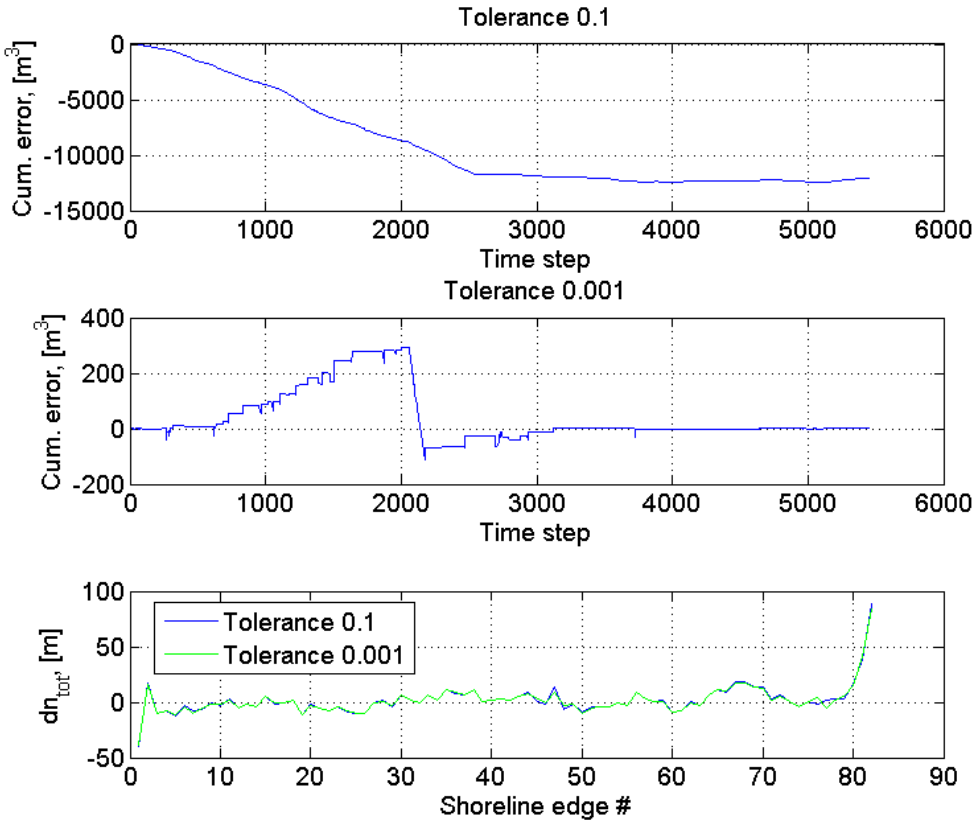

Figure 5.7 Top and middle: The sediment volume conservation error for two different tolerances for a practical example. Bottom: The total change in shoreline position (dn_{tot}) for the two runs

6 Validation

6.1 Equilibrium Slope

The aim of this example is to verify that the Sand Transport module in MIKE 21 Flow Model FM is able to predict the equilibrium slope of a straight flume.

The model is a straight flume, 30 m long and 2 m wide, which has a moveable bed. Initially, the bed level is -0.4 m along the entire flume. Now a fixed discharge of 0.5 m^3/s (corresponding to q = 0.25 $m^3/s/m$) is entered in the upstream end, while the downstream water level is fixed to 0.0 m. Under these conditions, as the bed of the flume is initially horizontal, an accelerating flow is created causing an increasing sediment transport rate along the flume and subsequent erosion of the bed. This process continues until the bed of the flume matches the slope of the surface water level indicating stable conditions.

The problem is to simulate the equilibrium bed level of the flume under the given conditions.

6.1.1 Numerical solution

The unstructured mesh shown in Figure 6.1 was used for the model. The bed resistance type was defined as a Manning number M with a constant value of 32 $m^{1/3}/s$. The model was run for a simulation time of 42 hours.

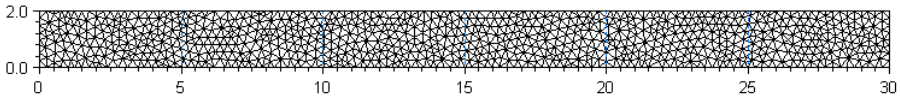

Figure 6.1 Mesh grid bathymetry

The water level adapts itself to the change in bed level during the morphological simulation. The change in the upstream water level during time is shown in Figure 6.2.

As the water level downstream is fixed to 0.0 m, Figure 6.2 shows that the resulting slope of the water level, I, is 0.03 m to 30 m, i.e. I_0 = 0.001.

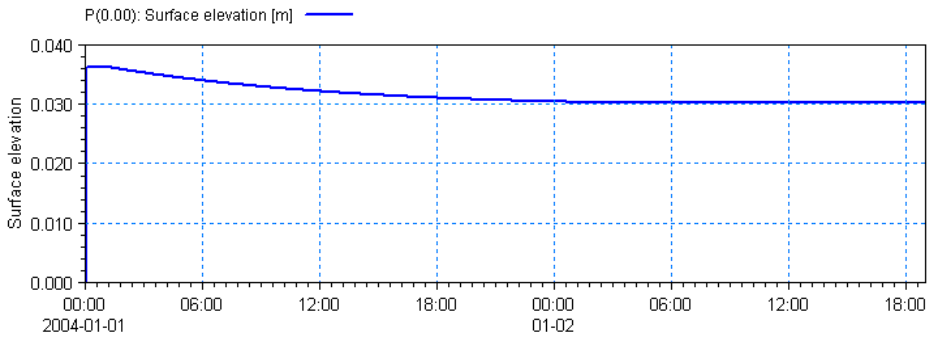

Figure 6.2 Water level at the upstream boundary during simulation

Figure 6.3 shows the development of the bed level during the simulation.

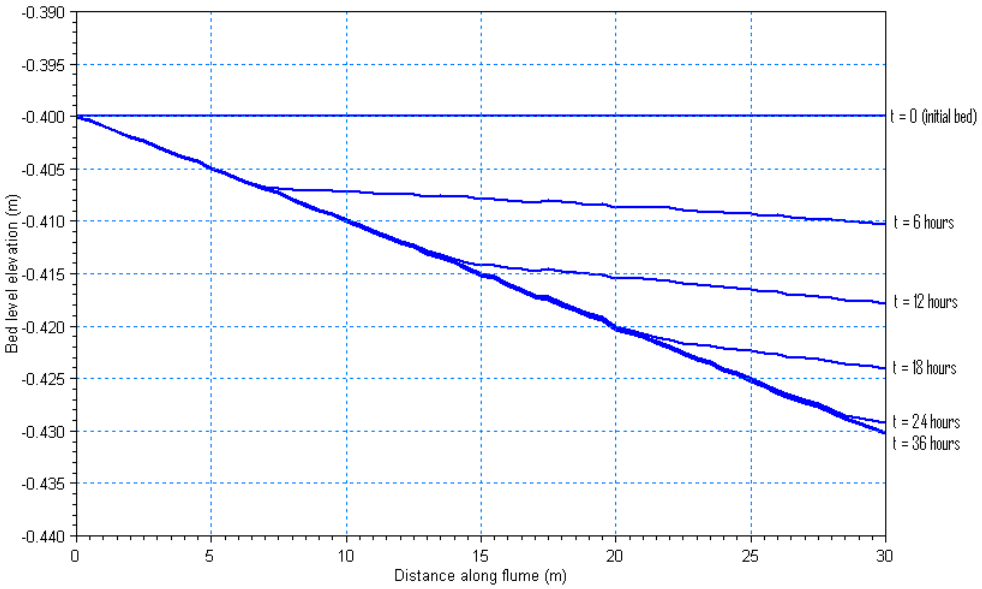

Figure 6.3 Longitudinal profile of the bed of a simulated flume at 5 times during a morphological simulation showing the development towards an equilibrium slope

Figure 6.3 shows that after 36 hours a stable solution is reached with a constant slope of the bed level. It can be seen that the bed level at the downstream point has eroded a little more than 0.03 cm, which corresponds to the resulting rise in water level at the upstream point.

6.1.2 Theoretical solution

The standard equation for natural depth, y_0, in a wide flume is:

$$y_0 = \left(\frac{q}{M\sqrt{I_0}} \right)^{3/5} \tag{6.1}$$

Then, if the hydrodynamic conditions from the simulation are inserted, the theoretical natural depth will be y_0 = 0.43 m, which is in very good agreement with the findings from the numerical morphological model.

6.2 Dune Erosion in Shoreline Model

The dune erosion model has been validated against the dune erosion experiment by Van Gent et al (2008). They measured the dune erosion rate in a large experimental facility. The experimental setup is shown in Figure 6.4. The waves were generated at the wave board (at 0 m).

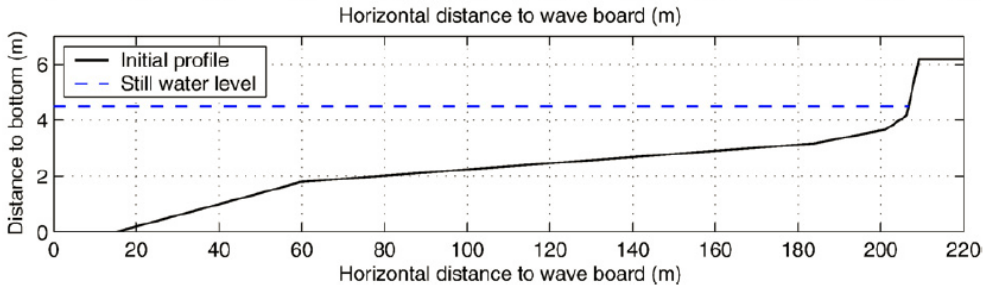

Figure 6.4 Experimental setup

The dune erosion model was setup to represent the test T01 where the wave conditions were H_{m0} = 1.5 m and T_p = 4.9 s.

The used model parameters were

- dune erosion slope tan(α_{re}) = 0.1
- max slope tan(α_{be}) = 0.2
- Calibration factor γ_r = 0.9
- Calibration factor C_s = 0.002

The comparison between the measured and modelled dune erosion is shown in Figure 6.5. A strong correlation between the measured and modelled dune erosion is observed.

The dune erosion is observed to happen quickly in the beginning when all the waves attach the foot of the dune and slower towards the end of the experiment as the foot of the dune has moved shoreward and upward along the slope tan(α_{re}) causing less waves to reach the foot of the dune which in turn significantly slows down the erosion rate. The comparison in Figure 6.5 shows that the model describes these mechanisms well.

It is noted that the bar which develops in the measured profile after 6 hrs (around 188 m from the wave board) cannot be described by the shoreline model because the coastal profile is prescribed to the model before starting the simulation.

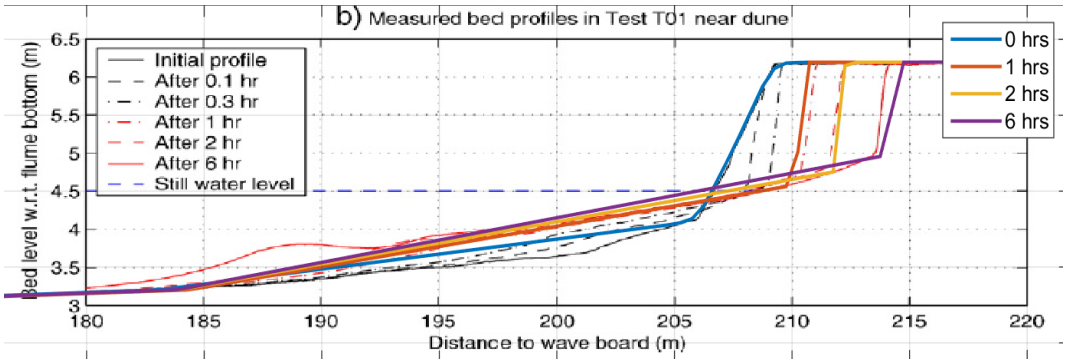

Figure 6.5 Comparison between the measured and modelled dune erosion. The thick full lines shown the modelled dune erosion.

7 References

/1/ Bendegom, L. van (1947), *Some considerations on River Morphology and River Improvement*, De Ingenieur, 59, No. 4, p. B1-11

/2/ Booij, R. and Kalkwijk, J.P.T. (1982), *Secondary Flow in estuaries due to the curvature of the main flow and to the rotation of the earth and its development*, Report 9-82, Lab. Of Fluid Mech., Dep. Of Civil Eng., Delft Univ. of tech, Delft

/3/ Brøker Hedegaard, I. (1985), *Wave Generated Ripples and Resulting Sediment Transport in Waves,* Series paper No. 36, Inst. of Hydrodynamics and Hydraulic Engineering, Technical University of Denmark.

/4/ Dally, W.R. and Brown, C.A. (1995), *A modeling investigation of the breaking wave roller with application to cross-shore currents,* J. of Geophys. Research, Vol. 100, No. C12, pp. 24.873-24.883.

/5/ Deigaard, R., Fredsøe, J., and Hedegaard, I.B. (1986), *Mathematical model for littoral drift,* Jour. of Waterway, Port, Coast. and Ocean Eng., ASCE, Vol. 112, No. 3, pp. 351-369.

/6/ Deigaard, R., Fredsøe, J., and Hedegaard, I.B. (1986), *Suspended sediment in the surf zone*, Jour. of Waterway, Port, Coast. and Ocean Eng., ASCE, Vol. 112, No. 1, pp. 115-128.

/7/ Deigaard, R., Asp Hansen, E., Justesen, P. and Brøker, I. (1994), *Sediment transport in the surf zone due to oblique incident waves,* MAST Gregynog Workshop, Gregynog, Wales.

/8/ De Vriend, H. J. (1981), *Steady flow in shallow channel bends,* comm. on Hydraulics 81-3, Dept. of Civil. Eng., Delft Univ. of Tech.

/9/ De Vriend, H. J. and Struiksma, N. (1983), *Flow and bed deformation in river bends,* Proc. ASCE Conference Rivers '83, New Orleans, p. 810

/10/ Doering, J.C. and Bowen, A.J. (1995), *Parameterization of orbital velocity asymmetries of shoaling and breaking waves using bispectral analysis,* Coastal Engineering (26)1-2, pp. 15-33.

/11/ Elfrink, B., Brøker, I., Deigaard, R., Hansen, E.A. and Justesen, P. (1996), *Modelling of 3D Sediment Transport in the Surf Zone,* Conf. of Coastal Engineering 1996, Proceedings.

/12/ Engelund, F. and Fredsøe, J. (1976), *A sediment transport model for straight alluvial channels,* Nordic Hydrology, 7, pp. 296-306.

/13/ Engelund, F. and Hansen, E. (1967), *A monograph on sediment transport in alluvial streams,* Teknisk Forlag, Danish Technological University, Copenhagen, Denmark.

/14/ Fenton, J. (1985), *A fifth-order Stokes theory for steady waves,* J. Coastal, Port, Waterway and Ocean Eng., ASCE, Vol.111, pp. 216-234.

/15/ Fenton, J. (1990), *Non-linear wave theories,* The Sea, Vol. 9, Ocean Eng. Science, Part A, Wiley, N.Y.

/16/ Fredsøe, J. (1984), *The turbulent boundary layer in combined wave-current motion,* Journal of Hydr. Eng., ASCE, Vol. 110, No. HY8, pp. 1103-1120.

/17/ Fredsøe, J. and Deigaard, R. (1992), *Mechanics of Coastal Sediment Transport,* Advanced Series on Ocean Engineering, Vol. 3, World Scientific.

/18/ Fredsøe, J., Andersen, O.H., and Silberg, S. (1985), *Distribution of Suspended Sediment in Large Waves,* Journal of Waterway, Port, Coastal and Ocean Engineering, ASCE, Vol. III, No. 6, pp. 1041-1059.

/19/ Galappatti, R. (1983), *A depth-integrated model for suspended transport,* Report No. 83-7, comm. On hydraulics, Dept. of Civil Engineering, Delft Univ. of Technology.

/20/ Guy, H:P, Simons, D.B. and Richardson, E.V. (1966), *Summary of alluvial channel data from flume experiments, 1956-1966*, U.S. Geological Survey Professional Paper 462-I, Washington D.C.

/21/ Ikeda, S. (1980), *Incipient motion of sand particles on slopes*, Rep. of Found. Eng. & Constr. Eng., Saitama Univ., Japan.

/22/ Isobe and Horikawa (1982), *Study on water particle velocities of shoaling and breaking waves*, Coast. Eng. in Japan, Vol. 25, pp. 109-123.

/23/ Jansen, P.H., van Bendegom, L., van den Berg, J., de Vries, M., and Zanen, A. (1979), *Principles of River Engineering*, Pitman Publishing.

/24/ Kaergaard and Fredsoe (2013), *A numerical shoreline model for shorelines with large curvature*, Coastal Engineering 74 (2013), p. 19-32

/25/ Kalkwijk, J. P. Th, and de Vriend, H. J. (1980), *Computation of the flow in shallow river bends*, J. Hyd. Res., 18, No. 4, p. 327.

/26/ Kalkwijk, J. P. T., and Booij, R. (1986), *Adaptation of secondary flow to nearly horizontal flow*, J. Hyd. Res, 24, No. 1, p. 18.

/27/ Kikkawa, H., Ikeda, J., and Kitagawa, A. (1976), *Flow and bed topography in curved open channels*, J. Hyd. Div., ASCE, Vol.102, No. HY9

/28/ Koch, F.G. (1980), *Bed level computation for axis-symmetric curved channels*, Rep. R567-1X/W308 part1, Delft Hyd. Lab.

/29/ Kwan, S. (2009). A two dimensional hydrodynamic river morphology and gravel transport model (Doctoral dissertation, University of British Columbia).

/30/ Lane, E.W. (1953), *Progress report on studies on the design of stable channels by the Bureau of Reclamation*, Proc. ASCE, Irr. And Drain, Div., Vol. 79

/31/ Larson, M., Erikson, L. and Hanson, H. (2004): *An analytical model to predict dune erosion due to wave impact*. Coastal Engineering Vol. 51, pp. 675-696

/32/ Luque, R. F. and van Beek, R. (1976), *Erosion and transport of bed-load sediment*, Journal of Hydraulic Research, 14, No. 2, pp. 127-144.

/33/ Meyer-Peter, E. and Müller, R. (1948), *Formulas for bed load transport*, Proc. 2nd Congr. IAHR, Stockholm, Vol. 2, paper 2

/34/ Nielsen, P. (1979), *Some Basic Concepts of Wave Sediment Transport*, Institute of Hydrodynamic and Hydraulic Engineering, Technical University of Denmark, Series Paper 20.

/35/ Nouh, M.A. and Townsend, R.D. (1979), *Shear stress distribution in stable channel bends*, Proc. ASCE, J. Hyd. Div., 105, HY10

/36/ Odgaard, A.J. (1981), *Transverse bed slope in alluvial channel bends*, J. Hyd. Div, ASCE, Vol.107, No.HY12

/37/ Olesen, K.W. (1987), *Bed topography in shallow river bends*, Faculty of Civil. Eng., Delft Univ. of Tech, Report 87-1

/38/ Parker, G. (1983), *Theory of meander bend deformation,* Proc. ASCE Conf. Rivers '83, New Orleans

/39/ Raudkivi, Arved J. (1988), *The Roughness Height under Waves,* Journal of Hydraulics Research, Vol. 26, 1988, No.5.6.

/40/ Rijn, L. C. van (1984), *Part I: Bed load transport,* J. Hyd. Eng., 110, October, "Part II: Suspended load transport", J. Hyd. Eng., 110, November

/41/ Rozovskii, I.L. (1957), "*Flow of water in bends of open channels*", English translation: Israel Progr. For Scientific Transl. Jerusalem, 1961

/42/ Rubey, N.W. (1933), *Settling Velocities of Gravel, Sand and Silt Particles,* Amer. J. of Science, 5th Series, Vol. 25, No. 148, pp. 325-338.

/43/ Struiksma, N., Olesen, K.W., Flokstra, C., and de Vriend, H.J. (1985), *Bed deformation in curved alluvial channels*, J. of Hyd. Res., Vol. 23, No.1

/44/ Swart,D.H (1982), *The nature and analysis of random waves in shallow water,* CSIR Research report 388/2, Stellenbosch, South Africa.

/45/ Talmon, A.M., Struiksma, N. and van Mierlo, M.C.L.M. (1995), *Laboratory measurements of the direction of sediment transport on transverse alluvial bed slopes,* J. Hyd. Res., Vol.33, no4, 1995

/46/ Van der Meer J.W. and Janssen, J.P.F.M. (1994): *Wave run-up and wave overtopping at dikes*. ASCE: Wave forces on inclined and vertical wall structures, ed. N. Kobayashi and Z. Demirbilek, pp. 1-27.

/47/ Van Gent, M.R.A., Van Thiel de Vries, J.S.M., Coeveld, E.M., De Vroeg, J.H. and Van de Graaff, J. (2008): *Large-scale dune erosion tests to study the influence of wave periods*. Coastal Engineering Vol. 55, pp. 1041–1051.

/48/ Vanoni, V.A. (1975), *Sedimentation Engineering,* ASCE manuals and reports on engineering practice, No. 54, New York

/49/ Vanoni, V.A. (1984), *Fifty Years of Sedimentation,* J. Hyd. Eng. ASCE, Vol. 110, No. 8

/50/ Wilcock, P. R. (1998). Two-fraction model of initial sediment motion in gravel-bed rivers. *Science*, *280*(5362), 410-412.

/51/ Wilcock, P. R., & Kenworthy, S. T. (2002). A two-fraction model for the transport of sand/gravel mixtures. *Water Resources Research*, *38*(10).

/52/ Wilcock, P. R., & Crowe, J. C. (2003). Surface-based transport model for mixed-size sediment. *Journal of Hydraulic Engineering*, *129*(2), 120-128.

/53/ Zyserman, J.A. and Fredsøe, J. (1994), *Data analysis of bed concentration of suspended sediment,* Journal of Hydraulic Engineering, ASCE, Vol. 120, No. 9, pp. 1021-1042

/54/ Zyserman, J.A., and J. Fredsøe (1996), *Validation of a deterministic sediment transport model for sheet-flow conditions,* Progress Report 76, pp. 1-7, Institute

of Hydrodynamics and Hydraulic Engineering (ISVA), Technical University of Denmark.